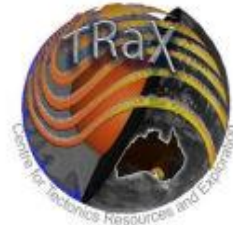


Mineralogy, petrography and stratigraphic analysis of gold-hosting units, Oberon prospect, Tanami Region, N.T.



THE UNIVERSITY
OF ADELAIDE
AUSTRALIA



Dylan Silcock – 1176459

School of Earth and Environmental Sciences, University of Adelaide, South Australia, 5005

Phone: 0406638322

Email: dylan.silcock@student.adelaide.edu.au

October 2011

Supervisors:

Nigel J. Cook, Cristiana L. Ciobanu

School of Earth and Environmental Sciences, University of Adelaide, South Australia, 5005



ABSTRACT

The newly-discovered Oberon gold deposit, Tanami Goldfields, represents a Paleoproterozoic mesothermal orogenic gold deposit hosted in the Tanami Group. Recent drilling has intersected extensive mineralised zones at various positions within the lower stratigraphy. Studying drillhole TID0065 using a number of different techniques, the project set out to understand the lithostratigraphy of the sequence and its relationship with gold mineralisation, constraints on depositional environments and associated hydrothermal alteration, along with correlations to other deposits in the region.

The sequence consists of a dolomitic mudstone, grading up into a phyllite, with a siltstone protolith. This meta-sandstone represents the main host for gold mineralisation and is similar to that seen in the Coyote deposit. Conformably overlying this unit is a rapidly-deposited well-defined turbidite sequence. Gold is also hosted in the overlying Boudin Chert unit, a graphitic, pyrite rich rock that has hosts distinctive diagenetic boudin structures. The Boudin Chert represents a transition into an anoxic sediment-starved environment. Increased clastic input along with a drop in sea level further defines the rest of the sequence, with a siltstone, mudstone and sandstone package and intercalated volcanoclastics and ignimbrites noted in the upper part of the drillhole extending into the Killi Killi Formation.

Mineralisation is predominantly stratabound but thrust stacking provides a secondary control to the gold distribution pattern. Gold mineralisation is associated with Na-enrichment and K-depletion; albite is the dominant feldspar in the gold-hosting assemblage. This demonstrates a possible sodic metasomatism of an alkali assemblage. The wide variation in chlorite composition, expressed as varying proportions of chamosite and clinocllore end-members between lithologies, is suggestive of multiple fluid phases and/or alteration events, including possible 'seafloor metamorphism' prior to hydrothermal activity.

Primary alteration in the deposit is represented by an earlier chlorite-sericite assemblage and a later stage calcite-dolomite alteration in certain lithologies at the base of the sequence. Using chlorite thermometry, peak metamorphic temperatures were calculated to be at 366 ± 21 °C (i.e. greenschist facies); conditions reach amphibolite grade less than a kilometre away. Electron probe microanalysis suggests the mineralising fluids were volatile-rich, as demonstrated by the high F content of biotite and apatite.

Future exploration potential for deposits of this type should focus on identification of Fe-enriched turbidite sequences, chlorite-albite-muscovite assemblages and the presence of arsenopyrite. Graphitic oxygen-deprived beds enriched in a range of trace elements with strong pyrite alteration are also good indicators of gold mineralisation.

INTRODUCTION

The Tanami gold fields, straddling the N.T. – W.A. border, host Northern Australia's most productive Paleoproterozoic Orogenic gold deposits with several mines currently in production (Figure 1, 2). The region also hosts a series of other more recently discovered deposits that have potential to be exploited in the future; relatively little is known about them. One such case is the recently discovered Oberon deposit, located ~50 km NW of the world-class Callie deposit. The Oberon prospect shares many characteristics with the surrounding regional goldfields, and has potential to be host high-grade deposits and be put into production once sufficient ore reserves can be proven.

Very little information has been published in Oberon until now partially due to the minimal exploration undertaken on the area. This is partly due to the heavy alluvial cover that dominates the Tanami region requiring extensive drilling to determine the subsurface geology (Crispe *et al.* 2007). Although some surface outcrop does exist, these are, however, poorly exposed and heavily weathered.

Oberon had previously undergone some relatively shallow drilling penetrating into the Madigan beds, with some low-grade intersections located near surface. Three drillholes targeted deeper mineralisation from 2008 onwards. TID0064 was the first of these holes with intersections at 17g/t Au. This however did not penetrate into the high-grade mineralised zone due to drilling complications. TID0065 (the hole studied here) was the next to be completed, intersecting far better mineralised zones. Two other holes TID0067 and -68 were delayed due to an extensive wet season in 2010-2011 and have only recently recommenced. Although core logging and assaying have been undertaken by Newmont², the deposit is poorly understood, particularly with respect to deposit formation and the lithostratigraphy of the host rocks.

Several of the surrounding deposits are, however, well documented with various types of studies being undertaken. These include fluid inclusion studies to determine temperature of ore deposition

and geothermobarometry to ascertain the metamorphic evolution of the host rocks (Huston *et al.* 2007, Tunks & Cooke 2007, Williams 2007). These studies have placed good constraints on the individual deposits and on variations across the district. In order to evaluate the mineralisation at Oberon in a similar context, and to compare it with other deposits in the area, petrographic, mineralogical and geochemical analysis of core samples has been undertaken. Particular emphasis has been placed on interpreting the rock sequence at Oberon, including identification of rock types, characterisation of alteration and metamorphic mineralogy, and correlating the sequence with others in the district.

The aims of this project are to determine the link between the lithologies and their associated gold mineralisation. One key query is whether the gold precipitation *is* associated with the Fe-rich host lithologies and/or graphitic beds or has it undergone redistribution (remobilisation) following initial deposition from the hydrothermal fluids? These questions have been addressed by petrographic analysis and Scanning Electron Microscopy (SEM), accompanied by core logging undertaken on-site at the Tanami mine. Quantitative mineral compositional data allow for comparison with other deposits in the region that share similar characteristics such as host lithologies and similar mechanisms of gold precipitation (such as depressurisation, and redox interactions between host lithologies) . An attempt will be made to constrain peak metamorphic temperatures using geothermometry based on the compositions of minerals such as chlorite.

The present project focuses on why mineralisation occurs where it does, and its chemical controls. The project is one of two being carried out simultaneously on Oberon. In the second project (Meria 2011), the focus is on the distribution of gold at the micro- and macroscales. Outcomes from both projects will give a better understanding of the gold distribution, improved chemical and physical constraints on the rocks hosting the mineralization and will help develop genetic models for the Oberon deposit. Comparison will be made with lithological and chemical characteristics of other known surrounding goldfields in the Tanami region, as well as mesothermal (orogenic) gold deposits in general as defined by Groves *et al.* (1998).

GEOLOGICAL SETTING

The Tanami region (Figure 2) lies roughly 600 km NW of Alice Springs. The region is part of the North Australian Craton with the Arunta Complex located to the south and the Kimberly region to the NW (Crispe *et al.* 2007).

The region contains a number of world-class orogenic gold deposits (the Tanami Goldfield). At the present time, the following mines are in operation: the world-class Callie deposit hosted in limestone (188 t Au at an average grade of 5.3g/t, the Dead Bullock Soak goldfield hosted in the Schist Hills iron member (SHIM) (16.4 g/t at 3.9 g/t) and the Tanami goldfield (50.6 t Au). Other noteworthy deposits that are not currently in production include Groundrush (hosted in the Killi Killi Formation), Coyote and Minotaur (Crispe *et al.* 2007, Huston *et al.* 2007). These other deposits in the region are significant for understanding Oberon since they share certain aspects such as mineralogy, stratigraphic setting and mechanisms of gold deposition (Figure 3, 4).

Lithostratigraphy

The oldest unit in the region is the Archean Gniess which outcrops to the South West of the Tanami as the Billabong Complex; this constitutes the basement of the region (Page *et al.* 1995). The Tanami Group unconformably overlies the Archean basement (Cooper & Ding 1997), and consists of the lower Dead Bullock Formation and the overlying Killi Killi Formation. The Tanami Group sequence is dated at between ~1.87–1.86 Ga based on $^{207}\text{Pb}/^{206}\text{Pb}$ isotope analysis of detrital zircons (Crispe 2006). The lower member of the Killi Killi Formation is known as the Madigan beds.

The Dead Bullock Formation is broken into two main sub-units: the Ferdies (also referred to as Davidson) and Callie Members (also referred to as Blake Beds). The lower parts of the Ferdies Member have only recently been drilled by Newmont, with promising intersections of gold-hosting lithologies being reached at a depth of >2 km in the Callie mine known as the Auron Beds.

The Ferdies Member is a Fe-rich, feldspathic, fine-grained quartz sandstone which contains interbedded siltstones and carbonaceous siltstones. The overlying Callie Member comprises finer-grained siltstones, sandstones and carbonaceous shale, and also contains intersections of volcanic tuff. In the transition zone with the Killi Killi Formation, this unit grades into laminated siltstones and cherts.

The Killi Killi Formation is a rapidly deposited sequence of turbiditic units that have been dated at between 1864 and 1844 Ma (Bagas *et al.* 2009). The tectonic setting of the Killi Killi Formation has been interpreted as an active continental margin, most likely during the collision between the southern Arunta and Northern Halls Creek Orogen (Bagas *et al.* 2009).

The depositional environment of the sedimentary sequences seen in the Tanami region is subaqueous, with interspersed bimodal magmatism. Sedimentation of the Tanami Group occurred at the same time as a magmatic event in the region at ~1,800 Ma. (Crispe *et al.* 2007). Expressions of bimodal volcanism are present in the Tanami Group, including dolerite intrusive; tuffs are recognised in the Killi Killi Formation. A series of oblique thrusts striking N to NW reflect convergence of the region; this phase was associated with the introduction of gold mineralisation. Although evolution of the deposit mainly occurred in an intra-cratonic setting, events from the Arunta and Halls Creek orogens also influence the region (Crispe *et al.* 2007). The Tertiary period saw the development of paleochannels that are now preserved at depth by the alluvial cover that dominates the region.

Overlying the Killi Killi is the Nanny Goat Volcanics (Figure 3, 4). The upper section of the unit contains felsic volcanics referred to as the 'Feldspar-quartz ignimbrite (Pn1') and 'Feldspar-

ignimbrite (Pn2)' (Hendrickx 2000). At the base of the Nanny Goat volcanics is a turbidite sequence that has been refined as the top section of the Killi Killi Formation. The intrusive unit has been referred to as the 'Birthday suite' (Crispe *et al.* 2007) or the Winnecke Granophyre of Blake (1976). This is an intrusive and shallow intrusive unit that has crystallisation ranges from 1,825 Ma to 1,810 Ma. Crispe *et al.* (2007) described the intrusive as very potassic with high SiO₂ (>70.7 wt%). The assemblage also contained biotite and hornblende, along with one sample that reflected a peraluminous composition.

Metamorphism and deformation

Deposition of the turbidite sequences ceased upon onset of the Tanami Event at 1830 Ma. Although the Tanami Orogeny underwent peak regional metamorphism at amphibolite facies, the greenschist facies is more commonly expressed in the inlier. Assemblages of quartz-biotite-muscovite or quartz-sericite are dominant. Syn-deformational granitic intrusions produced localised contact aureoles. Expressions of higher facies metamorphism (e.g. presence of andalusite, garnet or cordierite) are largely restricted to these contact aureoles (Scrimgeour & Sandiford 1993; Scott 1993; Valenta & Wall 1996; Vandenberg 2002; (Crispe *et al.* 2007).

Ore-forming fluids are interpreted to have originated from the inversion of the principle stresses in the Stafford event at 1803–1791 Ma from the NW to the south of the North Australian Craton (Huston 2006). Mineralising fluids then penetrated from the lower crust creating the Callie deposit. Recent Geoscience Australia publications have suggested that reactivation of previous deep shears from the Tanami event acted as a platform for the transport of fluids from the study of deep penetrating seismic surveys (Goleby 2008); see Figure 5.

The Tertiary period saw a development of paleochannels that are now preserved at depth by alluvial cover that dominates the region, making exploration difficult.

Mineralisation and associated alteration

The main gold-hosting sequences of the Tanami Group are the Callie Member (Callie Laminated Beds), which represent the main mineralised zone in the Callie mine. The Schist Hills Iron Member (SHIM) acts as a host sequence for the Dead Bullock Soak goldfield (Smith 1998). The overlying Killi Killi Formation is another important host sequence in the Coyote deposit. The Oberon deposit is currently *assumed* to be hosted in within the Killi Killi Formation (see schematic section Fig 29).

Alteration seen in the Tanami field, including at Oberon, is expressed in regionally widespread chlorite-carbonate assemblages that are associated with a stage-three syn-metamorphic alteration event (Tunks & Cooke 2007) synchronous with orogenic gold deposition. Comparable alteration is common in orogenic ore deposits formed at greenschist facies (Groves *et al.* 1998, Moritz 2002). The Golden Mile deposit (Kalgoorlie, W.A.) exhibits a chlorite/muscovite + carbonate + pyrite style of alteration (Phillips 1986), which is, in many ways, similar to that seen at Oberon.

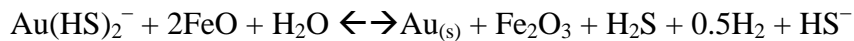
As with many mesothermal orogenic deposits there is little solid evidence of the source of the hydrothermal fluids that led to mineralisation and associated alteration. Elsewhere in the Tanami Region, fluid inclusion studies have shown ranges of fluid temperatures between 190 °C (shallow deposits) to 430 °C (deeper deposits). Fluid inclusions have been shown to contain 4-14 wt% NaCl and a relatively high proportion of CO₂ (Huston *et al.* 2007). CO₂±N₂-rich fluid inclusions are also abundant in shallower mineralised zones (Mernagh & Wygralak 2007). The origin of the fluids is still uncertain with possible various stages of fluid alteration giving isotope signatures suggesting fluid mixing. A metamorphic fluid (Adams 1997) or a magmatic fluid are the two most plausible sources (Wygralak 2005; Huston *et al.* 2007), although it is likely that the source fluid was a combination of the two (Groves *et al.* 2003).

The mechanism of gold deposition has been disputed with vastly differing models. A decarbonisation depositional model supported in recent publications (Huston *et al.* 2007, Williams 2007) suggests interaction between the mineralising fluids and carbon-rich host rocks causing

depressurisation, gold precipitation from the fluids and associated effervescence of CO₂. The source of the carbon was considered to be graphite in the mud- and siltstones. Structural controls are said to be an important factor in this processes, with anticlinal closures, shear zones and structural corridors concentrating the ore fluids into the graphite-rich host lithologies (Huston *et al.* 2007) (Williams 2007). The following reaction has been proposed:



(Lambeck *et al.* 2011) suggested that gold is not deposited by the de-carbonisation, since the Total Organic Carbon (TOC) is never present in sufficient quantities (only 0.1% in the Callie deposit) to enable decarbonisation reactions. Instead they consider the good correlation between Au grade and the Fe-rich sediments to infer that Fe-oxides in the rock acted as a redox agent, triggering Au precipitation from solution.



(Lambeck *et al.* 2011)

Fluid inclusion studies have shown that CH₄ was released in the deeper, higher temperature deposits, while the higher level deposits (such as Callie) had more CO₂±N₂ incorporated in fluid inclusions.

METHODOLOGY

Fieldwork and sampling

The initial phase of the report was to undertake a literature review of published/unpublished material on ore deposits and lithostratigraphy in the Tanami region. Although Oberon is a relatively new discovery and there is only limited information available, other deposits have been copiously

studied and provide a starting point to understand the regional geology. Comparisons can then be implied to the surrounding Tanami region's geochemistry and lithostratigraphy.

Sampling was undertaken on the discovery hole TID0065 at Oberon, Tanami. This drillhole is 900 m in length and intersects a package of lithologies that host the Oberon orebody. The entire 900 m was logged with special attention to lithological units, their associated contacts, alteration styles, faults and other large-scale structures within the sequence. Since the study was carried out on only a single hole, structural orientations were not mapped.

Along with core logging, the cores were comprehensively photo-documented. Sampling was undertaken by selecting 5-20 cm lengths of core in sections of the drillhole that represented either the main lithological units or special lithological features (e.g. contacts and alteration). Limited sampling was also undertaken on-site at the Oberon deposit, where there is no surface outcrop but rock chips could be collected from water monitoring bores. These materials provided a good indication of lithologies in the immediately adjacent area (such as visible garnets).

Forty-six samples were prepared as polished thin sections for petrographic analysis. Fifteen samples of particular interest were carbon-coated for higher magnification investigation by the SEM and quantitative analysis of mineral compositions by electron microprobe (EMPA).

Analysis

Optical analysis used a Nikon Eclipse LV100 polarising and reflected light microscope equipped with the DS-Fi1 camera. Each thin section was photographed at various magnifications (x5, x10, x20, x50) to document lithology, rock textures, alteration and mineralogy. Polarising and cross polarising light was used for the silicate minerals; ore minerals were observed under reflected light. The optical work also allowed particular slides to be selected for further analysis under the SEM.

SEM analysis was undertaken on the Philips XL30 FEG-SEM (Adelaide Microscopy), using an accelerating voltage of 15 kV, spot size of 4 and 10 mm working distance. The SEM is equipped with an EDAX EDS X-ray detector allowing for semi-quantitative spot analysis of minerals of interest to provide basic compositional information. Given the fine groundmass size (<1micron) of the Oberon lithologies, the resolving power of the SEM allowed for fine details to be observed. The instrument is also equipped with a back-scatter electron (BSE) detector allowing high-resolution images containing compositional information.

Microprobe (EMPA) analysis was carried out using a CAMECA SX51 instrument at Adelaide Microscopy. EPMA work targeted the same samples that were analysed by SEM. Analysed grains were pre-selected. Rock-forming minerals analysed included chlorite, biotite, muscovite, apatite, and alkali- and plagioclase feldspars. The instrument was operated at 15 kV; 16 elements were analysed. The beam current was 20.76 nA, accelerating voltage 15 kV and take-off angle of 40°. Standards, spectral lines, count times and minimum detection limits are summarised in Table 1. Between 7 and 10 spots per mineral per thin section (if it exists in the section) were measured to give a good representation in that lithology and eliminate outliers. Points were taken as systematically as possible and over the entire sample area to ensure an accurate representation as well as variations are recorded.

Whole rock geochemical data was supplied by Newmont. This consisted of assays at 0.5m intervals beginning at 300 m (giving 715 individual data points). The element set analysed was: Na, Ca, S, K, Mg, Al, Fe, Si, and Ti (as wt%) and the trace elements Ag, Au, As, Ti, Cr, Ni, Mn, Sc, Th, Be, Ba, Bi, Cr, Cu, Ga, La, Mo, Tl, U, V, W, Zn and Zr in ppm. Detection limits for the trace elements varied between mineral from 0.5 to 10 ppm. As a result, some rare earths and other trace elements (e.g., Ga, La, Mo, Tl, U, W, Th, Sc, Ag and Cd) present at concentrations of around or below the detection limit are poorly represented in the final dataset.

Data Processing

The Newmont assay data were evaluated and plotted using ioGAS statistical software. Initially, data points were separated into lithological units based on core logging. Probability plots were generated to determine the major elemental distributions through the lithologies. Zirconium was also plotted against likely immobile elements (e.g. Ti, Al, V) to help define primary lithologies. Partitioning of mobile elements (e.g. K, Na, Ca) in lithological units based on their enrichment and depletion was also undertaken. Alteration can also be determined from the distribution of elements such as S, Fe, Mg, Na and Ca. Plots between Au and major elements was undertaken to determine correlations of certain elements with higher gold grades.

Lithological unit boundaries were defined using key geochemical data that differentiate distinct lithologies (e.g. Ca, Mg enrichment in the lower 'Puck' sequence). Some boundaries are, however, difficult to define due to the gradational superimposed alteration. For example the base 'Puck' sequences contain intervals of phyllite/sandstone that are difficult to distinguish by visual inspection of core alone. Several elements are nevertheless characteristically enriched or depleted in both these sequences (Figure 18, 19). Relatively unaltered sedimentary units such as the upper sandstone units were used as a control to measure enrichment and depletion. These units have had not undergone the same degree of hydrothermal alteration as the lower greenschist and Fe-enriched lithologies.

EMPA data for chlorite, apatite, feldspar, white mica and biotite were processed to determine variation in both the end-members and additional minor elements, e.g. fluorine in chlorite. Mineral end-members were plotted on ternary diagrams and scatter plots.

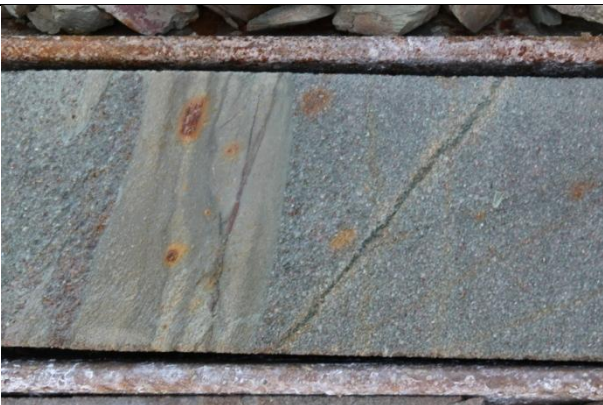
Peak metamorphic temperatures were derived by chlorite geothermometry using the calibrations of Cathelineau (1988), Jowett (1991) and Kratinoidis & MacLean (1987).

RESULTS

Simplified stratigraphy

The base of the stratigraphic column is the ‘Puck’ sequence, a fine-grained calcareous mudstone metamorphosed at greenschist facies with a unique textural fabric that easily defines the unit (see below). The dolomitic Puck unit grades up into a pelitic mudstone, also with a strong greenschist alteration and then into the overlying Fe-enriched turbidite facies. This well-defined package of conforming Bouma sequences hosts the majority of Au mineralisation in Oberon. The turbidite is marked by flame structures and rip-up clasts. The turbidite then grades into a series of less defined packages with smaller grain size.

The Boudin Chert unit marks a major transition into a fine-grained deep sea succession with a severely reduced clastic input. The clear decisive marker for this unit is diagenetic chert boudins that have developed in a S- and Fe-enriched environment, leading to extensive pyrite development. The deepwater sequence then develops, upwards, into a unit with very well-defined bedding that is referred to here as the ‘Zebra’ rock due to its pronounced black and white striping. Overlying the deep water succession is another expression of turbidites which then grades up into shallower deltaic deposits that also contain intercalations of volcanic rocks.



Madigan Beds/Killi Killi (turbidite):

Turbidite sequences lie conformably above the ‘Zebra’ unit. The contact is marked by rip-up clasts and flame structures. The unit consists of repeating units that make up a Bouma sequence. The sequence repeatedly grades up from a coarse-grained sandstone into a shale. Sedimentary features seen in the beds include a ‘hummocky’ cross-stratification, cross stratification; these clearly define a weak bedding that ranges in size from massive to 2 cm.



The Killi Killi also demonstrates very-well defined bedding with both white and black bands (image at 139m). This is very similar to the 'Zebra' rock. It could be that this was deposited by an equivalent process.

← top (120 m): Contact between the very well-defined beds of the

← lower (139.4 m): Intersection of finer mud in coarse sandstone



← lower (159.2 m): Fine-grained well laminated turbidite, with overlying mudstone package.



Volcanic Tuff (110-115 m)

A 10 m-thick tuff intersection with a felsic composition and fine glassy matrix occurs within the Killi Killi. Quartz-Feldspar symplectites are observed, together with feldspar, quartz, muscovite and some chlorite alteration.

← Tuff intersection (note core image has reflection on it).



Ignimbrite (236-351.7 m):

This 50 m-thick unit has a distinctive red colour with large 0.5mm quartz phenocrysts supported in a sericitised fine-grained matrix with a glassy fabric. The upper contact (possibly reversed) is yellow with large 1-3 mm-sized quartz phenocrysts. Below this is a limited fine-grained grey 'surge base' that is commonly seen at the base of ignimbrites. The deeper contact (at 280 m) appears conformably on top of the quartz dolerite intrusive.

The quartz-rich dolerite unit displays a marked 'cooked' contact at the top of the unit. This is absent at the bottom of the unit. The unit is a pale red colour, coarse-grained and is altered to a yellowish colour at the cooked contact.

← (upper) Yellow top (236.5m) contact with surge deposit (white).

← (lower) Base contact (351.7m)



Grey Arkose Quartzite (~279-351 m) *note, depth only estimate due to faulting of sequence

The quartzite conformably overlies the 'Zebra' unit, rip-up contacts of 'Zebra' are seen to mark the contact. The arkose quartzite is a medium-grained composition made up of ~65% quartz and ~25% plagioclase and 10% chlorite and sericite alteration. It may represent a base of a turbidite succession as it has undergone rapid deposition, evident from the rip-ups of the underlying lithology. The unit is homogeneous in composition, and displays massive bedding; no sedimentary features are distinguishable despite some rip-up clasts in the lower sections.

← (upper) Massive quartzite at 305m

← (lower) Rip-up clasts at 360m and injections of feldspathic sandstone (now quartzite) into the underlying 'Zebra'.



"Upper Dirty Zebra" (transition zone) (~350-385 m)

This unit is transitional to a 'dirtier' sediment that has a greater clay component and also contains pyrite; the thickness of the beds is less consistent. The lighter bands are now a silty grey colour, with lesser feldspar.

The contact between the overlying turbidite is seen in adjacent picture, with the fine-grained 'Zebra' rock being ripped up into the overlying rapidly deposited turbidite.

← Upper contact with rip-up with the overlying quartzite.



'Zebra' rock (184-350m)

Very well-defined black and white beds, each 20-50 mm in thickness. Very fine-grained, claystone. The unit has a fairly consistent bedding size ranging between 5 and 20 mm. The lighter beds are predominately albite-rich, while the dark beds are finer grained, quartz-rich, and also contain pyrite. Chlorite and muscovite makes up the groundmass.

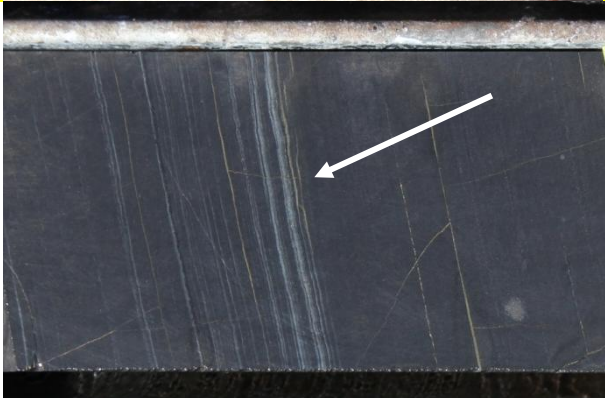
← Mudstone with very well defined bedding with pyrite alteration.



Lower Dirty 'Zebra' (Transition) (350-420 m)

Transition into dirtier sediment, banding/bedding is on a finer scale and less consistent. The white beds are more mudstone rich and no longer a pure white. Transition into sulphide-rich (pyrite) horizons demonstrates the grading contact between the zebra rock and the Boudin Chert below it.

← Lower dirty 'Zebra' Banding is less consistent and bands no longer have distinct black and white style.



← Very fine-grained 'Zebra rock' which at 430 m displays a transition into Boudin Chert. This represents the base of 'Zebra rock', grading up from Boudin Chert, introduction of small lighter bands of quartz-albite assemblage, which grades up into the thicker banding seen in the image above.



Boudin Chert (420-485 m)

This easily identifiable chert sequence is marked by the presence of large (20-40 mm-sized) diagenetic boudins, graphite-rich beds, strong iron enrichment and the presence of sulphides (pyrite ± chalcopyrite). The abundance of these features diminishes downwards in the sequence and grades towards a sandstone which is the upper reaches of the Turbidite below it.

← (upper) diagenetic chert boudins (450m) in the Boudin Chert. Graphitic beds along with pyrite rich layers possibly represent primary bedding.

← (lower) 100% graphite beds (435m) mark the transition in the sediment deprived Boudin Chert.



Puck Group (greenschist) (>490 m)

The base sequence of the discovery hole is a rock that has been heavily metamorphosed to greenschist facies and which is the main host sequence for gold mineralisation. The name Puck is derived from the Shakespeare play '*A Midsummer Night's Dream*,' Puck is the servant of Oberon, the 'king of the fairies'.

The sequence is generally a fine-grained chlorite-muscovite-plagioclase turbidite which grades from a coarse plagioclase-rich sandstone to phyllite. At the base, the Puck Group grades into a dolomitic mudstone with a distinct primary bedding feature (chlorite altered dolomite cavities). The base unit hosts no gold mineralisation.

Although this unit displays the same style of greenschist assemblage throughout, there is variation in mineralogy, texture and style of alteration, suggesting that a number of different protoliths are represented within the Group. These differences in the protoliths give vastly different textural patterns and gold grades making it important to distinguish the unit based on protolith of the greenschist.

The Puck Group sequence consists of: (i) the transitional boundary zone between the turbidite unit and the overlying 'Zebra' rock; (ii) a coarse-grained turbidite unit (sandstone to greywacke) immediately below, which grades into (iii) a fine-grained sandstone containing laminated beds and grading to a micron-scale feldspathic sandstone. The latter is the dominant lithology in the highest-grade gold mineralised zone. In the mineralized zone, networks of small quartz-filled fracture veins and associated calcite alteration are noted. With the base unit a dolomitic mudstone.



Puck Group turbidite - very coarse sandstone protolith (~540-615 m)

The coarse component of the turbidite package. Grain size range from 1-4 mm in the coarse sections. Flame structures and rip ups are commonly seen due to the rapid deposition. Feldspar and quartz grains range from rounded to very angular in different Bouma packages.

← Contact between fine grained siltstone and coarse grained sandstone.



↑ (upper) Fine-grained phyllite with arsenopyrite mineralisation



↑ (lower) Green phyllite with cross cutting quartz and calcite vein.



Puck Group turbidite - siltstone/phyllite protolith (~540-795 m)

The top section of the Turbidite, the groundmass consists of a fine-grained (μm -scale) schist containing chlorite, sericite, quartz and at lower depths, also plagioclase and K-Feldspar. Accessory apatite and rutile are common throughout the matrix. The grain size ranges from 200-500 μm in the upper turbidite sequences and 10-50 μm in the finer-grained shales.

This interbedded sandstone and siltstone unit is the main host for the gold mineralisation and exhibits a comparable microscopic banding to that seen in the upper sequences. The unit above has no graded contact as this is cut off by a fault, however sections are seen with the silty laminated 'Zebra' banding, suggesting a conformably contact with the overlying 'Zebra' rock.

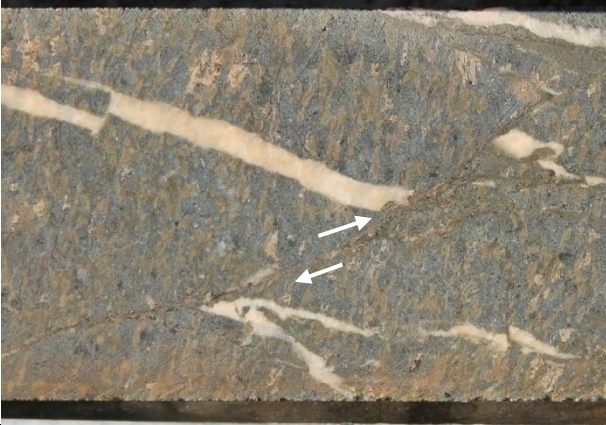
The base unit shows very well-developed Bouma sequences ranging from 10 to 30 m. Contacts between the finer-grained upper section and the coarser-grained base are seen in as a series of flame structures. This indicates a high-energy, wet environment of deposition. Massive graded bedding at the base with angular clasts at 2-5 mm at the base grading to a silt at the top. Sedimentary structures, including bedding and some flow structures are seen at the top of the sequence.

The coarse component of the Turbidites grades out at depths greater than 540m, leaving predominately the siltstone. This then grades into the lower contact of the turbidites with the dolomitic mudstone which is conformable; a clear flame structure is seen at 610 m. This shows that wet sediment was rapidly deposited on top of the mudstone.

ii) Puck Group- Dolomitic Mudstone (base section). (~815-900m)

The unit is a dolomitic mudstone with a contact with the rapidly deposited turbidite repeated over 100 m in the core due to faulting. The mudstone displays a fabric that can range from pods of 2-10mm across. The mudstone sequence contains no gold mineralisation.

Shearing is commonly seen and early quartz and carbonate veins have undergone intense deformation.



← (upper): The unique texture of the Puck sequence, cream rimmed green centre aggregates range between 3-20 mm.

← (lower): Typical green fabric of the Puck sequence. Shearing can be seen with reference to the carbonate veins being displaced



Sandstone (10% biotite) (830m)

Sections of this sequence exhibit relatively little chlorite alteration, if any. These sections instead contain abundant biotite, a mineral which was not found in any other lithology. Textures unique to this lithology include biotite with retrograde chlorite intergrowths replacing the biotite. Other distinct features include skeletal rutile replacement textures, such as those seen in sample DS33. Comparable textures can be seen by ilmenite within the biotite.

← Sandstone with biotite.

Structural observations

The drillcore exposed a series of crush zones along the entire width of the fault, major fault examples can be seen at the intervals 94m 435m and 800m. These vary in size (although they may be dependant of the drill core orientation) from 20 cm up to 10 m. These zones are interpreted to be a series of thrust stacking faults that have undergone very brittle fracturing. Some of these faults have been recrystallised (such as the Zebra rock in Fig 21) indicating they may predate the calcite alteration in the deposit.

Lithologies repeat throughout the sequence due the faulting - examples can be seen in the petrographic image table Figure 17. Samples DS33 and DS40 both contain biotite with retrograde chlorite replacement although they are separated by approximately ~100 m. DS38 and DS31 both have the same coarse sandstone matrix. Samples DS28 and DS 39 both have the same style

deformation of a quartz grain in the phyllite. DS32 and DS36 both demonstrate replacement of the quartz vein with late stage calcite.

Mineralogy and petrography

The **Felsic Tuff** intersection that occurs within the upper part of the Killi Killi Formation (110-115 m, sample DS1) has a hypocrySTALLINE felsic composition (e.g. *Img 11a*). The groundmass is made up of symplectitic quartz and K-feldspar, chlorite, apatite and sericite. The latter is an alteration product of K-feldspar and/or volcanic glass.

The **Ignimbrite** (236-251 m, sample DS6) has an intermediate composition, containing 1-2 mm-sized quartz and feldspar phenocrysts (at a ratio of 3:1) and hornblende. These are supported in a fine-grained groundmass that displays some laminated flow structures. The groundmass consists of a similar composition to the felsic tuff above, including symplectitic quartz and K-feldspar, sericitised prismatic K-spar and glass pods along with extensive chlorite. Grain boundaries are very irregular and chiselled, concordant with a volcanic unit. Euhedral orthoclase has undergone sericitic alteration (*Figure 15:f*) along with the K-spar in the symplectite. Grains of monazite found in the volcanic lithology show deformation stretching (*Figure 15:d*).

The **Quartz-diorite intrusive** is a holocrystalline, massive and equigranular relatively homogenous rock with a small proportion of porphyblasts (*Figure 6:d*). Grain size is fine- to medium-grained (0.1-0.8 mm), indicating intrusion at a relatively shallow depth. The rock is very silica-rich (~70 wt%). The groundmass is relatively euhedral with some 1-2 mm-sized porphyblasts of quartz and plagioclase (samples DS6 & DS7). The lower section of this unit becomes more plagioclase-rich, eventually grading to a granodiorite towards the base (section DS08). Sample DS08 has an increased grain size and a groundmass of plagioclase with overprinting chlorite and sericite alteration (*Figure 11:f*).

The **Grey Arkosic Quartzite** (*Figures 11d-e*) has a medium-grained, recrystallised quartz-feldspar assemblage in a ratio of 70:30. Alteration makes up ~20% of the assemblage, in the form

of sericite, and two stages of chlorite. Groundmass sized clinocllore and porphroblasts of chamosite 0.7-1.2 mm in size. The base of the unit (sample DS08) grades into a more felspathic rich composition with a quartz/feldspar ratio of 60:40. Feldspars have undergone partial sericitization and incorporate some chlorite (Figure 11f).

The **Unaltered turbidite** grades up from a 1-3 mm-sized greywacke to fine siltstone sections (see Figure plate 6). The top of the turbidite unit is a siltstone (Figure 6e). The base of the turbidite unit hosts a very coarse-grained rock containing quartz, feldspar (albite and microcline), muscovite (see Figure 6:c,f) and rutile (6:g). Contacts between the coarse-grained sandstone base and the fine-grained phyllite on top can be seen (Figure 1:e). Detrital quartz has undergone previous recrystallization (Figure 10:c). The unit has undergone greenschist facies alteration, although this is not to the same extent as the base units that have much more pervasive alteration, possibly due to the high silica content. In addition to the primary rock constituents, zeolites were found in sample DS27 using the EMPA data (appendix, 1). The zeolite composition was not identified to a specific mineral.

The **'Zebra rock'** is a well-bedded unit, consisting of clearly-defined bed boundaries, 20-40 mm in size, consisting of black and white, hence the term 'Zebra rock'. The beds consist of very fine-grained dark layers (~5 µm) that are rich fine-grained dark layers of chlorite + muscovite + biotite + quartz ± apatite (euhedral) at 2-5µm (petrographic 8b & SEM 12b). The light-coloured beds comprise of muscovite + quartz + plagioclase ± chlorite ± apatite groundmass with a slightly larger grains size of 15-25 µm. The dominant albite-quartz assemblage gives a distinctive white colour.

The **Boudin Chert** hosts a series of 2-5 cm-size diagenic quartz boudins (see core image). The groundmass is of a similar assemblage to that of the 'Zebra rock' (chlorite + muscovite + detrital quartz + albite ± rutile). There is a high degree of iron and sulphide enrichment, this can be seen in the extensive pyrite alteration (up to 20% of some samples DS17 & 18) e.g. 12g and in the hematite veins seen in images 12d a, f and g. Image 12f shows a hematite vein that had been altered to incorporate Mg. The original hematite is preserved next to the quartz, while an Mg-bearing hematite

or spinel (darker on the BSE image) is in close contact with chlorite. Ilmenite has undergone a retrograde reaction to rutile (image 12c). Image 12e demonstrates the microcrystalline groundmass for the Boudin Chert which is representative of much of the Oberon deposit. Dolomite that incorporates Fe into the matrix can be seen in image 10c.

The '**Puck Group**' is the name given to the base sequence that exhibits extensive greenschist alteration, it comprises of a base of dolomitic mudstone which grades up into a sandstone, then into a well-developed turbiditic sequence. To reflect differences of compositional variation in grain size, mineral assemblage and alteration the top and bottom sections of the Bouma sequence.

The Puck Group - gold-hosting phyllite makes up the top section of the Turbidite units. This was a well-bedded siltstone that had been partially altered to a muscovite-calcite-quartz-chlorite groundmass. The rock has undergone extensive greenschist alteration along with deformation that caused larger detrital grains in the rock have undergone a grain size, as can be seen in Fig 9b. It hosts the gold mineralisation, which is more obviously expressed as large (2-4 mm-sized) arsenopyrite crystals associated with gold mineralisation (Meria 2011) Image 14c. The arsenopyrite is commonly, but not exclusively seen in quartz veins, other sulphides include pyrrhotite, pyrite and chalcopyrite (see 14b). The rock itself is made up of a fine-grained assemblage of quartz, muscovite, feldspar and chlorite \pm rutile. Foliation in the rock is defined by the chlorite- muscovite assemblage which can be seen in Fig 9c

At the base of the Bouma sequence there is a **coarse-grained greywacke** (see 7b) that grades up to a **sandstone**. This unit contains detrital quartz, muscovite and microcline, along with reworked quartz grains. Grain size ranges from coarse clasts (1-3 mm in size) to the much finer-grained matrix minerals (often micron scale). Grain morphology ranges from sub-angular to rounded. The **matrix** of this unit consists of fine-grained quartz and feldspar with minor chlorite.

The Puck Group - dolomite is calcareous mudstone which has undergone metamorphism to dolomite along with pervasive chlorite/sericite alteration. Dolomite was seen as a primary bedding

feature that often defined the fabric of the Puck unit. This was particularly evident in the lowest sections of the unit that contained blotches in its structures that are 2-10 mm in size (see dolomite photos). These are possibly a primary bedding feature onto which various stages of hydrothermal alteration are superimposed. The primary sedimentary feature is known as a fenestral cavity a feature of inter-tidal mudstones and limestones. These nodules are often filled with calcite, which can be seen in the samples to be altered to dolomite-chlorite.

The mineral assemblage is chlorite-muscovite-quartz-dolomite-plagioclase feldspar \pm albite \pm K-feldspar \pm rutile \pm ilmenite (Figure 10b). Sulphides include pyrite, pyrrhotite, arsenopyrite \pm chalcopyrite \pm cobaltite \pm gersdorffite (Figure 14a). Other trace minerals include galena, cassiterite, xenotime, sphalerite, monazite and zircon. Albite porphyroblasts (1-3 mm in size) exist in sample DS46 (893.8m) it exhibits a poikiloblastic texture that then grades into an anti-perthite (K-Spar with chlorite and quartz inclusions) (see Figure 8g).

Dominated by Fe- rich and sulphide alteration along with Na-rich and C rich-graphitic beds, the **boudin chert** may have been deposited in a euxinic environment, or one that is relatively stagnant and lacks rapid water circulation. This results in the depletion of oxygen resulting in a generally anoxic environment. H₂S is generally present as a result of anaerobic respiration: the abundant pyrite in this unit is thus potentially biogenic rather than hydrothermal. Total organic carbon (TOC) is also elevated and as a result can form graphitic beds, as seen in this deposit (See core image 435m). The unit is also enriched in key trace elements such as Mo, Cu and U that are also commonly associated with organic-rich black shales.

The less extensively altered intersections in the lower Puck sequence and the sedimentary puck contain **biotite**, making them compositionally distinct from the rest of the unit, e.g. samples DS33 (phillyite) and DS40 (Ca-puck). The biotite has partially undergone a retrograde reaction to chlorite giving a distinct green and brown striped grain (petrographic 7c and SEM 12g). Sample DS33 12e shows a interlayer biotite, muscovite and chlorite. SEM image shows the three phyllosilicates in the

deposits all interlayer, with biotite, chlorite and muscovite all interlayer within the same grain. The unit also hosts 'skeletal' rutile textures, such as those seen in image 12f.

Numerous examples of **late-stage calcite veining** are seen in the samples. Image 4e shows a sheared quartz vein that has been reconnected due to the passage of late stage calcic alteration using pre-defined fluid pathways. Figure 21b shows brecciation of the phyllite unit and subsequent recementation by a later stage calcite event. This can also be seen on a larger scale in core Fig 31a where the 'Zebra' rock has undergone brittle deformation and has since been re-cemented by a late stage calcite. Recrystallization of calcite in metamorphic dolomite can be seen in Figure 4f.

The quartz vein in Figure 32 has undergone ductile deformation, this can also be seen on the microscale in Figure 9b which shows a quartz grain being incorporated into the fine-grained (<10 µm) groundmass. Rutile can also be seen to be incorporated into the rock matrix in Figures 10d and f. Pyrite in the boudin chert (Figure 9d) and quartz in the phyllite in Figure 9b are also evidence of the complex deformation history of the deposit on a microscopic scale. Quartz veins (eg. Figure 22) that have undergone multiple shearing and deformation events also demonstrate this on a larger scale.

The entire sequence has a pervasive greenschist chlorite and muscovite intergrowth assemblage (see image 13e)

Whole Rock Data

GOLD-HOSTING LITHOLOGIES

Gold is hosted in several lithologies in the Oberon sequence (Figure 16). Primarily the Fe + Mg enriched Bouma Chert and Fe enriched lower Turbidite unit. The gold mineralisation is commonly, but not exclusively hosted in a network of quartz-calcite veins associated with sulphide alteration

expressed as arsenopyrite (see Figure 14c). Visible gold is expressed in the host lithologies in quartz stockwork veins as a result of remobilisation from arsenopyrite (Meria 2011).

GEOCHEMICAL ANALYSIS OF LITHOLOGIES

(Lambeck *et al.* 2010) have shown that plotting Zr against various immobile and mobile elements for whole rock data can be useful in discriminating lithologies. Zirconium is suitable due to its stability with respect to hydrothermal alteration.

Zirconium concentrations from the whole rock dataset for drillhole TID0065 are plotted against (supposedly) immobile Ti, Al as well as elements generally considered more susceptible to movement during hydrothermal alteration such as V, Mg, Fe and Ca (Figure 17). These were then attributed to a group based on core logging observations and plotted on a log scale. The results show distinct groupings that correspond to different lithologies. Aluminium and Ti in particular give good indicators of the protolith of a particular rock and confirm that the gold-hosting turbidite plots in a similar part of the plot to the unaltered turbidite in the upper section of the hole.

In the Zr-Mg plot (Figure 17c) these lithologies are better separated based upon the alteration which possibly depleted the Mg. The relative Fe enrichment in the gold-hosting sequence compared to the unaltered turbidite is clearly seen in Figure 17d.

Figure 17e demonstrates Na enrichment in only some sections of the Au-hosting sequence. Notably, the highest Au grades coincide with the strongest Na enrichment. The gold-hosting lithologies are also enriched in K (Figure 17f). In contrast, the Ca Puck unit shows relative depletion in K (Figure 17h) and enrichment in Ca, V, Mg and Cr. These data point to the protolith of the gold-hosting lithologies, with enrichment in K and Na and Mg depletion attributable to primary rock composition or hydrothermal alteration.

The DS33 biotite-bearing mineralisation-hosting lithology plots in a similar area of the diagram as the turbidite, possibly indicating a shared source of detrital components. DS40 (the other biotite-

bearing sample) plots consistently together with the Ca Puck sequence, also indicating a possible shared protolith of a Ca-rich rock such as limestone, but a different intensity of alteration.

ELEMENT DISTRIBUTION & PROBABILITY PLOTS

Figure 19 shows a number of interesting features:

- a) Potassium is slightly enriched in the gold-hosting sequences; the highest Au grades correspond to 1.3-2.5 wt% K_2O . Potassium is depleted in the Ca 'Puck' sequence and K_2O is only 0.5 wt% in the biotite-bearing unit. The sandstone is similarly K_2O -poor. It is reasonable to assume that these are primary inherited features whereas the K-enrichment associated with alteration related to hydrothermal alteration.
- b) Sodium enrichment is also displayed by the gold mineralised lithologies; a notable increase in Au grade increase can be seen with those samples with highest wt% Na_2O .
- c) Calcium enrichment is noted in the lower puck unit, along with the two biotite-bearing units. This is presumably a primary compositional feature. Part of the sedimentary Puck unit plots consistently together with the sandstone. Some sections of the sequence do, however, show higher values (late-stage veining). Gold grades do not show any particular relationship with Ca.
- d) The Boudin Chert sequence has the highest levels of iron enrichment (e.g. sample DS17, 453 m in which hematite veins are associated with pyrite mineralisation). Significant gold grades in the Boudin Chert sequence correlate with >5 wt% Fe. The Madigan bed sandstone contains very little Fe and hosts no Au mineralisation.
- e) Elevated Mg levels are seen in the Ca Puck sequence, along with the boudin sequence, consistent with the Probe data indicating increased levels of clinochlore (Mg-rich) in this lithology. The Au hosting lithologies show relatively little Mg enrichment.

f) Aluminium is relatively constant and no lithologies are appreciably more aluminous than others.

g) and l) Sulphur values are higher in the Boudin Chert sequence and lower sections of the 'Zebra' sequence, dominantly in the form of pyrite (refer to core farm images). The gold-hosting turbidite sequence contains large euhedral arsenopyrite crystals and can be seen clearly as a spike in As concentrations on the figure.

A ternary K-Na-Ca diagram was plotted from the whole rock data. The carbonaceous Puck unit plots to the bottom left, indicating the very high degree of calcite enrichment. This is either a primary depositional feature or a consequence of late-stage calcic alteration. The Au-hosting lithologies plot towards to the Na-apex on the ternary diagram with the unaltered turbidites having very little Na. The unaltered sandstone has little Ca alteration and equal degrees of K and Na enrichment.

A Fe-Mg-S ternary plot (Figure 21) allows differentiation of the types of alteration across the lithologies. The Au-hosting unit indicates Fe enrichment and some S enrichment. The Ca rich puck shows negligible S. In Figure 22 Fe and S were also plotted in a scatter plot, showing a positive correlation between them in both the 'Zebra' rock and Boudin Chert. This demonstrates the primary pyrite composition in the rock, and possibly a primary enrichment.

Potassium and Na are plotted against each other to determine the albitisation of the assemblage, it demonstrates the Fe rich sandstone turbidite sequence (red) and 'Ca-Puck' have a higher degree of sodic alteration than the less altered sandstone (green). Immobile Al was plotted against mobile Ca to show the possible movement of mobile late-stage Ca^{2+} ions in the sequence. Again the lower 'Puck' sequence had elevated levels of Ca enrichment.

Mineral chemical data

Electron microprobe data was obtained for chlorite, feldspar, apatite, biotite and muscovite to determine the compositional variations between various lithologies.

FELDSPAR

Feldspar is found in both the detrital units and the altered lithologies. Alkali feldspar compositions (Table 2) vary from the Na-rich end-member (albite) to the K-end-member orthoclase (see Ab-An-Kfs diagram). Some intermediate compositions exist between K and Na, suggesting fine-grained mixtures of plagioclase and K-feldspar. Almost all analysed feldspars lie, however, within 10% of the end-member compositions. Almost no Ca was detected in the plagioclase feldspar indicating sodic alteration of an original more calcic plagioclase; intermediate compositions (oligoclase, sanidine and anorthoclase) were measured only in detrital plagioclase from the sedimentary units.

CHLORITE

Chlorite is found in all lithologies in drillhole TID0065. Analysed compositions are given in Table 3 and plotted on the Al-Mg-Fe ternary diagram as Figure 17. Chamosite (Fe-rich end-member) is the most common chlorite mineral in the sequence, with some reduced lithologies exhibiting extreme degree of Fe enrichment. Clinocllore is, however, the dominant chlorite mineral in the mineralised sequences. Very little Mn is present in the chlorites hence the Mn-rich end-member (pennantite) can be effectively ignored and Al used as the third element in the plot.

Chlorites are separated into groups A, B, and C based upon their end-member compositions and host lithology. Type A is a clinocllore found in the Boudin Chert sequence. This is consistent with the probability plot (Figure 19) showing elevated Mg levels in this unit. Type B is an intermediate composition chlorite contained in the unaltered turbidite and biotite hosting and Ca-Puck units. The

Boudin Chert sample DS17 contains both type A and B, indicating different stages of chlorite development. The turbidite hosts type B and C, due to alteration of some of these units into the Fe-rich chamosite.

APATITE

Apatite occurs throughout the entire sequence, and was analysed in 7 thin sections. Single compositions for each mineral in are shown in the table. Apatite has a consistent composition (Table 4), with the fluorapatite end-member dominant in all samples; no hydroxyapatite end-member was detected and the chlorapatite end-member component was minimal (max. 4% in sample DS45).

BIOTITE

Biotite is found in samples DS40 and DS33 (833.1 and 750.1 m, respectively; see Table 5, and 18core photo, SEM and petro Figures). Compositionally, the biotite ranges from approx. 50:50 phlogopite:annite (DS33) to much closer to the Mg-rich end-member phlogopite (DS40). DS40 contained biotite only in association with chlorite, resulting in lamellar intergrowths (see Figure 2c). Biotite is fluorine-rich. The highest F was detected in the biotite-rich lithology (1.50 wt%), the lowest in DS45, the 'Puck' carbonate (0.72 wt%).

SERICITE (WHITE MICA):

The white mica had a limited range of composition, with modest F content and a phengite component of 10-30% (Table 6). The samples from the Ca-rich Puck sequence had rather less F possibly do to partitioning into the co-existing biotite (Samples DS45 and -46). It is possible that the some of the higher phengite components may just be representative of the sub-micron interlayering with chlorite, giving an elevated Fe+Mg enrichment, not representative of the pure

white mica. The gold-hosting turbidite sample (DS35) had one of the highest phengite components. Interestingly, sericite from the dolerite had the highest F content, even if absolute F concentrations in the white micas are low in comparison with coexisting biotite (Table 7). The Fe/(Fe+Mg) ratio is constant in all analysed muscovites, in marked contrast to the coexisting chlorite.

Chlorite geothermometry

Various authors have suggested that chlorite compositions provide an estimate of the peak metamorphic temperature. Average temperatures were calculated for all 15 samples. Temperatures are derived from the proportion of silicon and octahedral Al in chlorite. Three different calibrations were applied. Of these, only the calibrations suggested by Jowett (1991) and Cathelineau (1988) gave reliable temperature estimates. The calibration of Kratinoidis and MacLean (1987) gave results that are unreasonably low.

Using the Jowett (1991) calibration, a peak temperature of 355 °C was calculated for sample DS46, the deepest sample in the Ca-rich Puck sequence (893.8 m). Sample DS33 (sedimentary Puck sequence, 750.1 m) gave a similar temperature estimate (345 °C). Other biotite-bearing samples: DS40 (Ca-rich Puck lithology, 833m); DS19 (Boudin Chert, 467m); and DS10 (unaltered upper turbidite sequence, Madigan Beds, 345.9 m) gave temperature estimates of 319 °C, 322 °C and 367 °C, respectively. The similarity of the temperature estimates from different lithologies gives confidence to the interpretation of these temperatures as realistic. The Jowett (1991) calibration is, however, not recommended for chlorite in which $Fe/(Fe+Mg+Mn) > 0.5$, so the Cathelineau (1988) calibration is preferred for calculation of peak temperature of the samples DS10, -18, -25, -27, -30, -31, -35, -38, -43 and -45.

The mean temperature estimate from all analysed chlorite is 341 ± 49 °C (Table 8). This places the deposit in the greenschist facies, consistent with mineral assemblages observed. The temperature estimate for the Puck sequence is 360 ± 20 °C and for Au-zone 344 ± 48 °C. The larger

S.D. for the gold mineralised zone reflects the larger variation in chlorite composition in these lithologies.

Table 8 shows the peak temperature for each sample, plotted against the stoichiometric value of Fe in the sample. This gave a marked negative correlation between Fe content in the chlorite and higher estimated temperature.

DISCUSSION

Host Unit Protolith

The entire sequence represents a sedimentary package with marine transgression and then regression associated with felsic volcanism and shallow intermediate intrusives. The schematic section (Figure 29) shows a series of fining-upwards turbidite sequences that exhibit a classical Bouma sequence. Deltaic shallow water successions of interbedded mudstones and coarse sandstones are seen at the top of the sequence. Deep water successions are expressed in the 'Zebra' rock package, while anoxic deep water has developed into the Boudin Chert. The base carbonaceous 'Puck' sequence represents a sediment-deprived carbonate-rich mudstone that has developed in an intra- or supratidal environment.

The evolving sequences can be considered as expressing changing tidal levels and sediment input. This is evident from the contacts between the lithologies in the core images at 139.4 indicating there had been a rapid change in sediment source and composition.

The turbidite package, an important Proterozoic gold host (Goldfarb *et al.* 2001), represent a rapidly deposited group of rock packages, each from 2 to 30 m in thickness and all fining upwards. The packages generally conform to typical Bouma sequences (Tucker 2001). The base of each

succession is a very coarse-grained sandstone grading up into a siltstone with poorly defined laminar bedding structures. This unit is the main host for gold mineralisation, possibly due to the relative ease of fluid percolation through the porous sequence (see Fig 7:a-b) for a typical fine and coarse Au host lithology). The setting for turbidite deposition is likely to have been off a continental shelf, at a time of high deformation that resulted in increased sediment input (Reading & Richards 1994). The clastic component is young due to the developing granitic intrusions. Zeolites found in some samples (e.g. DS27) prove that active volcanism occurred at the time of deposition. Zeolites are formed by the interaction of aluminosilicate-ash and salt water (Querol *et al.* 2002)

Killi Killi. The top unit in the **Madigan Beds** hosts an interbedded sequence of coarse sandstone, shale and siltstone with expressions of tuff. This possibly originated from below-wave base sedimentation with differing and rapidly evolving sedimentary inputs. The upper Killi Killi may represent a lower depth deltaic environment instead of a turbidite, as Bouma sequences are far less defined as those in the lower sections. One intersection contains a 10 cm micro-hummocky cross-stratification intersection indicating a deposition above storm base and below fair weather base according to (Dott & Bourgeois 1982).

The **Grey Arkose Quartzite**, is a rapidly deposited feldspathic sandstone that has undergone rapid deposition onto the underlying 'Zebra' units, seen in images 350 & 365m. Rip-up clasts demonstrate that the unit had a high energy deposition onto a wet underlying sediment. The unit could mark the base of a turbidite sequence, the top of which is not seen. The unit exhibits tri-grain boundaries (Figure 11d), indicating re-crystallisation of quartz. The unit also demonstrates two stages of chlorite, the darker Fe-rich chamosite prophyroblasts and the finer groundmass of the Mg end-member chlinochlore (Figure 11e).

The 'Zebra' Unit is a siltstone containing a series of very well defined beds separated into a darker very fine-grained (1-10 μm) quartz-chlorite-muscovite-calcite schist and a lighter coloured, slightly coarser grained (20-30 μm) albite-chlorite-muscovite assemblage. Pyritization of the unit is intensified with depth into the transition zone with the underlying Boudin sequence. The 'Zebra'

package is most likely a relatively deep water succession but with seasonal variation in sediment source and flux. In such a model, the darker layers represent the sediment-starved beds whereas the lighter-coloured layers represent periods of increased sediment input. The 'Zebra' package siltstone may represent the high stand system tract the base of the sequence representing the maximum flooding surface.

Dominated by Fe-rich minerals, sodic alteration, graphitic beds (high total organic carbon) and the presence of sulphides, the **Boudin Chert** (see core image at 445m) may represent sedimentation in a euxinic environment, or one that is relatively stagnant and lacks sufficient water circulation (Arthur & Sageman 1994) Fig 23. Oxygen depletion results in an anoxic environment. The strong correlation between S and Fe (Figure 22) demonstrates that Fe and S enrichment are possibly linked due to primary anoxic enrichment.

H₂S is generated as a result of anaerobic respiration and is expressed in the abundant pyrite in this unit, which has a geochemical signature distinct from that in the Au-hosting sequence. The marked enrichment of trace elements such as Mo, Cu and U is also consistent with an anoxic depositional environment. Formation of the boudin chert may have been as a result of changing sea levels giving rise to stagnant, pooled water. Another plausible explanation is an anoxic event, that results in the Earth's oceans being deprived of oxygen, these events have been noted in the mid Proterozoic (Arnold *et al.* 2004; Shen 2001). It may be synchronous with Proterozoic petroleum source rocks such as those seen in the Roper Basin to NE of the state in the Gulf of Capentaria.

The unit also hosts ellipsoidal chert nodules, presumably formed during diagenesis under a relatively shallow sediment load (1-5 m?). The Boudin Chert represents a major transition from the underlying rapidly deposited turbidite sequence to the overlying deepwater low-energy 'Zebra' succession. Petrographic analysis demonstrates a similar detrital component as the overlying Zebra unit, indicating it is possibly a heavily altered basal unit of this sequence.

The felsic to intermediate **volcaniclastic units** seen in image section 6 hosts matrix supported plagioclase and quartz ranging from 2-5 mm in size, these are seen at both the base and the top of the unit (Figure 11a-b). Euhedral plagioclase has been replaced by sericite. Grain boundaries are very sharp and chiselled.

The structure at the base of the '**Puck**' sequence exhibits a strong and textural fabric, possibly a primary sedimentary feature. The blotches seen in the 'Puck' unit are 3-15 mm across, with a high relief and are light green in colour. On initial inspection they appear to be large homogenous mineral overgrowths such as actinolite or epidote but SEM analysis demonstrated that they are in fact a fine-grained aggregate of dolomite and chlorite. The dolomite gives an indication that these may represent a primary bedding feature known as fenestral cavities. Such features are often seen in sediments formed in an intra-supra tidal environment (Tucker 2005, book sedimentary petrology). The cavities are often filled with calcite which has then undergone various degrees of alteration to incorporate minor chlorite, lending the aggregates a green colour.

The Ca-enriched 'Puck' sequence is a dolomitised mudstone enriched with both iron and magnesium. The groundmass is ~10 µm with chlorite reaching up to 100 µm in size and consists of quartz-feldspar-dolomite-chlorite±apatite±muscovite±rutile. Intersecting veins of calcite and/or dolomite (±wollastonite?) and quartz are common. Sedimentary banding is also commonplace ranging from 1-10 mm in size. The unit hosts no gold mineralisation despite its close proximity to the high-grade overlying Fe-enriched turbidites.

Regional stratigraphic comparison

The sequence is hosted within the Tanami Group, subdivided into two main lithological units the lower Dead Bullock beds and the overlying Killi Killi (Blake 1975). An underlying quartzite was identified by Cooper and Ding (1997). Various unconformable units such as the Nanny Goat volcanics overlie the Tanami Group.

The stratigraphy seen in the Oberon deposit has similar features to much of the regional stratigraphy however comparisons made between specific units is difficult due to the strong structural controls on the deposit (Fig 36 & 37). Distinctive marker units are nevertheless a good basis for correlation to other units. Units such as the Boudin Chert, with its distinctive 2-10 cm-sized boudins and heavy pyrite alteration are readily correlated to the Callie Boudin Chert member. Likewise the 'Zebra' unit with its distinctive bedding is similar to that of the Davidson Beds, Blake Beds (refer to Figure 34b).

The Killi Killi turbidite sequence is a thick package of turbidites expressed at the top of the Callie deposit. The sequence also hosts mineralisation in the Coyote deposit. The unit is made up of a coarse-grained lithic base comprising angular igneous-derived quartz, K-feldspar, lithic clasts and muscovite. The matrix is composed of a fine-grained clay-sericite-iron oxide assemblage. These observations correlate well with what is seen in the upper turbidite (at ~200m) at Oberon (see Figure 6). The main difference lies in the composition of the matrix. At Oberon, the assemblage is chl-ser-cal, and may represent a further alteration of the one described in the literature by (Blake 1979, Hendrickx 2000).

The Boudin Chert unit (BC) correlates well with the 'Davidson Beds' and the 'Blake Beds' described by Newmont¹. The BC represents the, the base of the 'Zebra' unit which correlates well with the 'Orac Formation' within the Davidson beds or, alternatively, the 'Callie Boudin Chert' (CBC) of the Blake Beds. This latter unit comprises well-developed chert nodules, inter-bedded in a sulphidic schist. Beds are comprised of feldspar, quartz and graphite. The described lithology appears comparable with what was seen in the Boudin Chert. The presence of Au mineralisation in both units lends further evidence to support this.

The overlying 'Zebra' rock shares some similarities with lithologies in the Davidson Beds, including the 'Maganiferous Chert' with its well-bedded graphitic horizons. Still better correlations can be made with the Upper Blake Beds (UBB), a series of 'rhythmically' banded graded beds, alternating between fine graphitic beds and non-graphitic banded quartz-sericite-chlorite

assemblages. Although no distinct graded bedded was seen in the 'Zebra rock', and the banding within it is a lot more pronounced, this is nevertheless the most probable correlation of the 'Zebra unit'. A logical conclusion is that the 'Zebra rock' represents a regional variation of one of the UBB members, with its well-defined banding being a localised expression of the beds, possibly indicating a deeper water package. A consequence of this would be that the Boudin Chert is, in fact, an equivalent of the CBC, since this underlies the UBB (Fig 36a).

The underlying turbidite and 'Puck' sequence prove far more difficult to correlate. Significant well-defined turbidite sequences are not noted from the lower units. They could thus represent a faulted section of the Killi Killi turbidite package, or, alternatively, a completely new unit unrecognised elsewhere in the district. This may also be the case with the underlying dolomitic mudstone, which is also not represented in any Callie stratigraphy. Conspicuously, dolomite is not mentioned in any of the literature relating to the Tanami Group, only minor carbonaceous intervals having been noted seen in the Tanami region. The only regional expression of dolomite is described by (Blake 1979) as the Birrindudu Group (Figure 4). This group has a low proportion of dolomite to sediment along with stromatolites. The depositional age is estimated at <1800 Ma, but the unit is poorly constrained.

The ignimbrite identified in the sequence is also problematic, in that a similar lithology is not recorded in the Tanami sequence. The only other known ignimbrite outcrops, ~100 km to the north, is the poorly-mapped Nanny Goat Volcanics (see map, Figure 3). "Feldspar-quartz ignimbrite" (Pn1) and "Feldspar-ignimbrite" (Pn2) are mentioned by Hendrickx (2000). Pn1 is described by Blake (1979) as an ignimbrite with a moderate phenocryst content, a quartz:feldspar ratio of 3-5:1 and replacement of some feldspar phenocrysts by sericite. Pn2 has a much lower quartz:feldspar ratio, with most plagioclase phenocrysts sericitised. The base of the Nanny Goat volcanics is a turbidite unit that has been refined as the top section of the Killi Killi Formation (Hendrickx 2000).

Structural orientation of the deposit

Although only a single drill core was studied, orientations of bedding and folding in the sequence can nevertheless be assumed. Several indicators suggest that it had in fact that there may have been a partial inversion of some of them. Evidence for this is seen in both sedimentary and volcanic units.

Volcanic: The second volcanic unit 235 – 278m had an inverted grading, the coarse quartz material was on the top while the base was finer grained and more oxidised (red in colour). The white laminated volcanic sections at the top may represent a surge flow deposit, a common feature at the base of an ignimbrite. This could also represent a cooked contact, or even tuff deposit at the top of the ignimbrite.

Sedimentary: Various sedimentary indicators in the deposit suggested that there was a distinct way up in relation to the sedimentary structures seen in the drill core. Structures included, cross bedding, hummocky cross stratification. Rip-up clasts of the dirty zebra into the turbidite sequence above was another very clear way up indicator. This was also seen in the flame structures seen in the turbidite sequence. A partial inversion of the sequence may be as a result of the drill hole intersecting a recumbent fold or the top of an anticlinal structure etc.

Faulting: There were many intersections based in the deposit that had very brittle contacts due to a series of brittle fault zones that existed throughout the sequence. The crush zones ranged from 10 cm up to 10 m in size, although this could also have been dependant on the orientation of the fault in comparison to the drill core angle.

Lithologies: Another key feature about the deposit was the fact that distinctive features such as rutile textures, deformation of quartz, detrital components such as rutile and even Au grades are repeated (see Figures in section 4.2). This could either be due to the fact that there were

predominately recombinant folds present or possibly the fact that the sequence seemed to be repeating itself due to the drill core crosscutting a very brittle thrust stacking regime

Evidence to suggest that these crush zones are in-fact faulted sequences comes from the repetition of units seen in the sequence. The distinctive dolomitic Puck 'blotches' are seen to be faulted up sequence into the overlying stratigraphy at the intervals 855 to 845 m and 840 to 815 m. Other examples of repeated units include a unique 20 cm intersection of hummocky cross stratification in the Killi Killi Formation which repeated twice in the same core sequence at the intervals 105 and 138 m and the contact between the zebra rock and the overlying turbidite was also repeated several times between 350 and 425m.

Gold Mineralisation

Gold mineralisation in the shallow deposits such as Callie has been disputed with various models put forward for the mechanisms that trigger precipitation of gold from the ore fluids. One model (Huston *et al.* 2007) suggests a TOC-rich rock that undergoes effervescence with release of CO₂.



Noting the association of gold with Fe-rich lithologies, Lambeck *et al.* (2011) suggests a different model, in which the Fe in the rock acts as an redox agent promoting precipitation of gold.



The first mechanism (decarbonisation) requires the presence of high TOC such as that found in the 'graphite rich beds'. No such strong graphite enrichment is observed in the phyllite and sandstone within the main mineralised zone of the deposit. Graphite beds are found exclusively in the Boudin Chert unit, and intersections above the mineralised zone in the Zebra unit.

Other instances of carbon are also seen in small amounts of carbonates in (e.g. Fig 10c). According to (Williams 2007) the graphitic beds in the sedimentary units were the source of the precipitated gold from the mineralising fluids. The micron sized chl-mus-cal-qtz 'dark' graphitic beds that as seen in the 'Zebra' unit demonstrate no mineralisation.

The highest gold grades are observed in the Fe enriched turbidites which lies above the carbonaceous rich 'Puck' sequence (see figure 19). The Ca-enriched 'Puck' sequence itself does not contain any mineralisation despite is close proximity to the high grade overlying Fe enriched turbidites. High gold grades are not seen above the Boudin Chert, this is possibly due to the impermeability of the overlying 'zebra' formation with is fine-grained (15-30 μm) matrix of albite-quartz.

Gold shows a correlation with Fe only in the Boudin Chert (see Fig 35). Correlation between the Fe-rich lithologies and Au grades are otherwise weak, possibly due to remobilisation of gold during late-stage deformation, or secondary Fe-enrichment. Chlorites associated with Au mineralisation always have $\text{Fe}/\text{Fe}+\text{Mg} < 0.7$ indicating that chamosite is not associated with Au mineralisation.

Gold mineralisation is associated with an enrichment of Na and depletion of K, probably as a result of sodic metasomatism resulting in the albitisation of most feldspar in the deposit. Potassium was mobilised during this alteration. Such a scenario is consistent with the whole rock data and zirconium plots which showed that the Au-mineralised zone is enriched with Na. Sodic alteration resulted in the stability of albite in the 'Puck' units. Microprobe analysis of feldspars shows >90% of the end-members are albite in the Au-hosting turbidite, demonstrating the strong correlation between Au grades and Na enrichment. The turbidite gold-hosting lithology also shows a depletion of Mg and enrichment of Fe.

Gold was possibly precipitated along a Redox front in the Fe-rich siltstones/turbidites containing chamosite (Fe-rich chlorite). Gold has possibly been deposited by a different method in the Boudin Chert – e.g. via decarbonisation of the highly graphitic beds. Fluids penetration was not consistent

throughout the lithologies with some unaltered lithologies containing biotite possibly being ahead of the Redox front.

The mineralised zone was then faulted after gold deposition, giving localised mineralised gold lode zones averaging at 10g/t. Faulting causes the entire sequence to be repeated multiple times along the length of the drillcore. This is evident from the Au-hosting sedimentary part of the 'Puck' unit to which Au is largely bound. This unit is possibly repeated many times due to thrust faults. Thrust stacking then re-distributed the primarily gold mineralisation in the Fe-rich turbidites and provides a secondary control on Au distribution, resulting in a 'patchy' distribution of gold grades.

Sequence evolution (protolith – alteration – metamorphism)

SEDIMENTATION

Deposition of units can be envisaged as follows:

1. Initial deposition of the base Puck sequence during a period of low sediment input in an intra to supra-tidal environment.
2. Marine transgression and along with increased clastic input led to the development of turbidite sequence.
3. Deep water succession of interbedded claystone deposited, the base of which developed into a eutectic environment deprived of O₂ and enrich with sulphur, iron, trace elements and a high TOC.
4. Sea level regression and sediment decrease lead to a deep water 'zebra' succession deposited contains more clay input. Further regression lead along with more terrestrial input of sediments formed interbedded siltstone and coarse sandstones in a possible deltaic environment (demonstrated by hummocky stratification), in a time of active volcanism depositing intervals of Tuff.
5. Ignimbrite deposited.

ALTERATION

Enrichment of Fe was seen in the gold hosting lithologies, Boudin Chert and turbidites. This may represent a primary compositional feature as opposed to an effect of alteration event. Iron enrichment could have been derived from when the unit was deposited on the seafloor. This is especially true for the Boudin Chert unit, as this was deposited in a eutectic environment, common place with banded iron formations in a reduced setting (Arnold *et al.* 2004).

The Puck group is very sodic enriched, expressed in the dominant albite-quartz-chl-ser assemblage (see Figure 10b) and may represent a product of sodic alteration. The biotite hosting sequences in the Puck unit may represent an assemblage that existed prior to sodic metasomatism. The feldspar ternary diagram demonstrates that this unit only hosts orthoclase. The albitisation of the potassic rich assemblages, such as alkali-feldspars and biotite into albite is (see zirconium plots) demonstrates the sodic alteration phase. This Na enrichment correlates well with high gold grades seen in the turbidite facies, indicating a possible co-enrichment.

Hydrothermal fluids resulted in a Mg enrichment the carbonaceous Puck and Boudin Chert. Evidence for late stage Mg-enrichment can be seen from various sources. Chlorite exhibits compositional variation from the Fe and Mg end-members as seen in Figure 26. Two generations of chlorite can be seen in the quartzite (Figure 11e), the darker iron enriched porphyroblasts, and a finer grained matrix of lighter clinocllore (Mg-enriched). The Fe-enriched chlorite represents first stage, the groundmass chlorite Mg chlorite is the later stage event. Further evidence for late stage Mg fluids can also be seen in SEM Figure 13f, a hematite vein has been compositionally altered to incorporate magnesium. The lighter original composition can be seen persevered next to the quartz while the darker Mg alteration can be seen next to the chlorites.

Mineralising fluids were oxidising, volatile-rich and possibly Mg-rich. At the same time as sulphide and gold deposition, the fluids altered the chlorite to T₂ Chlinochlore (see Ternary Diagram, Fig 26) along with ilmenite to rutile (see Figure 13c) and possibly biotite into retrograde chlorite, although this may be simply a retrograde metamorphic feature. The sodic alteration that resulted in albitisation of feldspars may have occurred synchronously with mineralisation, but more likely, was the product of an earlier alteration event ('seafloor alteration') that pre-dated gold mineralisation.

A distinctive feature of the biotite was its high fluorine content Biotite is fluorine-rich. The highest F was detected in the biotite-rich lithology (1.50 wt%), the lowest in DS45, the 'Puck' carbonate (0.72 wt%) which was interlayer with chlorite (see Figure 8c). The same high content was also seen in the apatites (~5 wt%). This suggests the fluid associated the mineralisation of biotite and apatite had a high fluorine composition. Contrary to this, the co-existing white micas had a very low fluorine content (<0.20 wt%). Table 6 also demonstrates that in comparison to the chlorites the white micas had little fluctuation in the Fe/Fe+Mg, indicating that the mica may not have been subjected to the same selective hydrothermal alteration. These factors lead to indications sericitic alteration post-dating the main mineralising hydrothermal event

Calcium takes multiple stages in the deposit, primary enrichment occurs alongside sedimentation such as that seen in the dolomitic Puck mudstone. Secondary enrichment can be seen in the numerous fine calcite veins throughout the stratigraphy. These veins are pervasive throughout the deposit and there are many instances in which they can be seen exploiting a pre-existing fluid pathway such as a quartz vein (e.g. Fig 9e & g). Metamorphism of calcite into dolomite can be seen in 9f. Very late stage calcite development can be seen on a larger scale in which it is re-cemented a faulted lithology (Figure 31 a & b), representing a very late stage event, post-dating the brittle thrust faults seen throughout the sequence. These various stages of development may indicate that it was not predominantly associated with gold mineralisation, but instead developing contemporaneously.

Calcium enrichment is seen in the unaltered biotite sequence, this may show that in fact Ca was mobilised from previous lithologies, leaving only an albite, K-spar assemblage.

METAMORPHISM

The entire sequence has been metamorphosed at greenschist facies during the Tanami Event, producing T₁ (chamosite) chlorite from pre-existing Fe₂O₃ enrichment in reduced beds. The assemblage also would have included biotite, this then underwent retrograde alteration to chlorite; remnants of previous assemblage are seen in samples DS33 -40. Biotite was also seen in unaltered sections, partially altered to chlorite (Figure 7c-d) but a pervasive chlorite-sericite assemblage is seen though out the entire sequence.

The peak metamorphic temperature based upon chlorite thermometry was calculated to be 366 °C (± 21 °C), i.e. upper greenschist facies. This compares closely with the data of Meria (2011) who obtained a temperature of ~380 °C in a similar lithology from arsenopyrite geothermometry using the calibration of Kretschmar & Scott (1976).

Regional expressions of amphibolite facies less than 1 km from the discovery hole have been noted, with an assemblage consisting of garnet, sillimanite and tourmaline (Figure 30 a & b). The only other expressions of amphibolite facies metamorphism seen in the region are to the east of The Granites, roughly 30 km SE of the deposit (Hendrix 2000a).

Exploration Potential

Future exploration for similar deposits can be based on the applied gold mineralisation model described in this report. Key indicators of mineralisation are:

1. Fe-enriched turbidite host sequence
2. Fe- and trace element-enriched graphitic beds

3. Sodic alteration assemblages such as albite-muscovite
4. Fluorine-rich biotite and apatite

Notes added in final revision

The use of a single hole TID0065 made structural interpretations difficult as there was little basis for correlation with the surrounding lithologies. The invocation of thrust stacking made the most logical sense at the time as there was no other good explanation for the repeated unit contacts above each brittle faulted zone in the drillcore. Without looking at surrounding lithologies and their orientations only the simplest of interpretations can be made and 3D structures such as antiforms and synforms are hard to determine. Repeating of lithologies based upon their repetition of sedimentary sources also makes logical sense as this was seen in examples such as the 'Zebra' rock which was seen at various intersections throughout the lithology due to a similar depositional environment. One early explanation for is that the repetition could have been due to the hole intersecting the limbs of a synform or similar structure.

The chlorite observed was described as resulting from an alteration event. While the chlorite itself may be derived from a regional low-grade metamorphic event there was evidence of different chlorite-bearing assemblages and compositionally-distinct chlorite generations. While it is expected that the $Fe/(Fe+Mg)$ ratio in chlorite would vary between lithologies (reflecting bulk rock composition), variation in the ratio was also seen in the same samples. This is a good indication that chlorite within those samples was formed during multiple events. A good example can be seen in Fig. 26 where a Mg-rich (clinochlore) chlorite co-exists with an intermediate chlorite species. A petrographic image of sample DS10 also demonstrates visually the different stages of chlorite, one being a darker, early stage Fe-rich chlorite (chamosite), while there is a fine-grained matrix

composed of Mg-rich chlorite (clinochlore). Which is as a result of hydrothermal alteration and which is a 'metamorphic' overprint is unclear.

The strong Na-enrichment seen in the 'Puck' sequence can be either a reflection of primary rock composition, or a post-depositional (and possibly pre-metamorphic) hydrothermal event. The lenses of so called 'unaltered' biotite-bearing lithologies in the 'Puck' sequence may represent less sodic enrichment and a more K-rich primary rock composition or alteration style.

Sodic enrichment is postulated to have been derived from a post depositional event, such as sodic metasomatism ('seafloor alteration'). This would have been accompanied by some removal of Ca from plagioclase resulting in albite as the stable plagioclase feldspar. The original protolith is hard to determine due to the similarity between the greenschist facies metamorphic assemblage and that which would result from hydrothermal alteration.

If the elevated Na is, however, a primary lithological feature, then the underlying dolomitic 'Puck' protolith could correspond to a shallow-water limestone with a moderate detrital input (as seen as the quartz, feldspar and rutile in the rock groundmass). An alternative explanation might involve a meta-evaporite in which Na is derived from halite or other Na-bearing minerals within the primary stratigraphy. This would also account for the variation in sea-level and coexistence of meta-evaporite and underlying limestone.

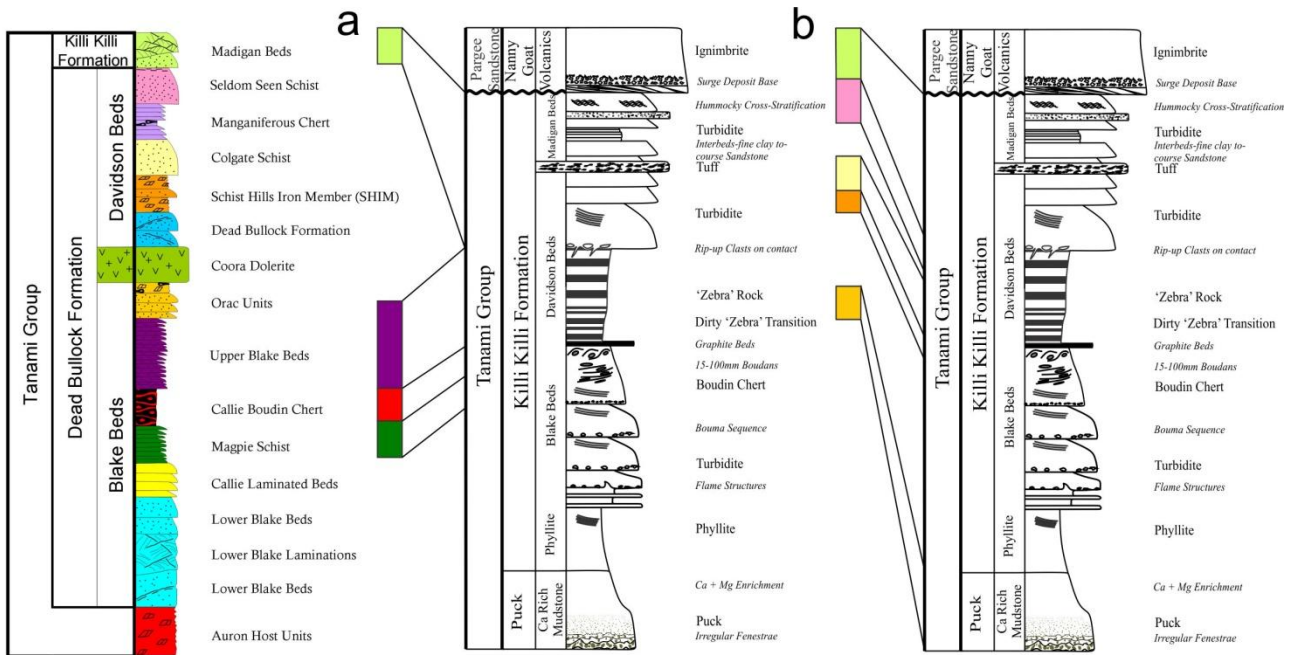


Fig 36a: Interpreted correlation between the Newmont Callie mine stratigraphy and the Oberon stratigraphy (this study). This is based on the marker unit of the distinctive Callie Boudin Chert and the Boudin Chert in Oberon. Connections are made between the Upper Blake Beds and the 'Zebra' package, the distinctive Callie Boudin Chert and the Boudin Chert (Oberon) and the Magpie Schist and lower Boudin Chert (Oberon).

Fig 36b: Correlation between the stratigraphy as interpreted by Newmont (Pascal Hill, pers. comm.) and the interpreted Oberon stratigraphy (this study). The Madigan Beds in the Killi Killi Formation correlated well with the Killi Killi package in the Oberon hole, which extends down to approximately the Orac Units. The tuff intersections are not described in literature as found within the Killi Killi Formation.

The Oberon package correlates with the upper section of the Dead Bullock Formation in the Tanami Group (Fig. 36a). Distinctive lithological units mark a connection between the Callie mine lithology and the Oberon lithologies. Examples of this include the Zebra package, which is defined by a series of well defined bands of very fine grained light and dark sediments with the Upper Blake Beds (Fig 36a), which also exhibits the rhythmic seasonal banding displayed in the 'Zebra' formation. Newmont geochemical data however correlated the upper and lower sections with the Seldom Seen Schist and Colgate Schist units respectively (Fig 36b). The Boudin Chert has acts as a unique marker unit for the Oberon sequence and is seen in the Callie stratigraphy (known as Callie Boudin Chert). The unit hosts distinctive 'Boudins' that mark the top of the mineralised zone in both the Callie and the Oberon stratigraphy. The underlying Magpie Schist correlates to the base of the Boudin Chert in Oberon (Fig 36a). Newmont interpretation however (Fig 36b) suggest as the Schist Hills Iron Member (SHIM) is the corresponding unit based on Geochemical interpretation. Finally the base Ca Puck unit does not distinctively match any of the Callie or regional stratigraphy it does however have a similar geochemical expression as the Orac Units in the Callie mine (Fig 36b)

ACKNOWLEDGEMENTS

Thanks go to Newmont for providing financial and logistical support. Particular thanks go to Pascal Hill for taking time out to explain in great detail what the project entails. Thanks go to all those at Adelaide Microscopy especially to Angus Netting, Benjamin Wade with regards to training and continued support on the use of the SEM, EMPA and petrographic equipment, along with Esther and Ken for their help with coating samples in a rush. Ian Pontifex is thanked for the timely preparation of thin sections and associated samples. I would especially like to thank my primary supervisor, Nigel Cook and co-supervisor Cristiana Ciobanu their continued support throughout the entire project at what seemed like all hours of the day which was vital for its completion.

REFERENCES

- ARNOLD G. L., ANBAR A. D., BARLING J. & LYONS T. W. 2004. Molybdenum isotope evidence for widespread anoxia in mid-proterozoic oceans. *Science* 304, 87-90.
- ARTHUR M. A. & SAGEMAN B. B. 1994. Marine black shales - Depositional mechanisms and environments of ancient-deposits. *Annual Review of Earth and Planetary Sciences* 22, 499-551.
- BAGAS L., ANDERSON J. A. C. & BIERLEIN F. P. 2009. Palaeoproterozoic evolution of the Killi Killi Formation and orogenic gold mineralization in the Granites-Tanami Orogen, Western Australia. *Ore Geology Reviews* 35, 47-67.
- BLAKE D. H. 1979. *Geology of the Granites-Tanami Region, Northern Territory and Western Australia*. Australian Govt. Pub. Service (Canberra).
- COOPER J. A. & DING P. Q. 1997. Zircon ages constrain the timing of deformation events in the the Granites-Tanami region, northwest Australia. *Australian Journal of Earth Sciences* 44, 777-787.
- CRISPE A., VANDENBERG L. & SCRIMGEOUR I. 2007. Geological framework of the Archean and Paleoproterozoic Tanami Region, Northern Territory. *Mineralium Deposita* 42, 3-26.
- CRISPE A. J. C. A. J. 2006. SHRIMP U-Pb analyses of detrital zircon: a window to understanding the Paleoproterozoic development of the Tanami Region, northern Australia. *Mineralium Deposita* 42, 27-50.
- DOTT R. H. & BOURGEOIS J. 1982. Hummock stratification- significance of its variable bedding sequences. *Geological Society of America Bulletin* 93, 663-680.
- GOLDFARB R. J., GROVES D. I. & GARDOLL S. 2001. Orogenic gold and geologic time: a global synthesis. *Ore Geology Reviews* 18, 1-75.
- GROVES D. I., GOLDFARB R. J., GEBRE-MARIAM M., HAGEMANN S. G. & ROBERT F. 1998. Orogenic gold deposits: A proposed classification in the context of their crustal distribution and relationship to other gold deposit types. *Ore Geology Reviews* 13, 7-27.
- HENDRICKX M. 2000. Palaeoproterozoic stratigraphy of the Tanami Region. *Northern Territory Geological Survey* GS 2000-13.
- HUSTON D., VANDENBERG L., WYGRALAK A., MERNAGH T., BAGAS L., CRISPE A., LAMBECK A., CROSS A., FRASER G., WILLIAMS N., WORDEN K., MEIXNER T., GOLEBY B., JONES L.,

- LYONS P. & MAIDMENT D. 2007. Lode–gold mineralization in the Tanami region, northern Australia. *Mineralium Deposita* 42, 175-204.
- LAMBECK A., HUSTON D. & BAROVICH K. 2010. Typecasting prospective Au-bearing sedimentary lithologies using sedimentary geochemistry and Nd isotopes in poorly exposed Proterozoic basins of the Tanami region, Northern Australia. *Mineralium Deposita* 45, 497-515.
- LAMBECK A., MERNAGH T. P. & WYBORN L. 2011. Are iron-rich sedimentary rocks the key to the spike in orogenic gold mineralisation in the paleoproterozoic? *Economic Geology* 106, 321-330.
- MERIA D 2011. Gold formatin and relation to arsenopyrite in the Tanami. B.S. Hons. thesis, University of Adelaide (unpublished).
- MERNAGH T. & WYGRALAK A. 2007. Gold ore-forming fluids of the Tanami region, Northern Australia. *Mineralium Deposita* 42, 145-173.
- MORITZ R. 2002. *What have we learnt about orogenic lode gold deposits over the past 20 years? Section des Sciences de la Terre, University of Geneva, Switzerland.*
- NEWMONT 2010. Tanami Geology Overview. Report (unpublished).
- NEWMONT 2011. Oberon Development. Report (unpublished).
- PHILLIPS G. N. 1986. Geology and alteration in the Golden Mile, Kalgoorlie. *Economic Geology* Vol. 81, pp. 779-808.
- QUEROL X., MORENO N., UMANA J. C., ALASTUEY A., HERNANDEZ E., LOPEZ-SOLER A. & PLANA F. 2002. Synthesis of zeolites from coal fly ash: an overview. *International Journal of Coal Geology* 50, 413-423.
- READING H. G. & RICHARDS M. 1994. Turbidite systems in deep-water basin margins classified by grain-size and feeder system. *Bulletin-American Association of Petroleum Geologists* 78, 792-822.
- SANDIFORD I. S. A. M. 1993. Early Proterozoic metamorphism at The Granites gold mine, Northern Territory; implications for the timing of fluid production in high-temperature, low-pressure terranes. *Economic Geology* August 1 vol. 88 no. 5, 1099-1113.
- SMITH L. D., PRING P. I., SANDO B.G. 1998. Dead Bullock Soak gold deposits. *Aust IMM Monogr* 22, 449–460.
- TUCKER M. E. 2001. *Sedimentary petrology: an introduction to the origin of sedimentary rocks.* Wiley-Blackwell.
- TUNKS A. & COOKE D. 2007. Geological and structural controls on gold mineralization in the Tanami District, Northern Territory. *Mineralium Deposita* 42, 107-126.
- WILLIAMS N. 2007. The role of decarbonization and structure in the Callie gold deposit, Tanami Region of northern Australia. *Mineralium Deposita* 42, 65-87.

Table 1. EMPA standards, minimum detection limits and count times (background and sample).

<i>Silicates EMPA Standards, spectral line, count times and minimum detection limits</i>					
Element	Standard	Line	Count time (secs.)		Approx (wt. %)
			Sample	Background	Detection Limit
F	Fluorite	K α	10	5	0.17
Na	Albite	K α	10	5	0.04
Mg	Almandine	K α	12	7	0.02
Al	Almandine	K α	20	10	0.01
Si	Almandine	K α	12	7	0.02
P	Apatite	K α	10	5	0.03
Cl	Tugtupite	K α	10	5	0.02
K	Sanidine	K α	10	5	0.01
Ca	Apatite	K α	12	7	0.02
Ti	Rutile	K α	10	5	0.02
Cr	Pyrope	K α	10	5	0.01
Mn	Rhodonite	K α	12	7	0.03
Fe	Almandine	K α	12	7	0.03

Table 2: Electron probe microanalyses of biotite in samples DS33 and DS40, showing end members, annite, phlogopite and fluorphogopite. (Minimum detection limits for EMPA (wt.%): F 0.17, Na 0.04, Mg 0.02, Al 0.01, Si 0.02, P 0.03 Cl 0.02, K 0.01, Ca 0.02, Ti 0.03, Cr 0.01; Mn, 0.03 and Fe 0.03)

Lithology	Ca-Puck	S-P (+bio)	Upper Turbidite	S-Puck (Au)	Turb (lower)	S-Puck	S-Puck	S-Puck
Number of analyses	N=5	2	8	17	4	2	15	4
(Wt.%)	46DS	40DS	10DS	30DS	27DS	35DS	31DS	38DS
CaO	0.50	0.02	0.06	0.18	0.33	0.08	0.14	0.18
Na ₂ O	7.70	0.14	2.07	9.37	3.55	3.11	4.50	3.72
K ₂ O	4.39	13.09	11.98	1.73	7.67	8.01	9.66	8.45
FeO	0.41	0.04	0.06	0.43	0.12	0.97	0.44	0.51
TiO ₂	0.01	0.00	0.01	0.02	0.01	0.05	0.02	0.03
MgO	0.01	0.00	0.00	0.03	0.00	0.01	0.02	0.01
SiO ₂	61.03	64.58	63.36	68.36	66.52	66.32	64.90	65.92
MnO	0.01	0.00	0.00	0.03	0.00	0.01	0.02	0.01
Cr ₂ O ₃	0.01	0.00	0.00	0.00	0.01	0.02	0.01	0.01
Al ₂ O ₃	19.54	18.25	17.91	18.15	18.99	19.52	18.64	19.05
F (wt.%)	0.02	0.00	0.00	0.02	0.03	0.02	0.01	0.02
Cl (wt.%)	0.03	0.08	0.04	0.07	0.04	0.01	0.05	0.04
Total	93.66	96.20	95.49	98.39	97.27	98.13	98.41	97.91
albite %	70.06	1.63	19.48	87.62	39.59	48.91	40.79	43.10
anorthite %	2.49	0.15	0.29	0.94	2.04	0.70	0.72	1.15
K-feldspar %	27.46	98.22	80.23	11.45	58.37	50.38	58.49	55.75

Table 3: Combined table of chlorite data and the chlorite thermometry. Calculations of temperatures are by the methods (*Minimum detection limits for EMPA (wt.%): F 0.17, Na 0.04, Mg 0.02, Al 0.01, Si 0.02, P 0.03 Cl 0.02, K 0.01, Ca 0.02, Ti 0.03, Cr 0.01; Mn, 0.03 and Fe 0.03*)

Label	46	33	40	19	18	10	20	25	27	30	31	35	38	43	45
Total Sample points	6	4	9	9	6	6	5	8	8	7	6	12	6	7	9
F (wt.%)	0.14	0.19	0.1	0.11	0.14	0.08	0.35	0.31	0.27	0.32	0.35	0.34	0.28	0	0.3
Ox%(Na)	0.04	0.02	0.1	0.15	0.05	0.02	0.05	0.03	0.17	0.11	0.05	0.08	0.11	0.05	0.07
Ox%(Mg)	15.25	14.99	18.15	20.07	12.12	6.49	21.93	8.59	9.03	6.9	7.28	7.02	7.78	10.3	13.62
Ox%(Al)	19.62	19.37	19.47	19.84	19.39	20.15	18.41	20.5	19.32	19.09	19.66	19.54	19.76	20.19	20.18
Ox%(Si)	24.73	25.13	26.59	27.35	25.71	22.97	32.38	24.2	28.31	25.98	22.57	23.82	24.46	25.35	24.84
Ox%(P)	0.04	0.01	0.05	0.01	0.03	0	0.02	0.02	0.05	0.1	0.04	0.05	0.04	0	0.06
Cl (wt.%)	0.01	0.01	0.01	0.02	0.03	0.01	0.05	0.01	0.03	0.03	0.01	0.01	0.03	0	0.01
Ox%(K)	0	0.06	0.13	0.03	0.02	0.04	0.19	0.25	0.27	0.06	0.02	0.23	0.19	0.14	0.11
Ox%(Ca)	0.04	0.03	0.05	0.03	0.06	0.02	0.03	0.11	0.09	0.12	0.04	0.05	0.05	0.11	0.6
Ox%(Ti)	0.08	0.1	0.07	0.04	0.02	0.05	0.02	0.07	0.07	0.06	0.08	0.25	0.08	0.06	0.73
Ox%(Cr)	0.01	0.06	0.1	0.01	<mdl	<mdl	0.01	0.02	0.04	0.01	0.06	0.05	0.08	0.02	0.01
Ox%(Mn)	0.09	0.05	0.03	0.06	0.03	0.21	0.04	0.08	0.05	0.04	0.07	0.06	0.04	0.06	0.03
Ox%(Fe)	24.09	24.84	19.92	18.6	28.9	34.61	12.93	32.01	28.4	32.63	34.35	34.4	33.33	29.87	25.59
Total	84.1	84.86	84.79	86.32	86.5	84.66	86.43	86.22	86.12	85.44	84.59	85.89	86.22	86.17	86.16
F	0.05	0.07	0.03	0.04	0.05	0.03	0.11	0.11	0.1	0.11	0.13	0.12	0.1	0	0.1
Cl	0	0	0	0	0.01	0	0	0	0.01	0.01	0	0	0.01	0	0
(OH)	15.95	15.93	15.97	15.96	15.95	15.97	15.89	15.89	15.9	15.88	15.87	15.87	15.9	16	15.9
total	16	16	16	16	16	16	16	16	16	16	16	16	16	16	16
Fe/(Fe+Mg+Mn)	0.47	0.48	0.38	0.35	0.57	0.75	0.25	0.68	0.64	0.73	0.73	0.73	0.71	0.62	0.51
% clinocllore	52.91	51.76	61.84	64.88	42.72	24.93	74.47	32.24	36.07	27.33	27.36	26.61	29.35	38.01	48.65
% chamosite	46.92	48.14	38.1	35	57.22	74.62	25.45	67.59	63.83	72.58	72.5	73.26	70.56	61.86	51.29
% pennantite	0.17	0.1	0.06	0.12	0.06	0.45	0.08	0.17	0.1	0.1	0.14	0.12	0.09	0.12	0.06
Alivc (KN)	1.61	1.59	1.45	1.43	1.59	1.86	0.97	1.76	1.42	1.57	1.87	1.79	1.73	1.64	1.67
Alivc (J)	1.33	1.3	1.22	1.21	1.25	1.41	0.82	1.35	1.04	1.14	1.44	1.35	1.31	1.27	1.36
Cath 1988	351	341	317	318	322	367	253	352	324	281	378	348	336	327	359
J 1991	355	345	319	319	330	380	251	362	328	294	390	360	348	337	365
Kr+N 1987	189	186	171	169	187	215	140	204	180	185	217	207	201	192	195

The three methods were used to derive a temperature. The Kratinoidis and MacLean (1987) method gave a particularly low temperature and was disregarded. The Jowerrr (1991) method was used in samples with less than 0.05 Fe/(Fe+Mg)

Various authors have suggested that chlorite compositions provide an estimate of the peak metamorphic temperature. Average temperatures were calculated for all 15 samples. Temperatures are derived from the proportion of silicon and octahedral Al in chlorite. Three different calibrations were applied. Of these, only the calibrations suggested by Jowett (1991) and Cathelineau (1988) gave reliable temperature estimates. The calibration of Kratinoidis and MacLean (1987) gave results that are unreasonably low.

Table 4. Representative electron probe microanalyses of apatite (means for each sample/lithology) and calculated end-member components. Minimum detection limits for EMPA (wt.%): F 0.17, Na 0.04, Mg 0.02, Al 0.01, Si 0.02, P 0.03 Cl 0.02, K 0.01, Ca 0.02, Ti 0.03, Cr 0.01; Mn, 0.03 and Fe 0.03.

(Wt.%)	30DS06	46DS10	33DS04	33DS10	40DS02	40DS07	40DS13	30DS10	45DS08	45DS13	45DS14	45DS16	35DS20
CaO	55.27	54.79	49.73	52.08	55.20	55.10	55.60	50.97	52.40	54.54	53.01	54.30	51.89
Na2O	0.16	0.07	1.28	0.07	0.06	0.17	0.02	0.09	0.20	0.17	0.37	0.09	0.06
K2O	0.01	0.02	0.12	0.22	0.01	<mdl	0.01	0.03	0.12	0.03	0.30	0.02	0.46
FeO	0.59	0.54	0.20	0.80	0.27	0.40	0.39	2.99	0.57	0.43	0.44	0.72	2.23
TiO2	0.02	0.03	<mdl	0.03	<mdl	<mdl	0.03	<mdl	0.02	<mdl	<mdl	0.03	0.09
MgO	0.00	0.05	0.01	0.21	0.04	0.18	0.03	0.47	0.06	0.03	0.02	0.13	0.28
SiO2	0.96	0.22	6.10	5.58	0.27	0.50	0.35	1.90	0.32	0.21	0.34	0.19	3.61
MnO	0.08	0.06	0.12	0.05	0.07	0.08	0.07	<mdl	<mdl	0.13	0.03	<mdl	0.11
Cr2O3	0.02	0.04	<mdl	<mdl	<mdl	<mdl	0.01	<mdl	0.02	<mdl	<mdl	<mdl	<mdl
Al2O3	0.10	0.06	1.91	0.04	<mdl	0.02	0.03	1.34	0.12	<mdl	0.11	<mdl	1.81
P2O5	38.82	39.31	35.49	37.22	39.51	37.97	39.39	36.46	35.58	38.22	37.89	38.03	34.26
F (wt.%)	5.40	5.70	6.24	4.61	4.00	5.09	5.23	4.30	3.90	4.32	3.87	3.81	4.39
Cl (wt.%)	<mdl	0.07	0.02	<mdl	0.06	<mdl	0.02	0.01	0.04	<mdl	0.26	<mdl	0.01
True total	96.88	96.12	95.96	97.03	96.09	95.24	96.77	94.95	90.03	94.43	93.26	94.11	95.51
P	5.70	5.81	5.16	5.36	5.82	5.69	5.78	5.46	5.65	5.76	5.78	5.75	5.13
Si	0.17	0.04	1.05	0.95	0.05	0.09	0.06	0.34	0.06	0.04	0.06	0.03	0.64
Total	5.86	5.85	6.21	6.31	5.87	5.78	5.84	5.80	5.71	5.80	5.84	5.78	5.77
F	2.96	3.15	3.39	2.48	2.20	2.85	2.87	2.41	2.32	2.43	2.21	2.15	2.46
Cl	0.00	0.02	0.00	0.00	0.02	0.00	0.01	0.00	0.01	0.00	0.08	0.00	0.00
OH (by difference)	0.00	0.00	0.00	0.00	0.00	0.00	0.00	0.00	0.00	0.00	0.00	0.00	0.00
Total	2.96	3.17	3.39	2.48	2.22	2.85	2.87	2.41	2.33	2.43	2.29	2.15	2.46
X OH	0.00	0.00	0.00	0.00	0.00	0.00	0.00	0.00	0.00	0.00	0.00	0.00	0.00
X F	1.00	0.99	1.00	1.00	0.99	1.00	1.00	1.00	0.99	1.00	0.96	1.00	1.00
X Cl	0.00	0.01	0.00	0.00	0.01	0.00	0.00	0.00	0.01	0.00	0.04	0.00	0.00

Table 5. Electron probe microanalyses of biotite in samples DS33 and DS40. (Minimum detection limits for EMPA (wt.%): F 0.17, Na 0.04, Mg 0.02, Al 0.01, Si 0.02, P 0.03 Cl 0.02, K 0.01, Ca 0.02, Ti 0.03, Cr 0.01; Mn, 0.03 and Fe 0.03)

(Wt.%)	33DS01	33DS02	33DS05	33DS06	33DS07	33DS08	33DS14	40DS01	40DS06
CaO	0.06	0.06	0.00	0.03	0.00	0.01	0.03	0.08	0.02
Na2O	0.11	0.08	0.00	0.06	0.04	0.06	0.08	0.07	0.03
K2O	8.99	9.30	9.15	9.07	9.36	9.27	9.33	7.49	6.51
FeO	18.44	18.17	17.23	18.04	19.33	19.29	18.49	16.70	16.18
TiO2	3.56	3.29	3.35	3.51	3.30	3.05	3.46	3.90	1.79
MgO	11.03	9.74	12.31	10.49	10.05	10.39	10.49	13.90	15.06
SiO2	34.97	33.32	34.75	32.61	34.67	35.05	35.41	35.49	33.78
MnO	0.04	0.07	0.00	0.02	0.06	0.03	0.02	0.08	0.04
Cr2O3	0.00	0.00	0.00	0.02	0.00	0.00	0.00	0.01	0.02
Al2O3	14.71	15.05	13.93	13.92	15.49	14.89	14.71	14.33	15.76
F (wt.%)	1.50	1.14	1.44	1.23	1.19	0.92	1.43	0.83	0.72
Cl (wt.%)	0.05	0.11	0.04	0.06	0.09	0.14	0.07	0.03	0.02
Total	93.30	90.18	92.20	88.98	93.53	93.02	93.42	92.75	89.90
F	0.75	0.59	0.73	0.65	0.60	0.46	0.72	0.41	0.36
Cl	0.01	0.03	0.01	0.02	0.02	0.04	0.02	0.01	0.01
OH	3.24	3.38	3.26	3.33	3.38	3.50	3.26	3.59	3.63
Total	4.00	4.00	4.00	4.00	4.00	4.00	4.00	4.00	4.00
TOTAL	20.12	20.35	20.04	20.14	20.29	20.24	20.24	19.63	19.66
Annite	40.64	41.56	38.34	41.97	42.67	42.66	40.72	36.08	35.86
Phlogopite	43.31	39.69	48.81	43.50	39.54	40.96	41.16	53.53	59.46
Fluorophlogopite	18.78	14.82	18.17	16.25	14.90	11.54	17.90	10.13	9.03
An/Ph	0.94	1.05	0.79	0.96	1.08	1.04	0.99	0.67	0.60

Table 6. Electron probe microanalyses for sericite (white mica) in samples DS46, -33, -10, -05, -43, -45, -25, -27 and -35. (Minimum detection limits for EMPA (wt.%): F 0.17, Na 0.04, Mg 0.02, Al 0.01, Si 0.02, P 0.03 Cl 0.02, K 0.01, Ca 0.02, Ti 0.03, Cr 0.01; Mn, 0.03 and Fe 0.03)

(Wt.%)	46DS21	33DS21	10DS18	05DS16	43DS17	45DS26M	25DS20F	27DS19	35DS22m
CaO	0.02	0.10	<mdl	0.01	0.03	0.05	0.11	0.04	0.03
Na2O	0.17	0.23	0.12	0.39	0.16	0.26	0.15	0.06	0.10
K2O	10.49	7.33	8.80	9.17	10.23	10.15	5.71	7.16	7.13
FeO	2.60	2.18	2.64	1.40	3.00	3.53	12.56	5.34	7.74
TiO2	0.11	0.11	0.15	0.04	0.40	0.25	0.20	0.54	0.36
MgO	1.49	1.33	1.12	1.41	1.67	2.26	3.16	2.23	2.06
SiO2	44.84	47.87	44.85	48.77	49.40	46.29	47.40	46.91	45.05
MnO	0.01	<mdl	0.02	0.03	0.02	0.02	0.04	<mdl	0.04
Cr2O3	0.01	<mdl	<mdl	0.02	0.02	0.06	0.02	0.07	0.05
Al2O3	30.20	33.13	30.76	35.48	31.57	29.81	23.19	30.79	29.79
F (wt.%)	0.05	0.18	0.12	0.30	0.25	0.30	0.18	0.34	0.38
Cl (wt.%)	0.01	0.01	0.02	0.00	0.00	0.04	0.02	0.01	0.03
Total	90.00	92.47	88.61	97.02	96.75	93.01	92.74	93.48	92.73
TOTAL	7.02	6.79	6.90	6.89	6.94	7.03	6.93	6.86	6.94
F	0.01	0.04	0.03	0.06	0.05	0.07	0.04	0.07	0.08
Cl	0.00	0.00	0.00	0.00	0.00	0.00	0.00	0.00	0.00
OH	1.99	1.96	1.97	1.94	1.95	1.93	1.96	1.93	1.91
Total	2.00	2.00	2.00	2.00	2.00	2.00	2.00	2.00	2.00
Fe/(Fe+Mg)	0.49	0.50	0.57	0.38	0.50	0.46	0.69	0.57	0.66
phengite component %	15.68	12.76	13.71	10.33	17.09	21.49	45.78	25.16	29.72
% F-end-member	0.60	1.87	1.42	3.04	2.64	3.25	1.99	3.71	4.13
% Cl-end-member	0.05	0.04	0.11	0.02	0.01	0.23	0.10	0.04	0.19

Table 7. Comparison of F (wt%) and Fe/(Fe+Mg) ratios in biotite, chlorite and apatite from selected samples. Sample DS33 containing the ‘unaltered’ assemblage contains a lower ratio of Fe/(Fe+Mg), along with less fluorine.

Mineral		DS10	DS18	DS19	DS20	DS25	DS27	DS30	DS31	DS33	DS35	DS38	DS40	DS43	DS45	DS46
Biotite	Fe/(Fe+Mg)									1.02			0.53			
	F (wt.%)									1.27			0.77			
Chlorite	Fe/(Fe+Mg)	0.75	0.57	0.35	0.25	0.68	0.64	0.73	0.73	0.48	0.73	0.71	0.38	0.62	0.51	0.47
	F (wt.%)	0.08	0.14	0.11	0.35	0.31	0.27	0.32	0.35	0.19	0.34	0.28	0.10	0.00	0.30	0.14
Apatite	F (wt.%)							4.85		5.43	4.39		4.77		3.98	5
Muscovite	Fe/(Fe+Mg)	0.57				0.69	0.57			0.50	0.66			0.50	0.46	0.49
	F (wt.%)	0.12				0.18	0.34			0.18	0.38			0.25	0.30	0.05

Table 8. Statistical analysis of the thermometric calculations. The entire chlorite dataset gives an average peak metamorphic temperature of 341 °C, whereas the lithology specific calculations calculate temperatures of 344 °C for the Puck Group and 360 °C for the Au-mineralised zone.

	Entire deposit (C)	Ca-Puck (C)	Au zone (C)
Minimum	207	-	-
Maximum	440	-	-
Mean	341	344	360
SD	39	48	20
Median	350	-	-

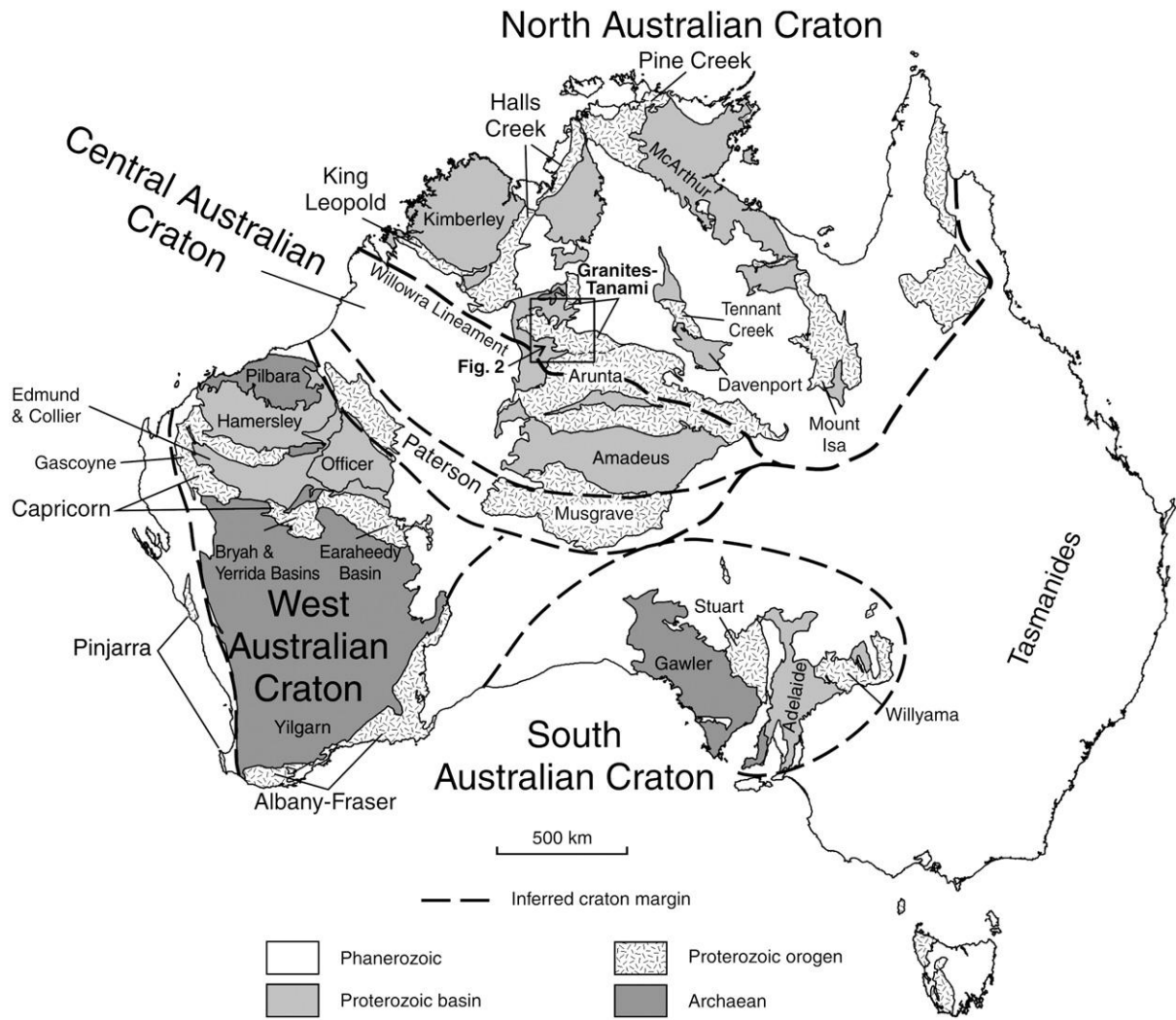


Figure 1. Map of Australia with Phanerozoic, Proterozoic and Archaean terranes showing the location of the Granites–Tanami Orogen, after Bagas *et al.* (2009).

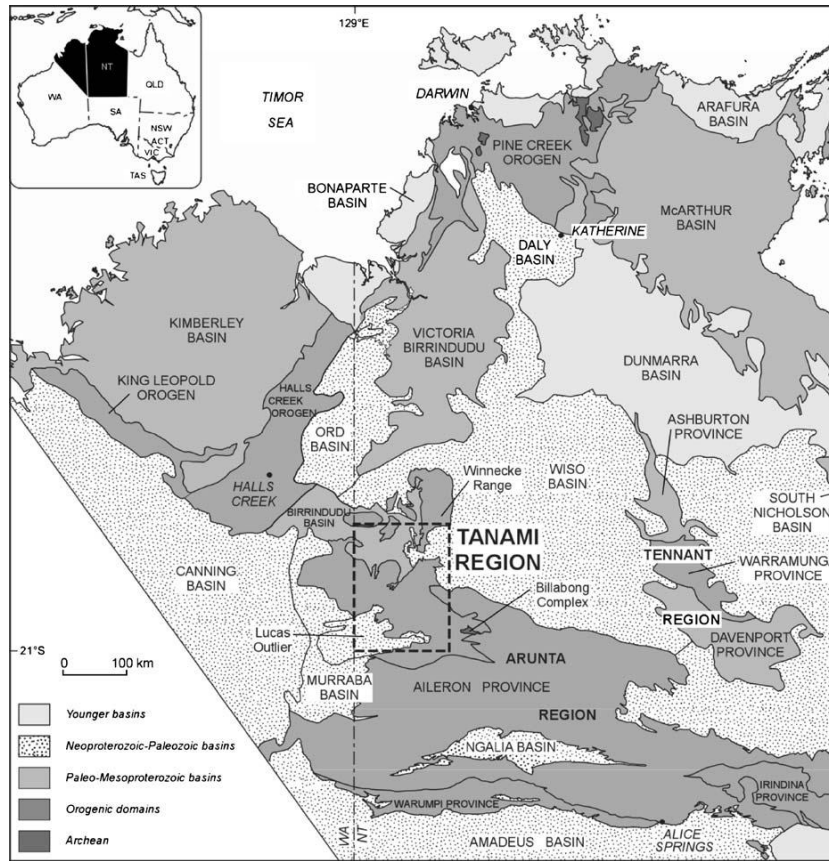


Figure 2. Map of the location of the Tanami goldfields (Tunks & Cooke 2007).

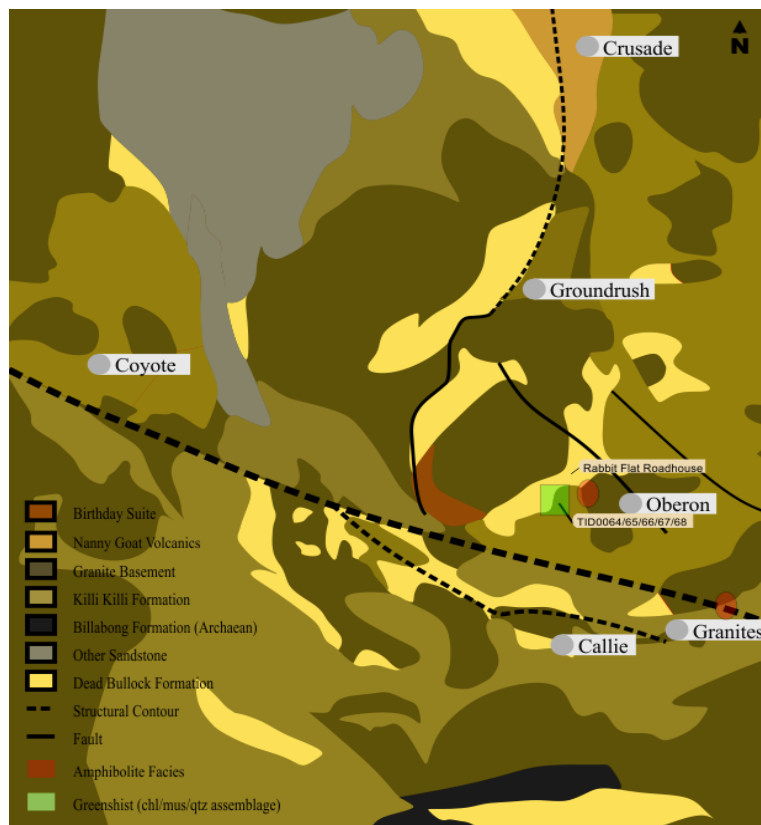


Figure 3. Regional map of the Tanami Goldfields. Shows lithology below alluvial cover which dominates the entire region. Archean basement (Billabong Complex) outcrops to the south of the gold fields. Nanny Goat volcanics can be seen to the north of the deposit. Oberon is hosted in the greenschist Tamani Group, regional expression of granulite facies can be seen. *Adapted from (Crispe et al. 2007)*

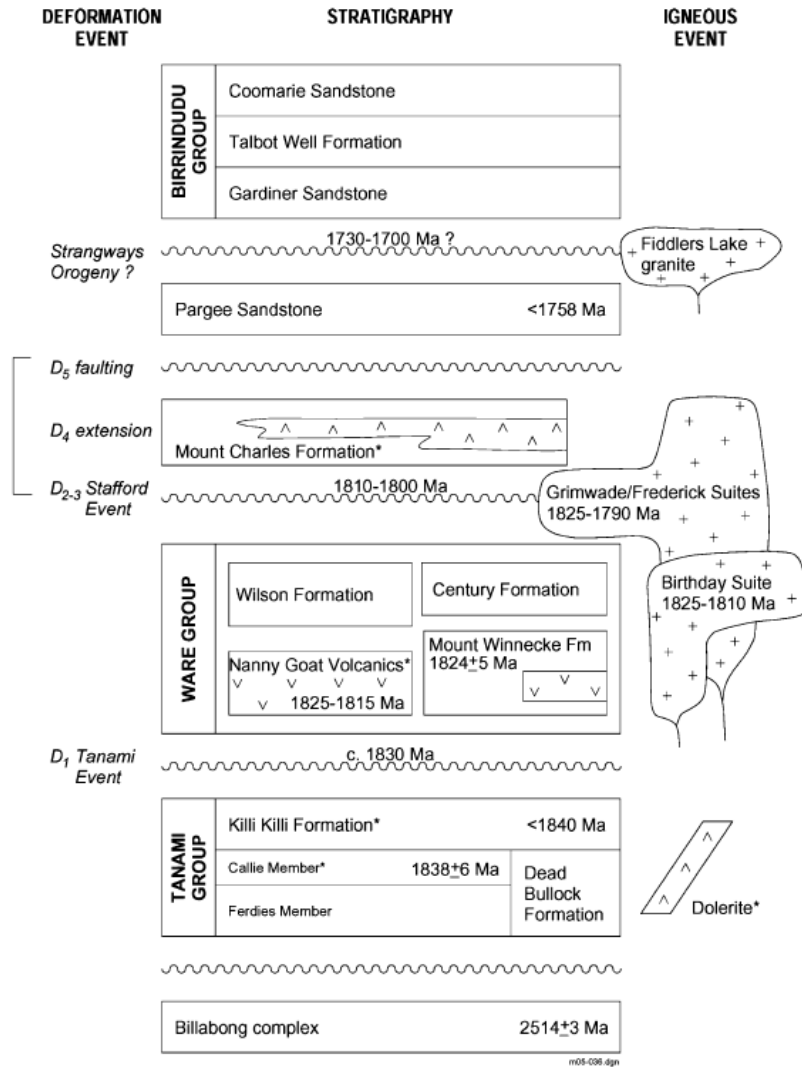


Figure 4. Chronological succession of the main units that make up the Tanami region. Archean basement unconformably overlain by the Paleoproterozoic Tanami Group, then Nanny Goat volcanics which is unconformably overlain by quartz, sandstone, lithic argillite and conglomerates of the Pargee Sandstone (sediments from the 1730 Ma Strangways orogeny), after (Crispe et al. 2007).

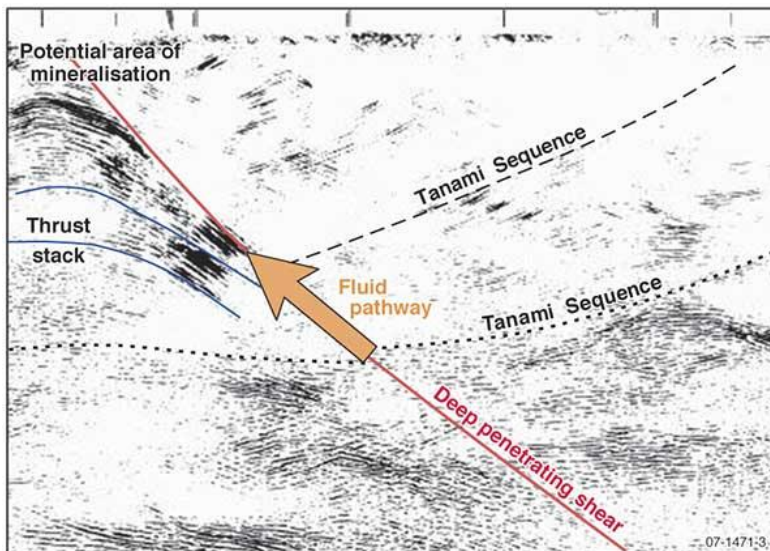
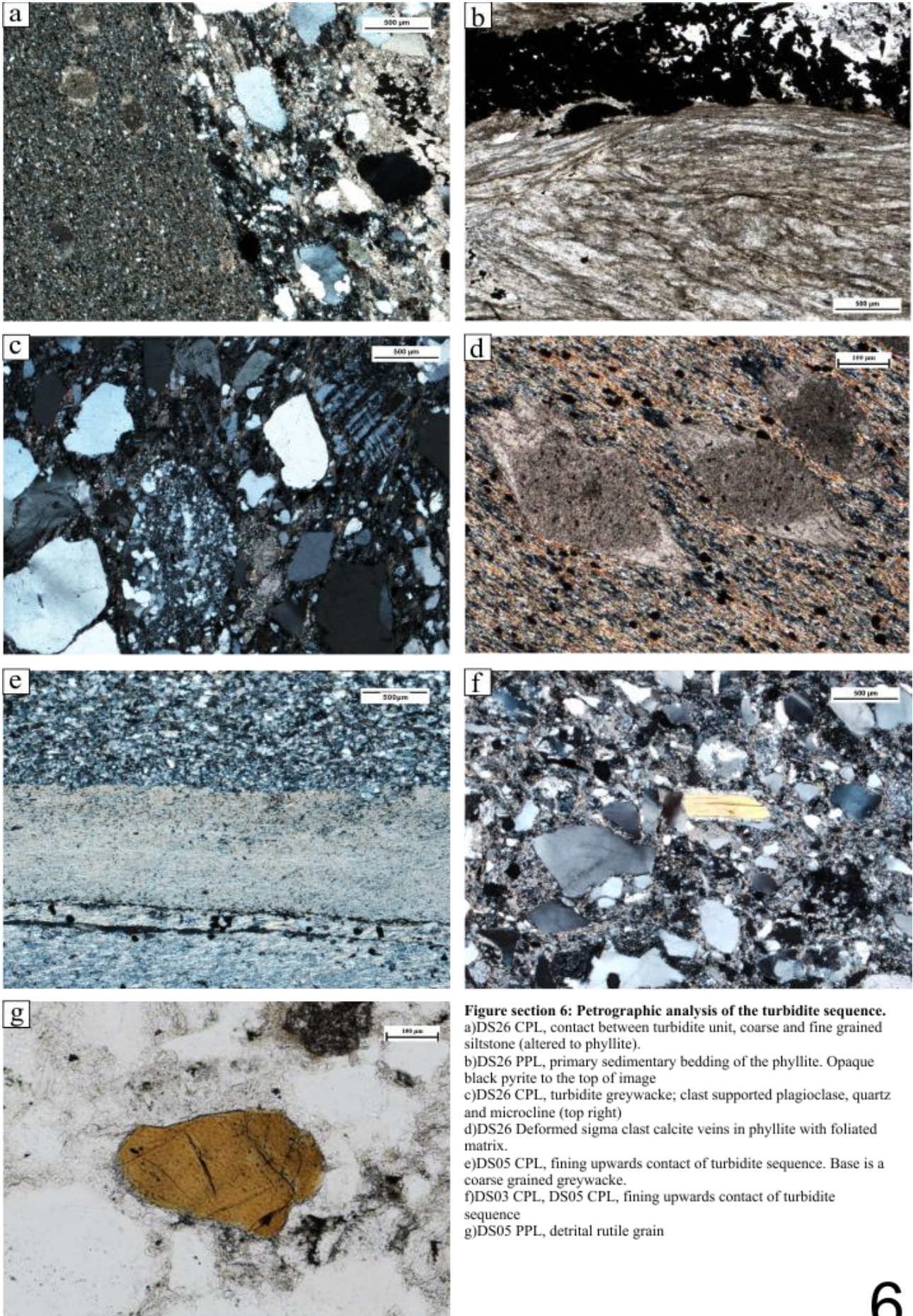


Figure 5. Deep penetrating seismic surveys demonstrating the fluid pathway along reactivated faults during the Stafford event of 1803–1791 Ma (Geoscience Australia 2007).

Figure 6-15. Petrographic and SEM images collected from samples DS 1-46. All main lithologies are represented along with specific textural features. Captions imbedded within the figures



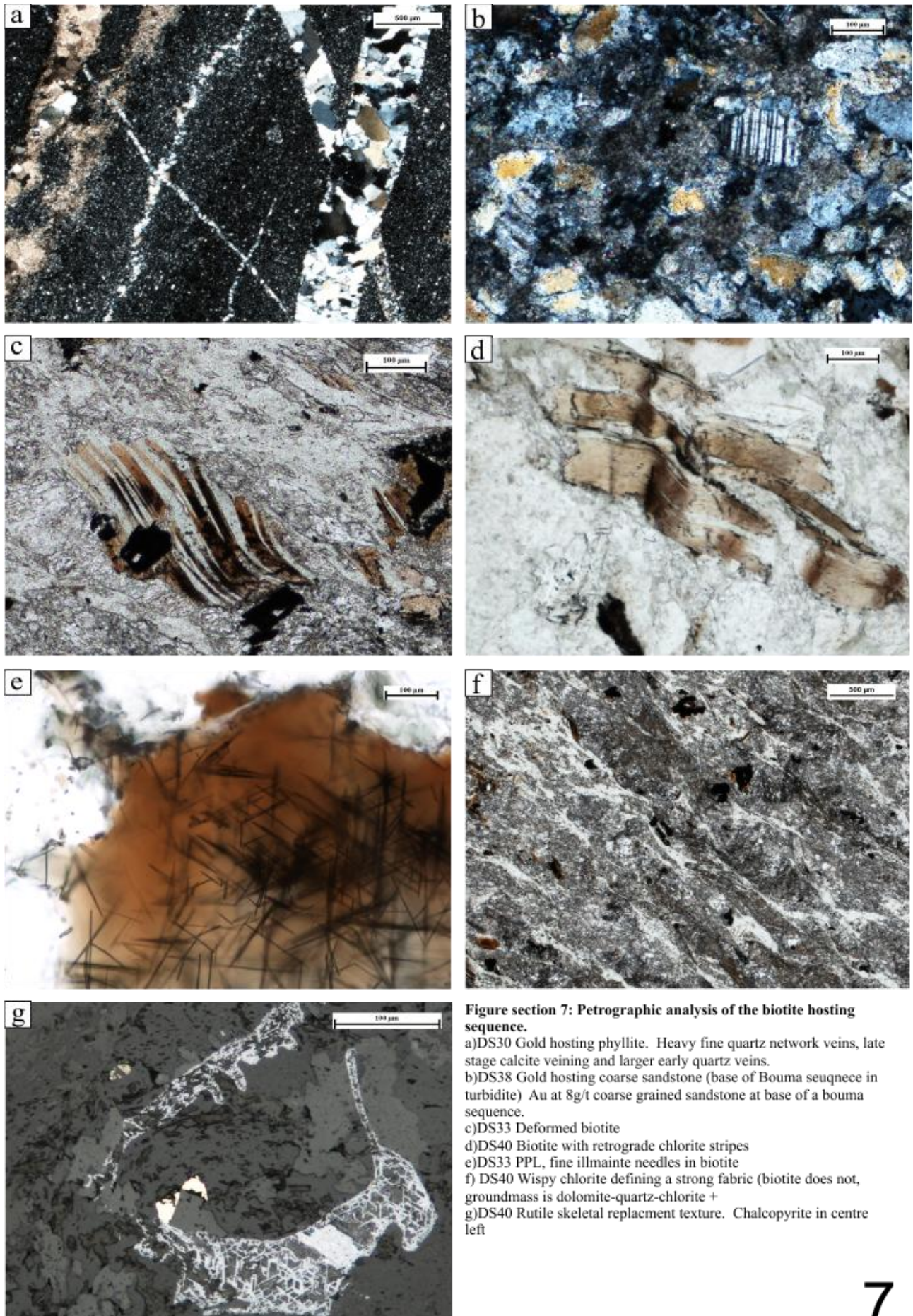


Figure section 7: Petrographic analysis of the biotite hosting sequence.

a)DS30 Gold hosting phyllite. Heavy fine quartz network veins, late stage calcite veining and larger early quartz veins.

b)DS38 Gold hosting coarse sandstone (base of Bouma sequence in turbidite). Au at 8g/t coarse grained sandstone at base of a bouma sequence.

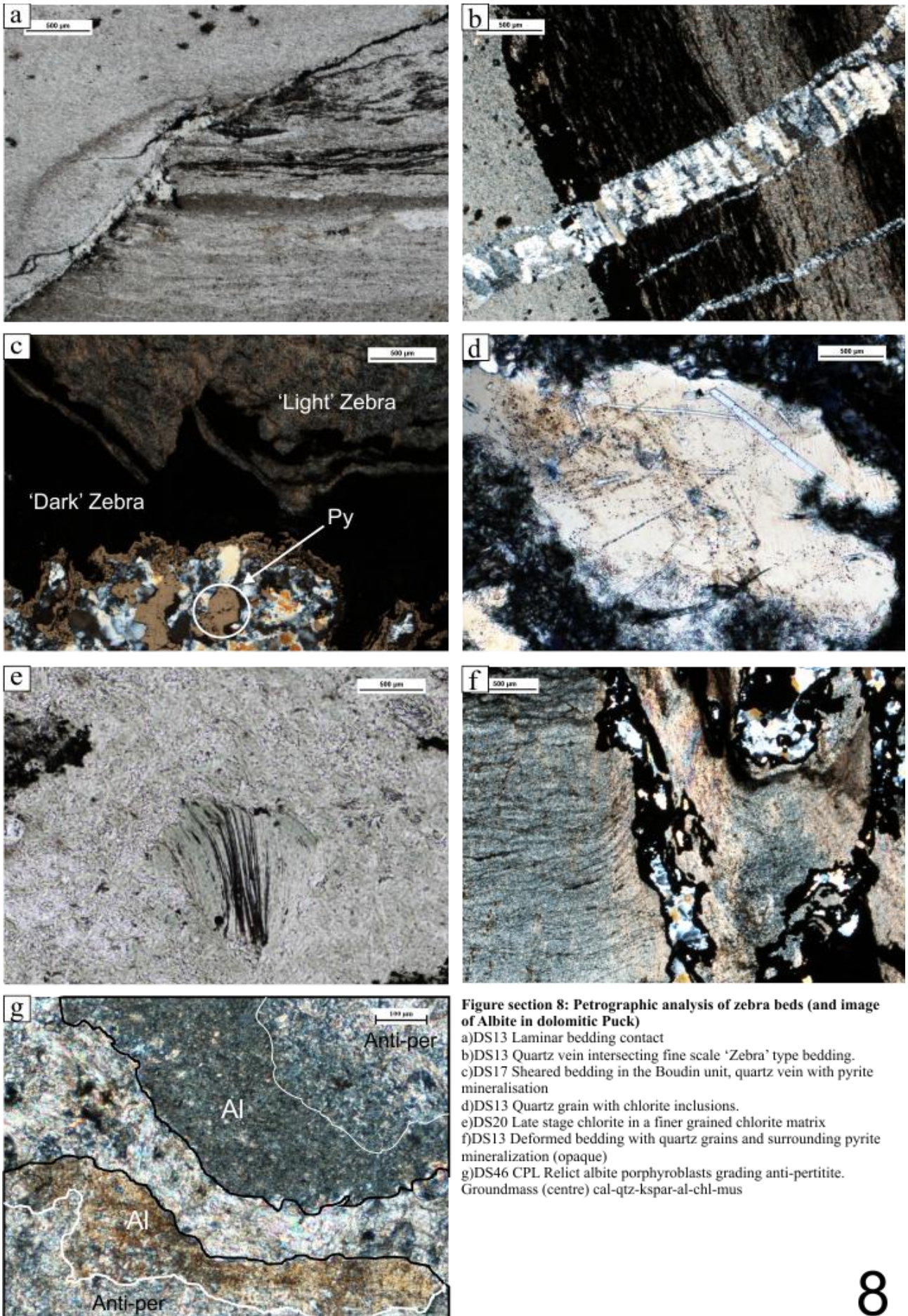
c)DS33 Deformed biotite

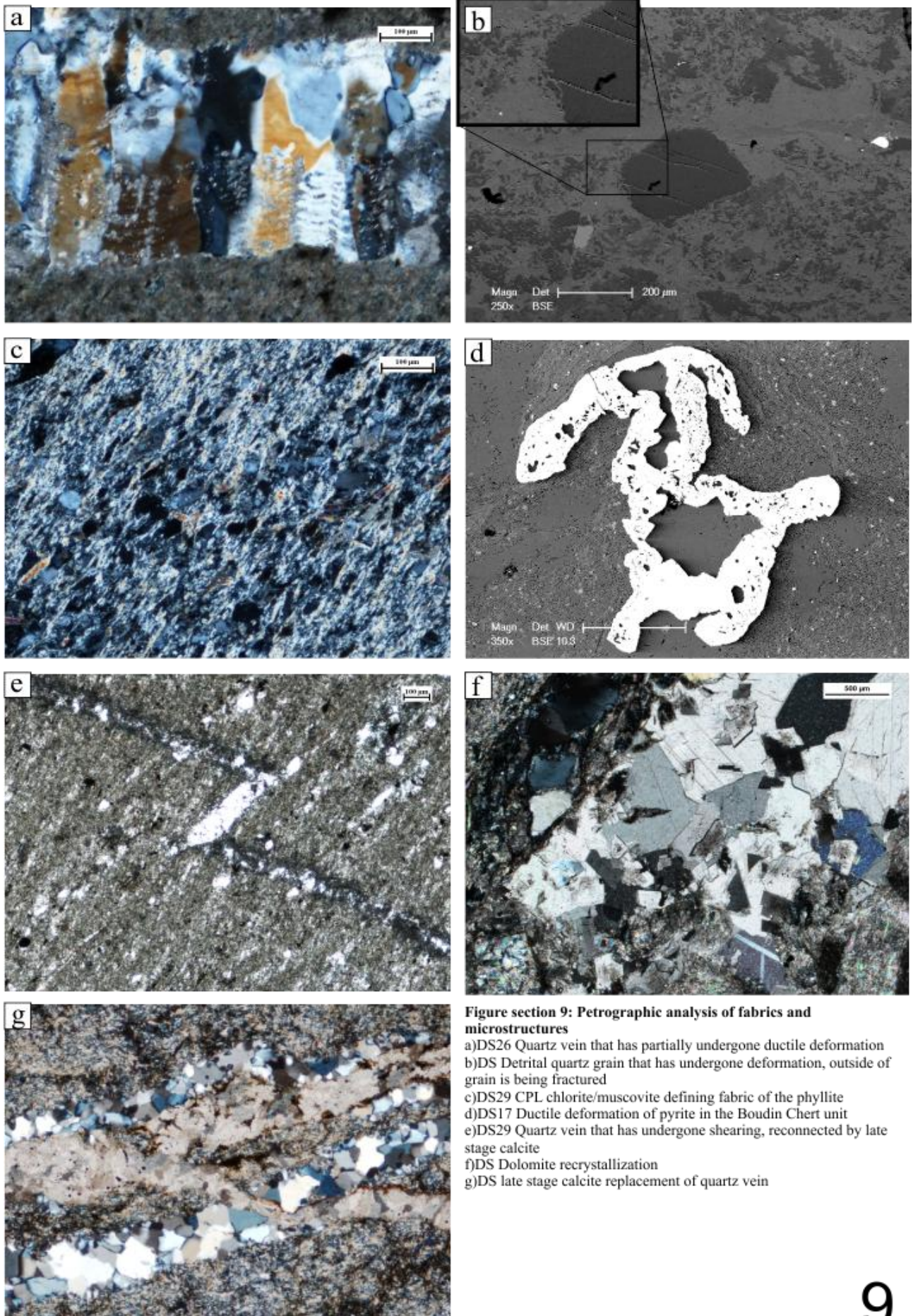
d)DS40 Biotite with retrograde chlorite stripes

e)DS33 PPL, fine ilmenite needles in biotite

f) DS40 Wispy chlorite defining a strong fabric (biotite does not, groundmass is dolomite-quartz-chlorite +

g)DS40 Rutile skeletal replacement texture. Chalcopyrite in centre left





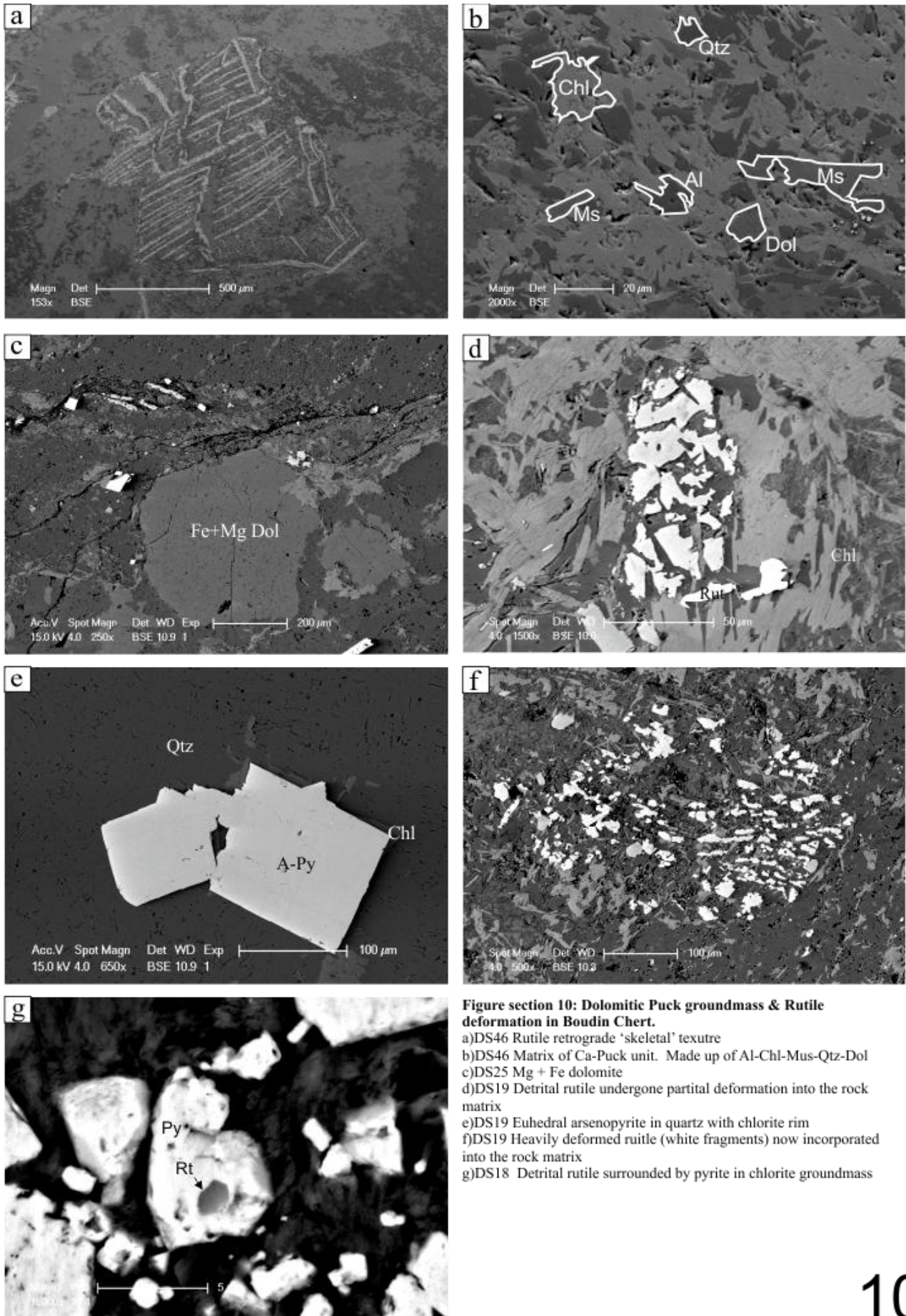
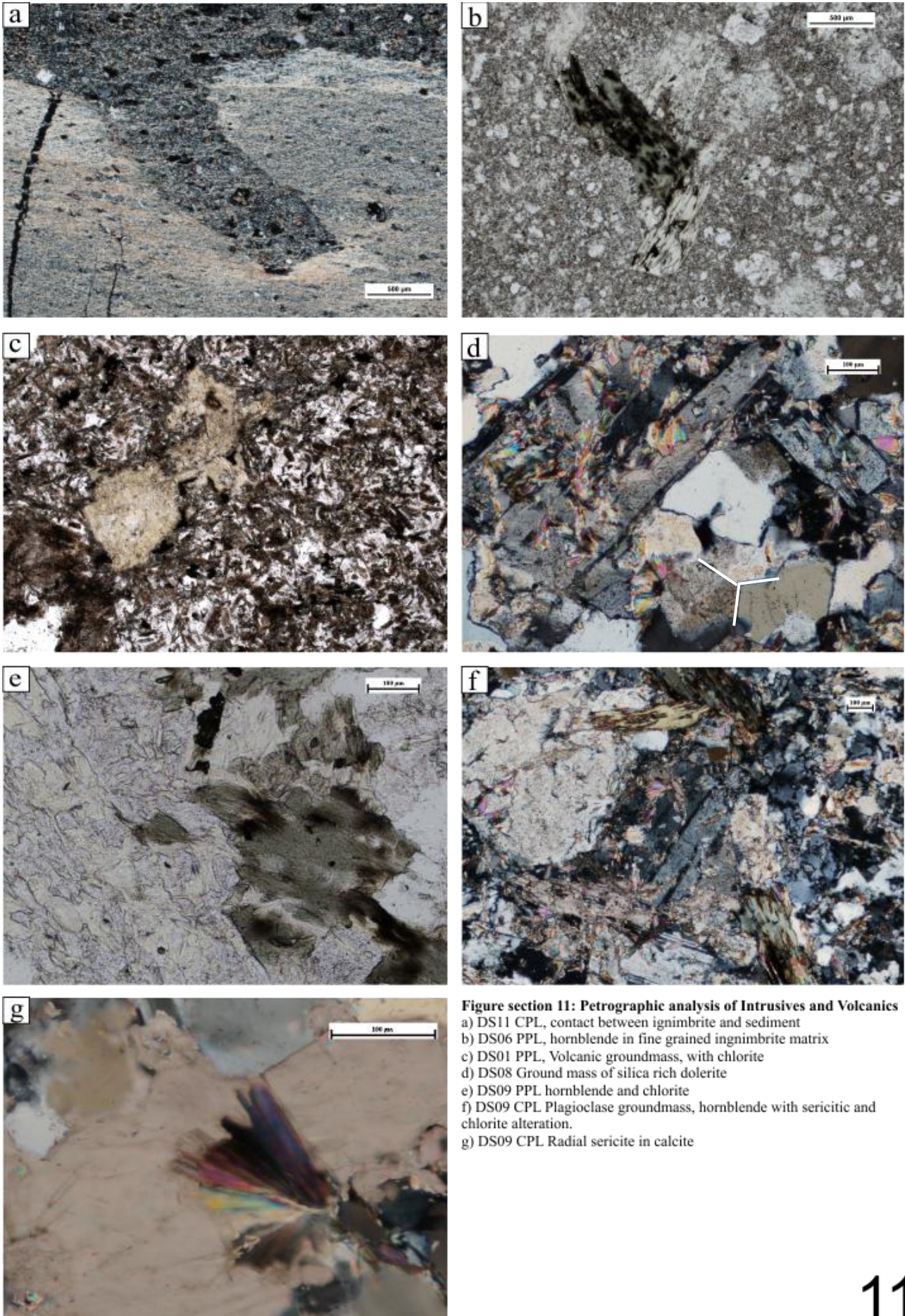


Figure section 10: Dolomitic Puck groundmass & Rutile deformation in Boudin Chert.

- a) DS46 Rutile retrograde 'skeletal' texture
- b) DS46 Matrix of Ca-Puck unit. Made up of Al-Chl-Mus-Qtz-Dol
- c) DS25 Mg + Fe dolomite
- d) DS19 Detrital rutile undergone partial deformation into the rock matrix
- e) DS19 Euhedral arsenopyrite in quartz with chlorite rim
- f) DS19 Heavily deformed rutile (white fragments) now incorporated into the rock matrix
- g) DS18 Detrital rutile surrounded by pyrite in chlorite groundmass



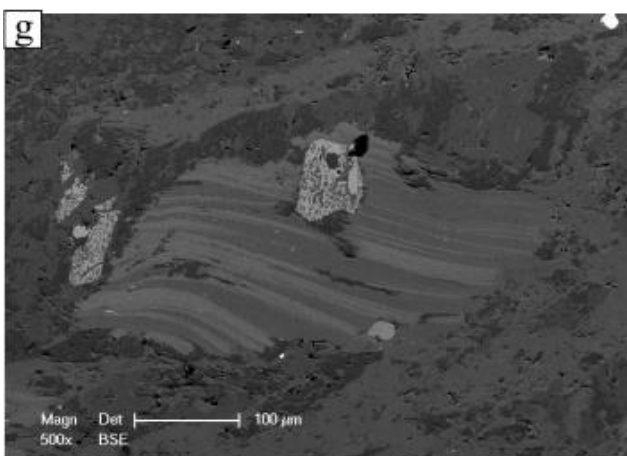
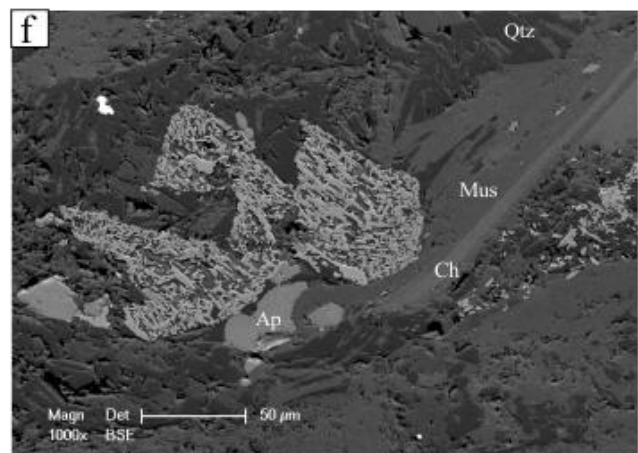
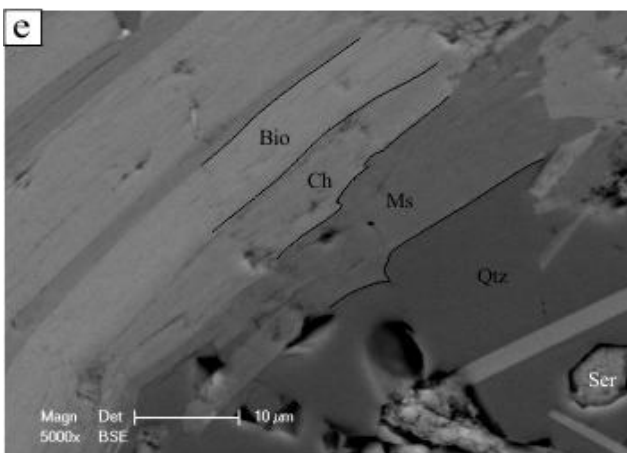
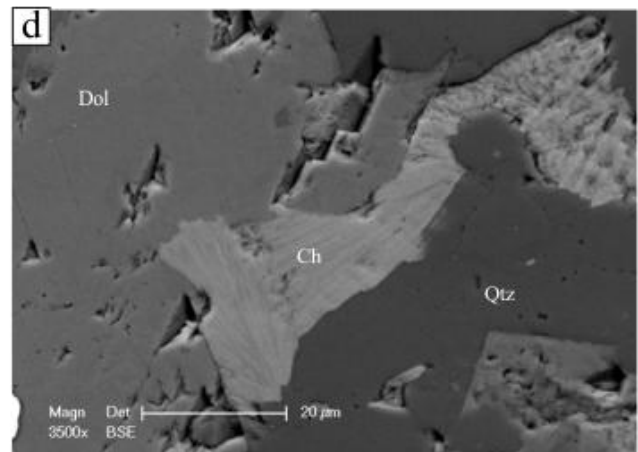
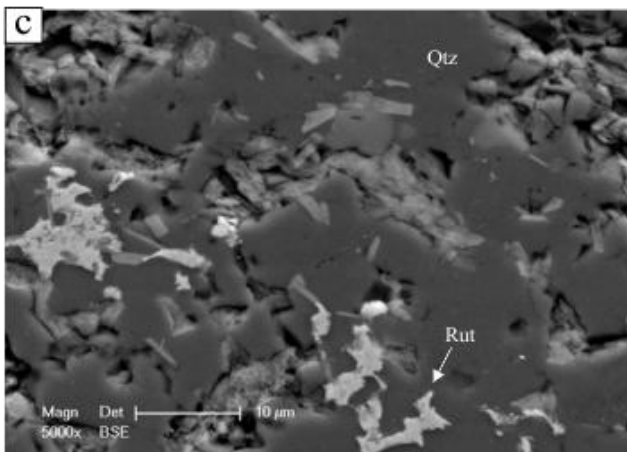
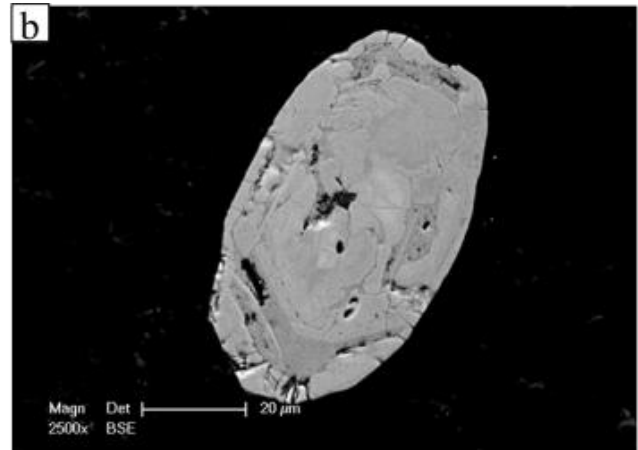
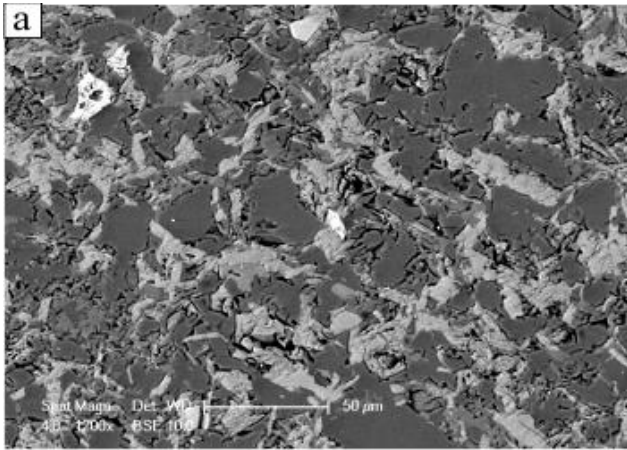


Image section 12: Au hosting (Ds30) lithology & Biotite hosting lithologies (DS30 & 40)

- a) DS31 Example of groundmass microstructure in coArse grained gold hosting lithology
 b) DS30 Zoned detrital zircon
 c) DS30 Matrix of gold hosting lithology, chlorite, rutile and carbonates
 d) DS30, a chlorite in between a quartz and carbonate
 e) DS33 Interlayered phyllosilicates, biotite, chlorite and muscovite, sericite alteration of plagioclase (bottom left)
 f) DS33 Rutile replacement textures
 g) DS40 Interlayered biotite and chlorite, rutile in centre

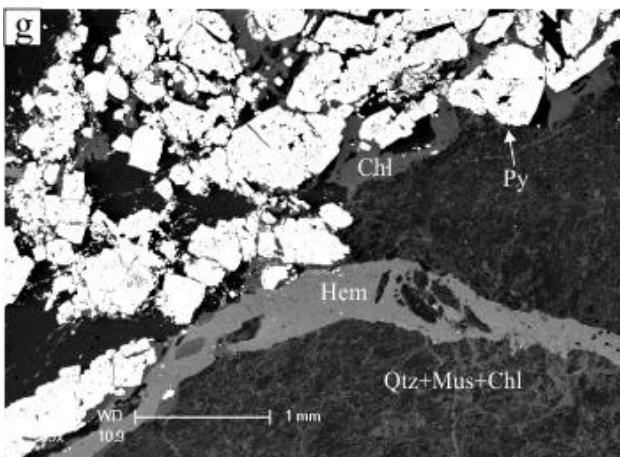
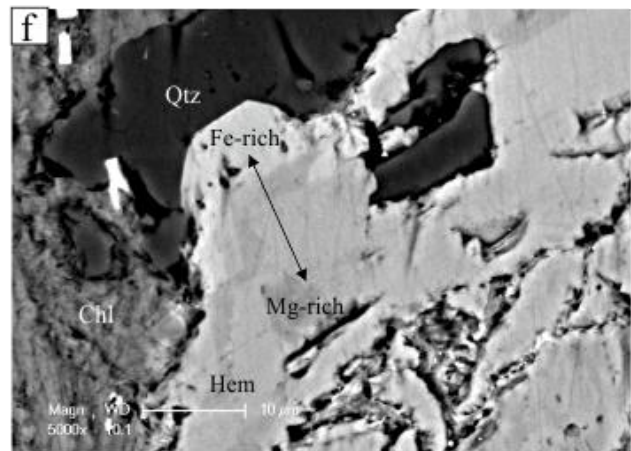
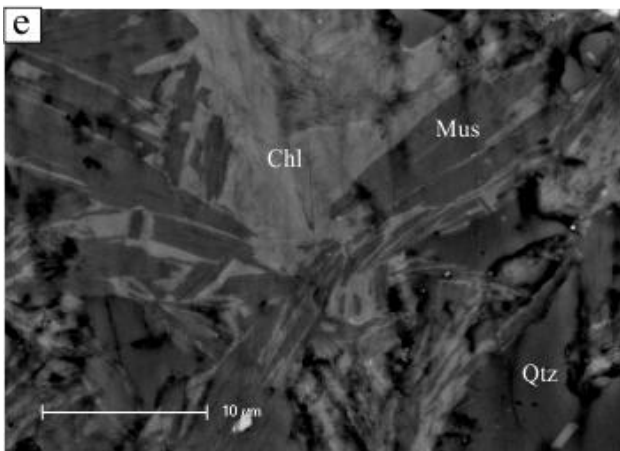
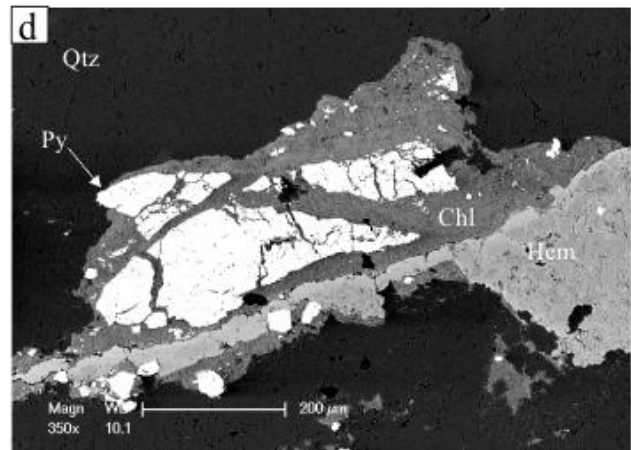
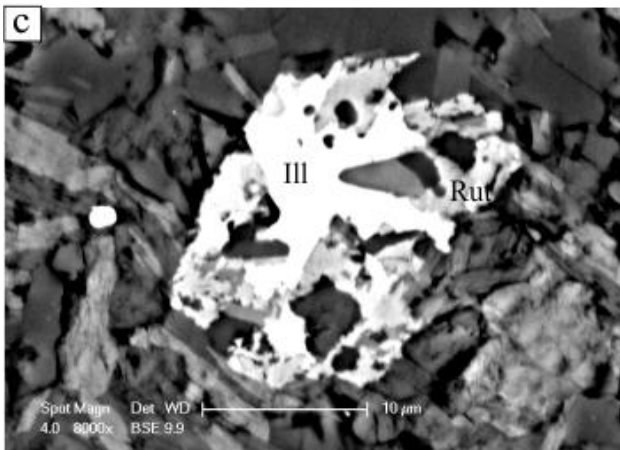
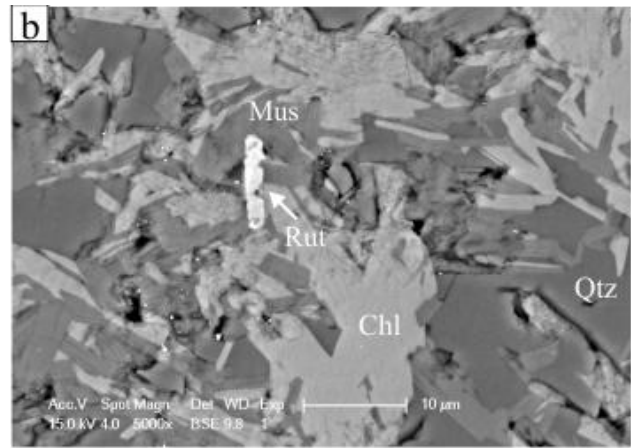
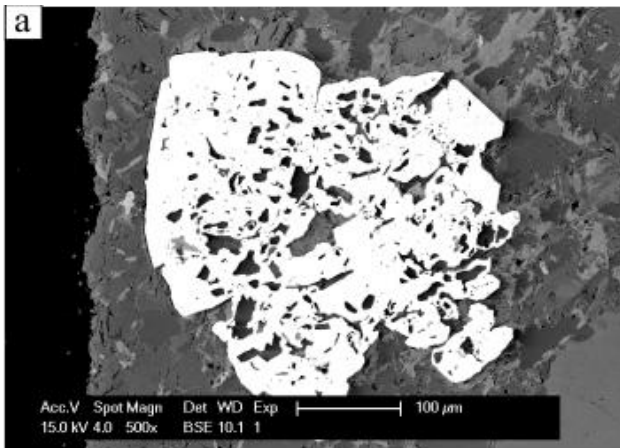
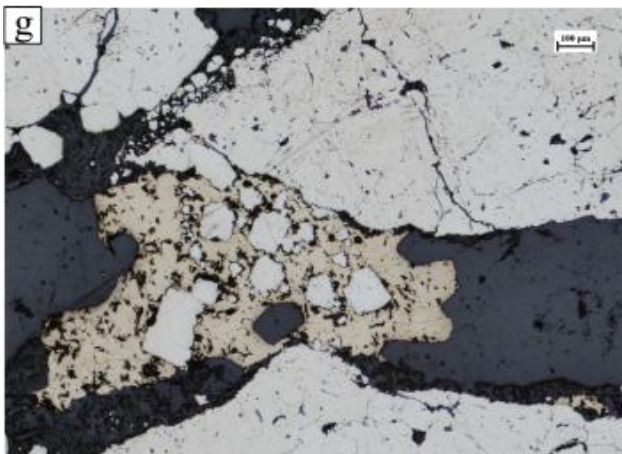
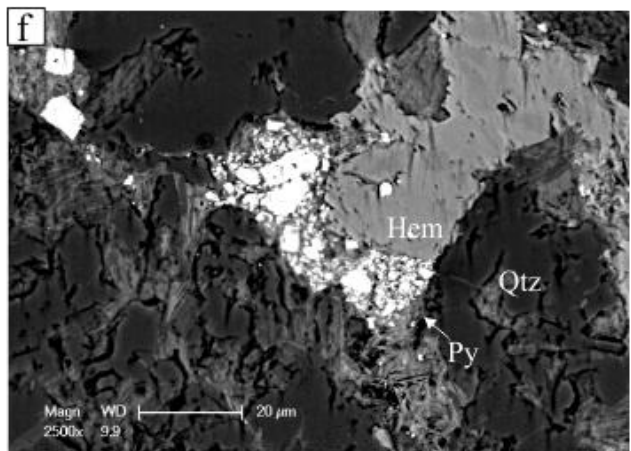
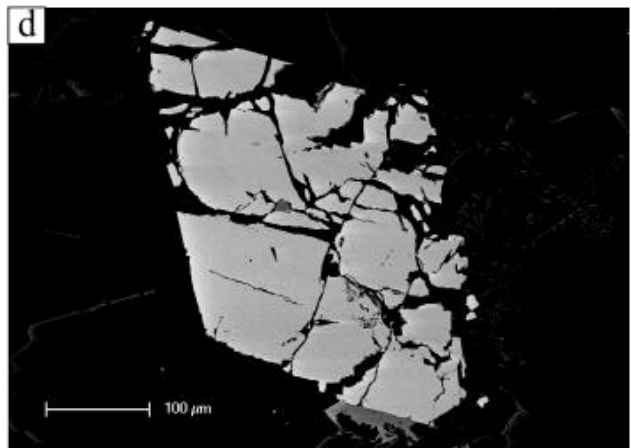
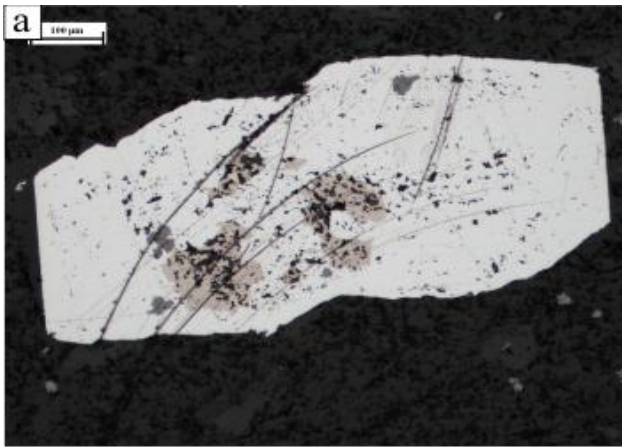


Figure section 13: SEM images of the Boudin Chert unit (and zebra in images a & c)
 a) DS24 Poikiloblastic pyrite with inclusions due to late stage growth around groundmass (black is edge of slide)
 b) DS18 Matrix chl/mus association
 c) DS25 Ilmenite, surrounded retrograde titanite
 d) DS18 Brecciated Qtz grain
 e) DS18 Microcrystalline relationship of muscovite and chlorite, usually found on the sub-mircon scale. (qtz+mus+chl in Fig:g representative of groundmass on larger scale).
 f) DS18 Grades from Fe rich to Mg rich.
 g) DS18 Chl-mus-qtz matrix (bottom), intense pyrite alteration (top) and hematite vein centre



Images section 14: Ore textures

- a) DS43 Arsenopyrite with inclusions of pyrrhotite and rutile
- b) DS25 Quartz vein with chalcopyrite mineralisation in pyrite
- c) Micron scale gold mineralization in arsenopyrite (D. Meria 2011)
- d) DS26 Early euhedral pyrite undergone re-working
- e) DS46 Reflected light image of a typical replacement texture.
- f) DS18 Hematite vein with pyrite, qtz-chl-mus groundmass
- g) DS17 Arsenopyrite + Pyrite

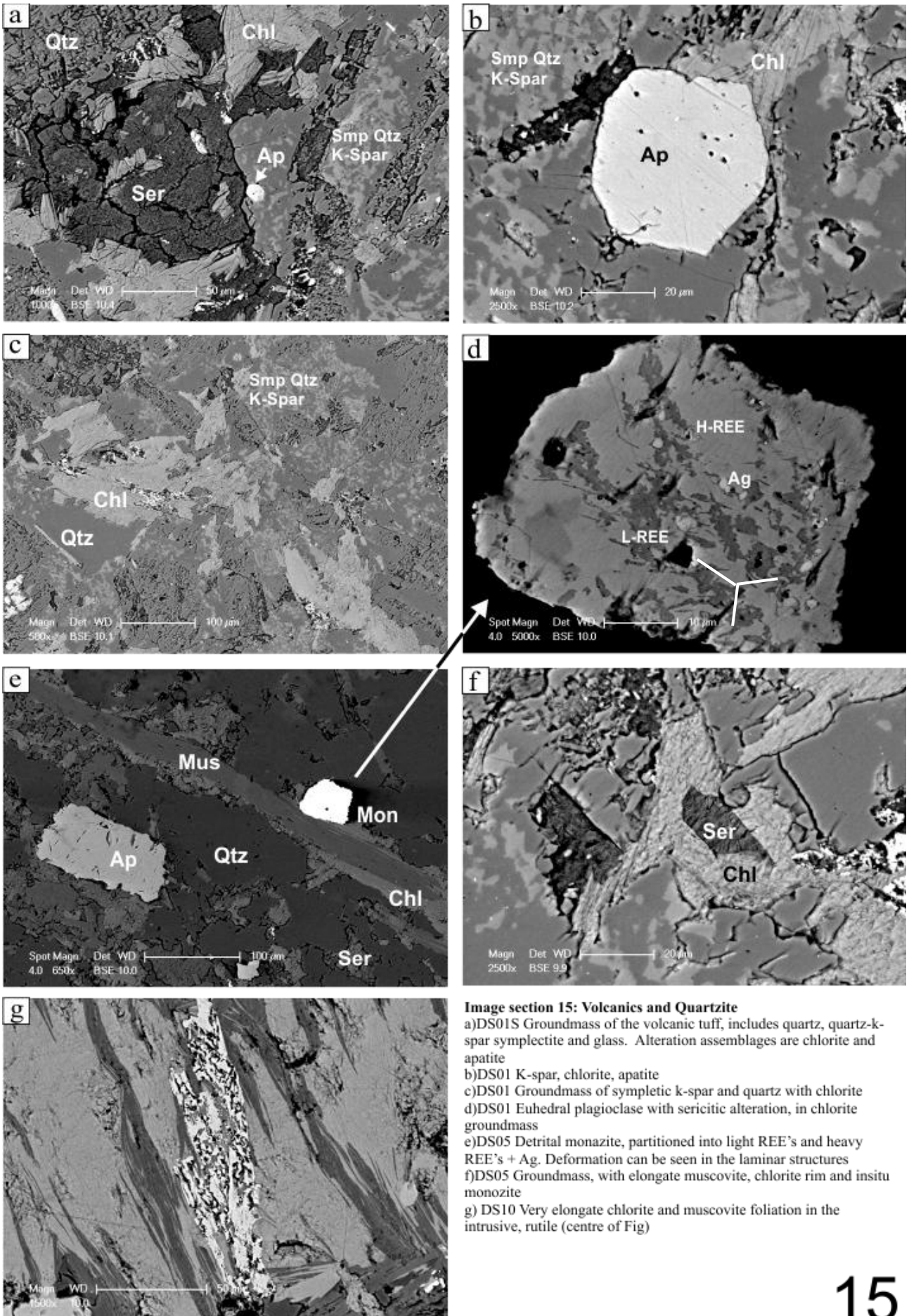


Image section 15: Volcanics and Quartzite

- a) DS01S Groundmass of the volcanic tuff, includes quartz, quartz-k-spar symplectite and glass. Alteration assemblages are chlorite and apatite
- b) DS01 K-spar, chlorite, apatite
- c) DS01 Groundmass of symplectitic k-spar and quartz with chlorite
- d) DS01 Euhedral plagioclase with sericitic alteration, in chlorite groundmass
- e) DS05 Detrital monazite, partitioned into light REE's and heavy REE's + Ag. Deformation can be seen in the laminal structures
- f) DS05 Groundmass, with elongate muscovite, chlorite rim and in-situ monazite
- g) DS10 Very elongate chlorite and muscovite foliation in the intrusive, rutile (centre of Fig)

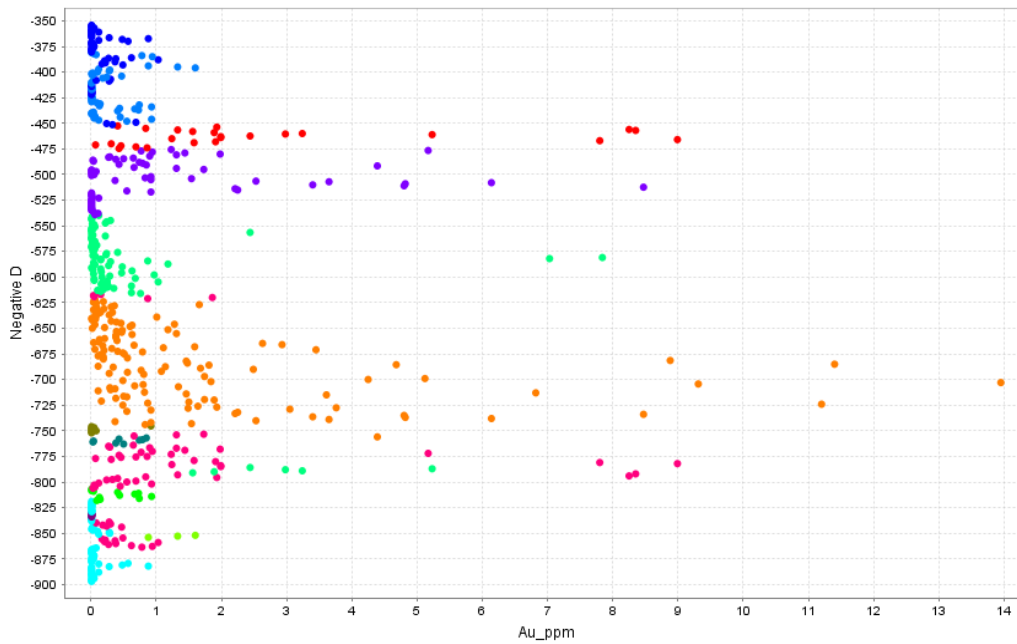
Figure 16**Au grade vs. Depth**

Figure 16. Variation of gold grades with depth in drillhole TID0065 divided by lithology, clearly showing gold enrichment at two distinct levels, the 'Upper mineralisation' hosted by the Fe enriched Boudin Chert (red and purple) and the 'Lower mineralisation' in the Fe-enriched turbidite (orange). Note for the sake of scale 3 gold assay values >25ppm are excluded from the graph in the orange turbidite unit.

Figure 17 two 17d and 17e. Is this Figure 17 or 18?

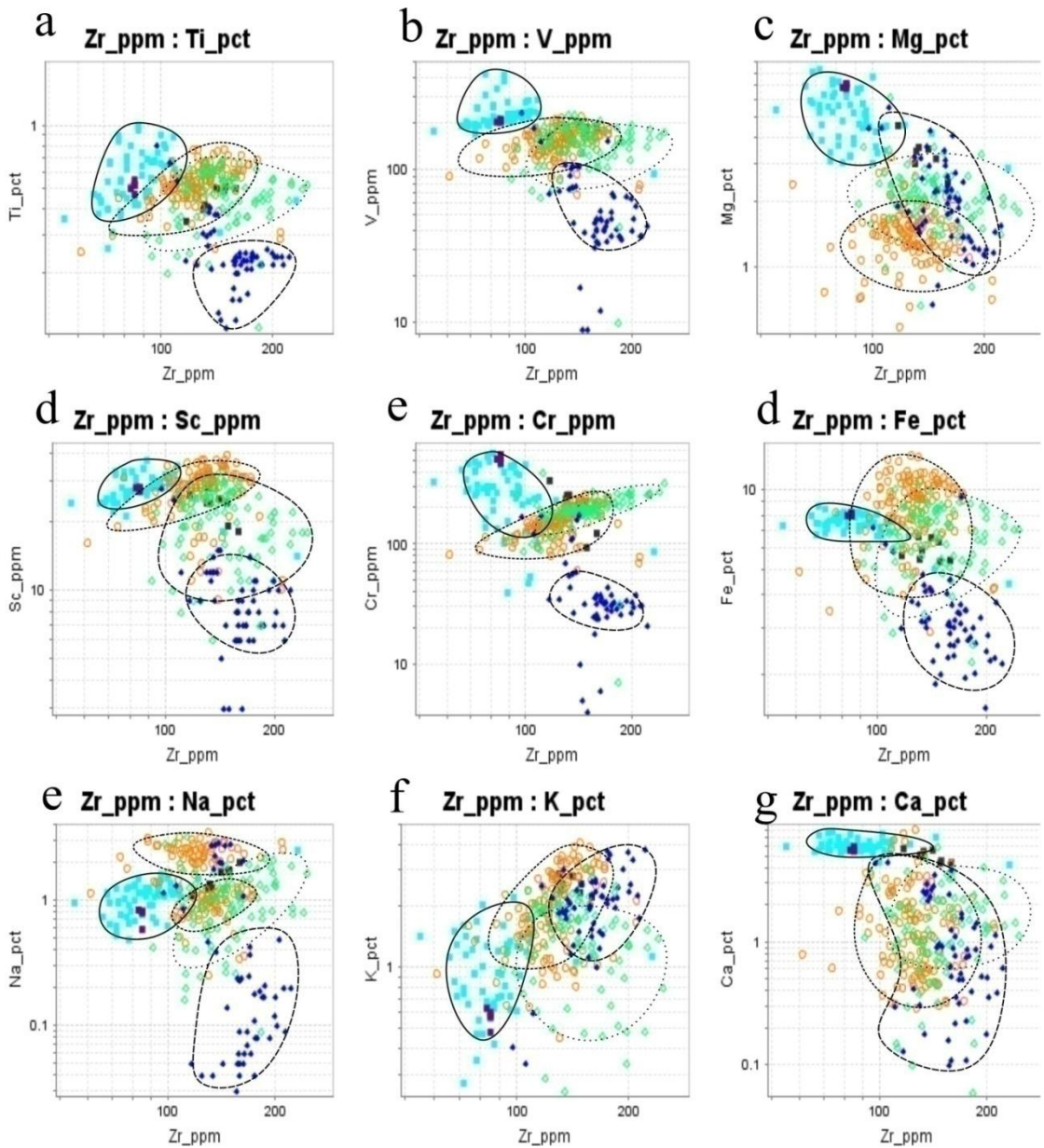

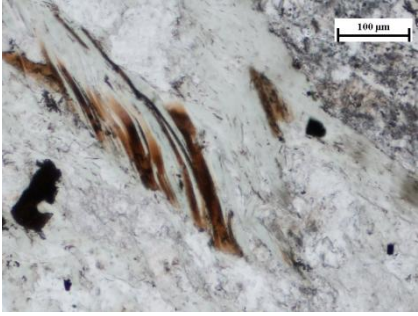
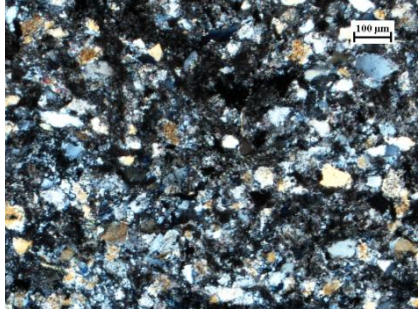
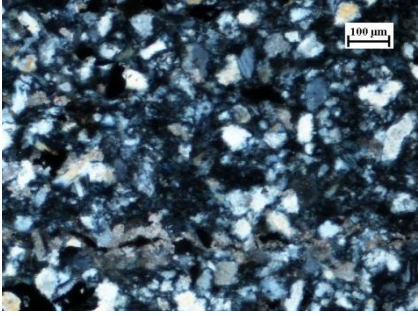
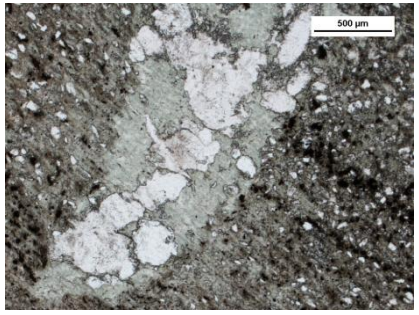
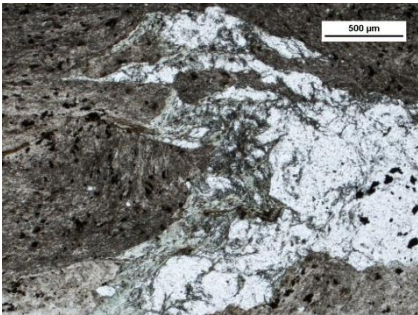


Figure 18 (8): Zirconium plotted against selected elemental groups to differentiate them base upon their chemical partitioning of elements. Relatively immobile Ti can be used as an indication of the primary enrichment and can be used as a good primary protolith tool between lithologies (the turbidite and Au hosting turbidite correlate well). Other more mobile elements active during hydrothermal alteration (eg: Mg, Fe, K, Ca) give an indication of their enrichment or depletion. The less altered turbidite gives an indication Ca-Puck is more enriched in V, Ca, Sc, Cr and Mg. Gold hosting lithologies are enriched in Fe, Na and depleted in K.



Figure 18

Comparisons between lithologies based upon petrographic observations.

<i>Lithology</i>	<i>Sample</i>	<i>Sample</i>
Sandstone (unaltered with biotite)	DS33	DS40
		
Coarse sandstone	DS38	DS31
		
Phyllite (with deformed quartz vein and chlorite)	DS28	DS39
		
	DS32	DS36

Phyllite with dominant calcite veins

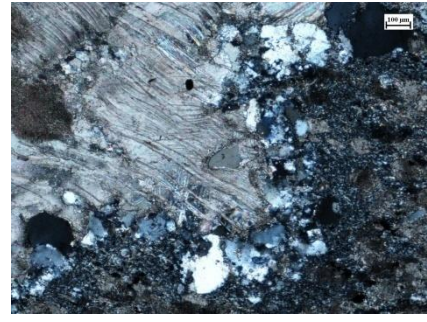
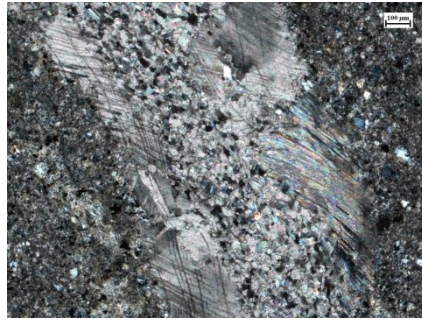
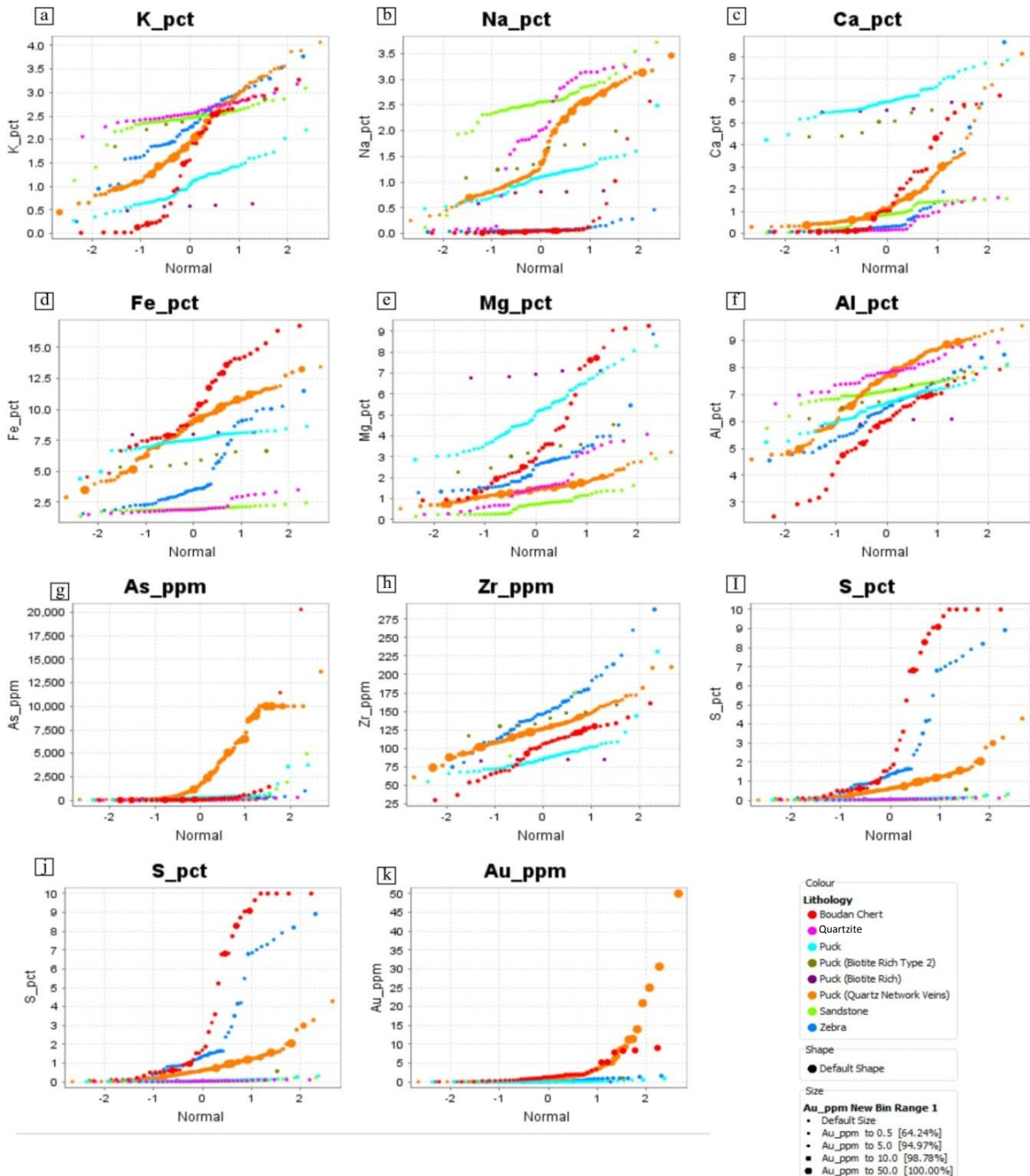


Figure 19



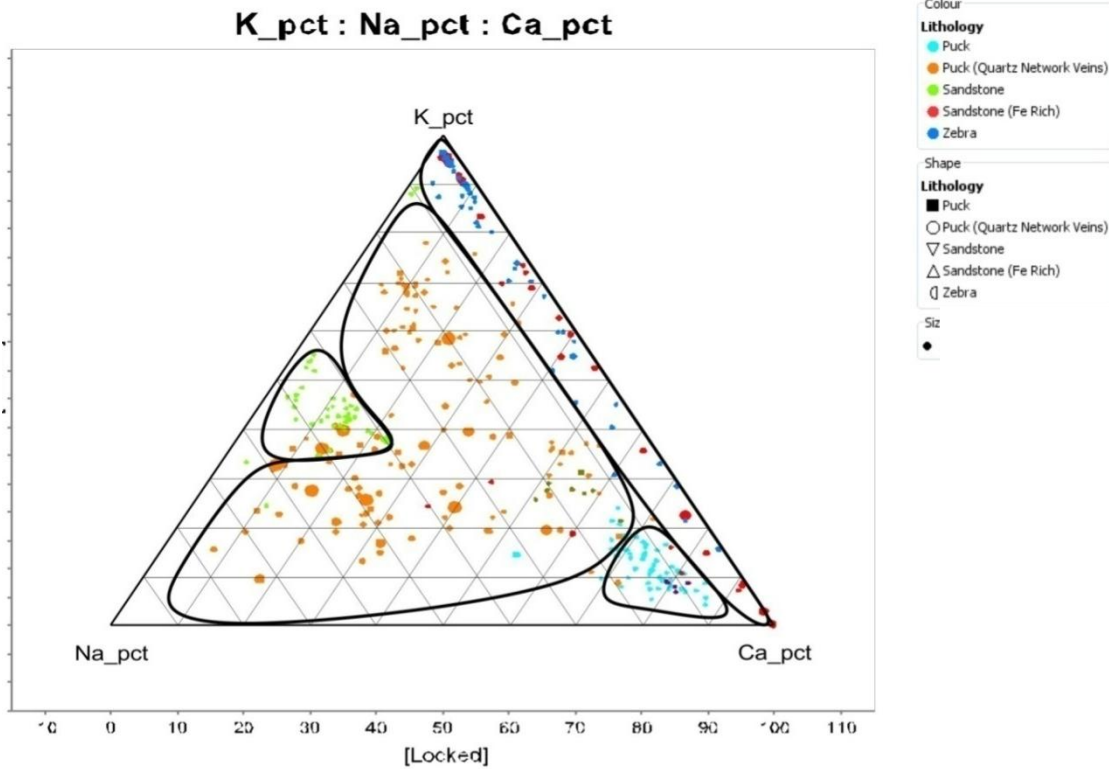


Figure 20: Distribution of K, Na and Ca in the lithologies. The Boudin Chert and the ‘Zebra rock’ show no sodic alteration. The calcareous members of the Puck unit are heavily

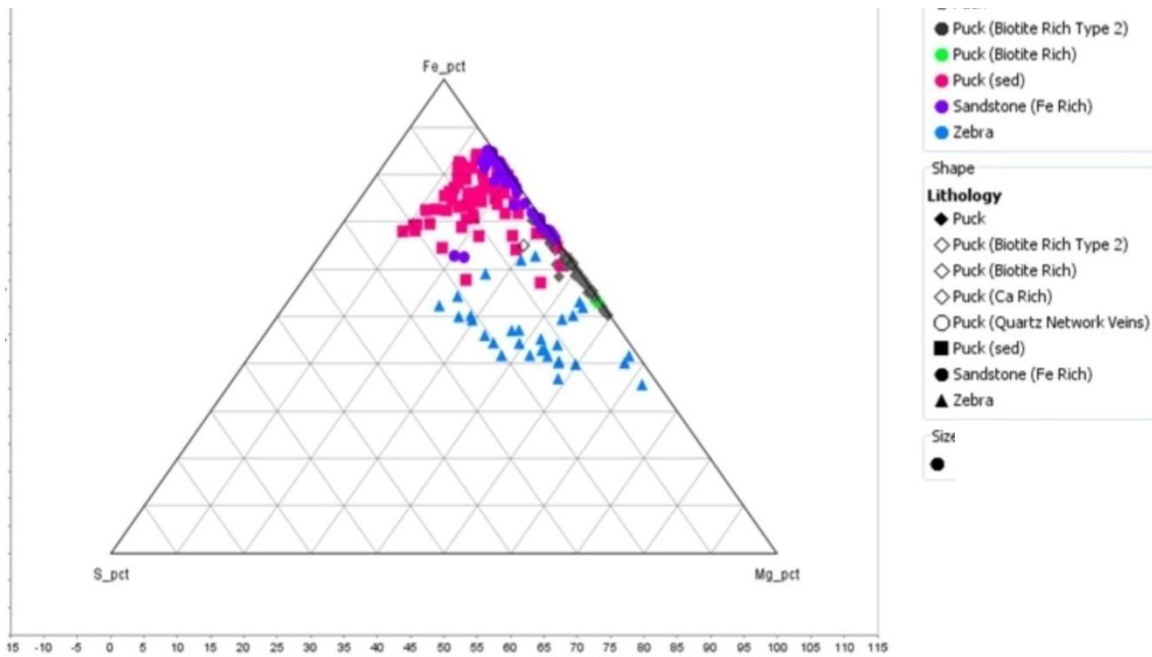


Figure 21: Fe, S and Mg plotted to differentiate the hydrothermal alteration of the units. The gold hosting turbidite (sed Puck) shows a degree of S and Fe enrichment.

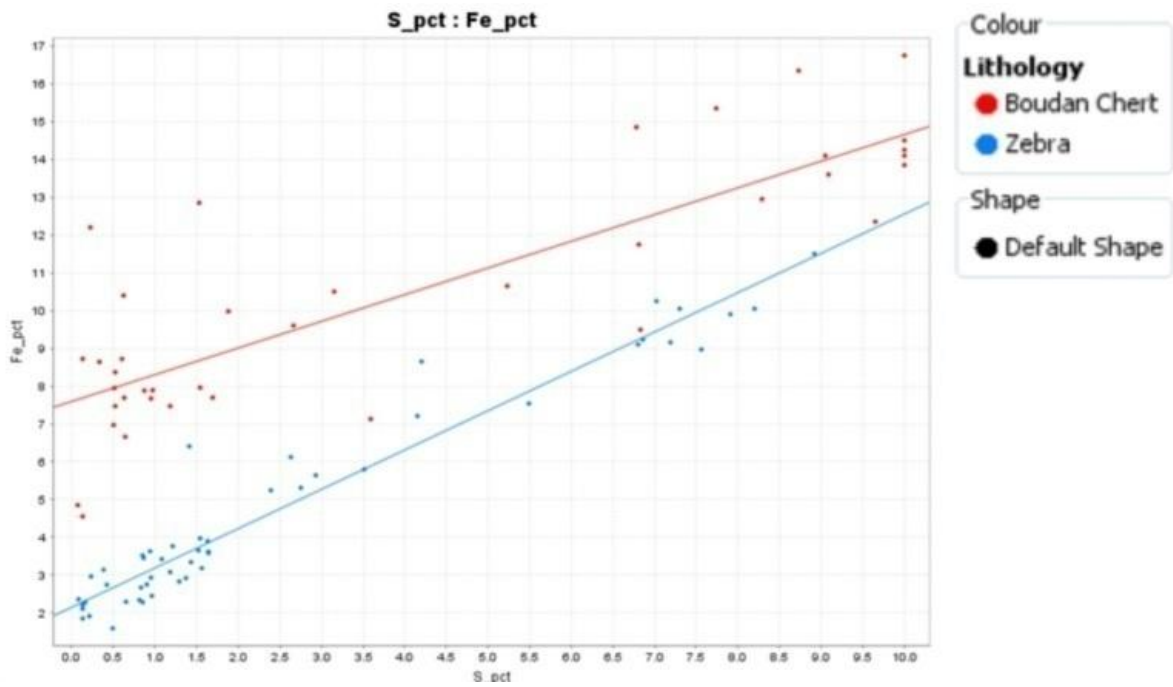
Figure 22

Figure 22: Binary plot between sulphur and iron. Shows a strong correlation in the Boudin Chert and overlying zebra between S and Fe, reflects pyrite mineralisation. Also may indicate Fe and S were both enriched at the same time, possibly at the time of the units formation on sea floor.

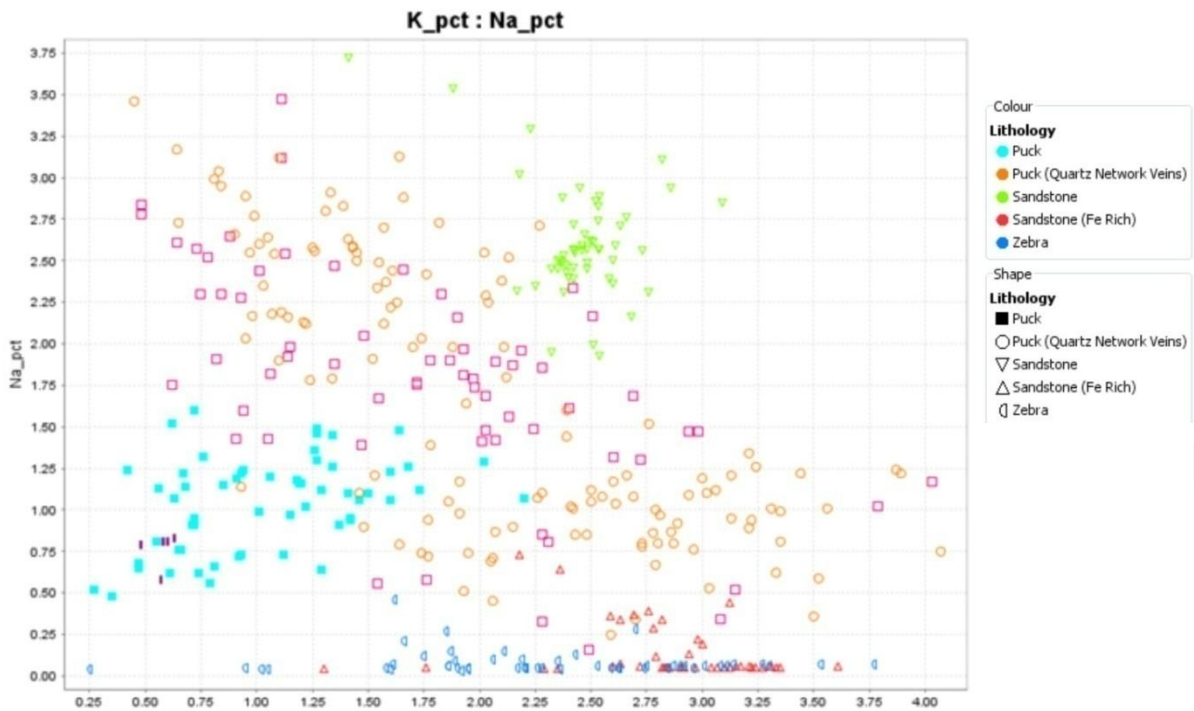


Figure 23: Binary plot between K vs. Na. The relatively unaltered sandstone (green) shows ~2.5% Na and ~2.5% K. The Au hosting turbidite however has been depleted in K possibly due to sodic metasomatism

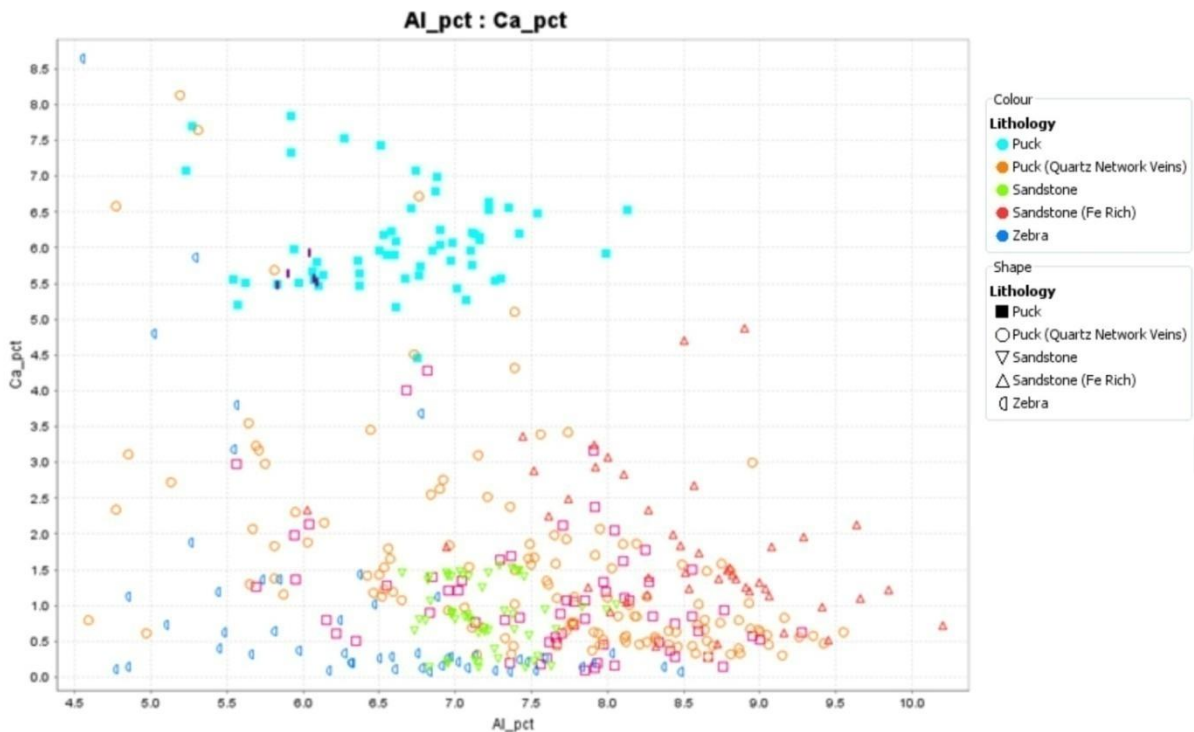


Figure 24: Binary plot between immobile Al vs. mobile Ca. The dolomitic Puck is enriched with calcium, while the other lithologies generally have little overall Ca. Ca enrichment is most likely a primary feature. Ca is predominantly found in dolomite/calcite, with no Ca found in Feldspars.

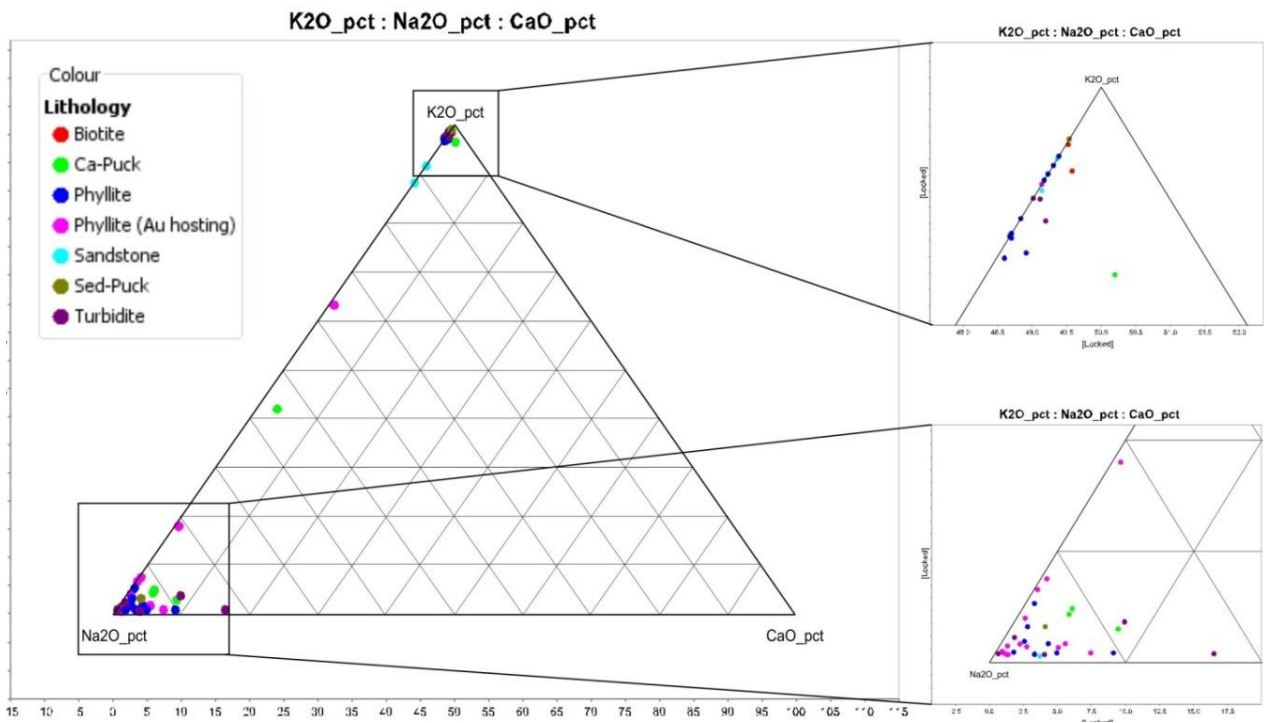


Figure 25. Ternary plot of feldspar probe data, end-members K vs. Na vs. Ca. All lithologies contain orthoclase, albite with sanidine found in the Au hosting turbidite. No Ca end-member Ca was detected in the samples, other than small amounts from that of the detrital components in the unaltered turbidite.

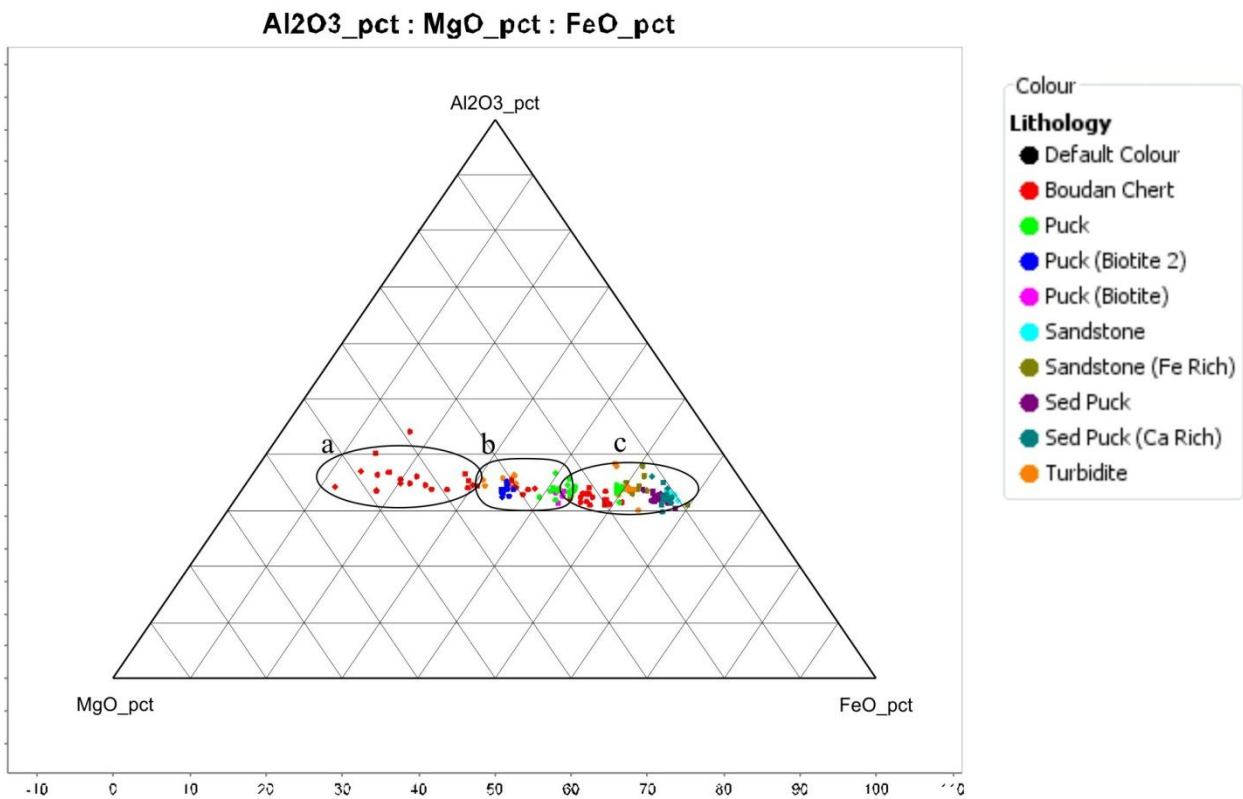


Figure 26: Ternary plot of chlorite end-members Mg & Fe, Al variation representing differing ratios, Mn was not plotted due to trace amounts in chlorite. Data base on electron probe microanalytical analysis of chlorites 15 samples. Type- A represents are Mg-dominant clinochlore species, from the Boudin Chert. Type- B has intermediate Mg/Fe = ~ 0.5 compositions, and occurs in lithologies such as the Ca-Puck and the unaltered upper turbidite sequence. Type- C represents the Fe-dominant chamosite species, typically associated with gold mineralization. The Boudin Chert sample DS18 hosts both types-A and -B, interpreted to represent two distinct generations of chlorite growth.

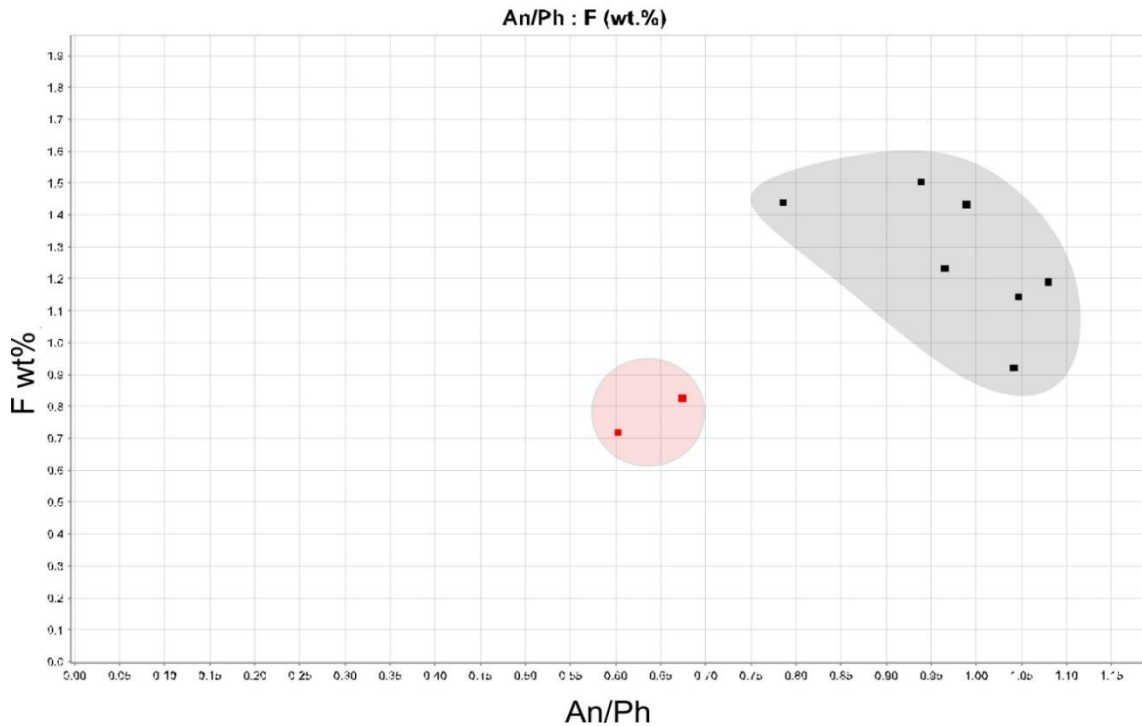


Figure 27: Compositional binary plot for biotite of F wt% vs annite/phlogopite. Samples DS33 (red) and DS40 (black), expressed in terms of annite and phlogopite end-members at wt% F. Sample DS40 has a higher F content and is hosted in the sedimentary sequence, DS40 is hosted in the Ca-Puck unit and has lower F content.

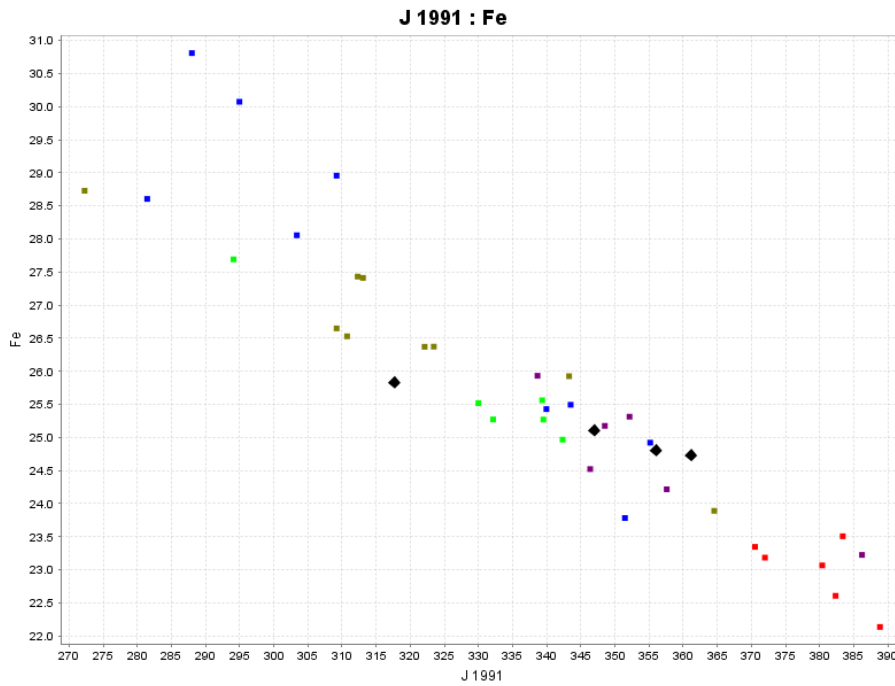


Figure 28: Binary plot of temperature estimates from chlorite geothermometry, Jowett (1991), vs. Fe a.p.f.u. for each analysed chlorite. The gold-hosting mineralogies are the Phyllite (turbidite) and Boudin Chert. Elemental Fe decreases with temperature increase in chlorite.

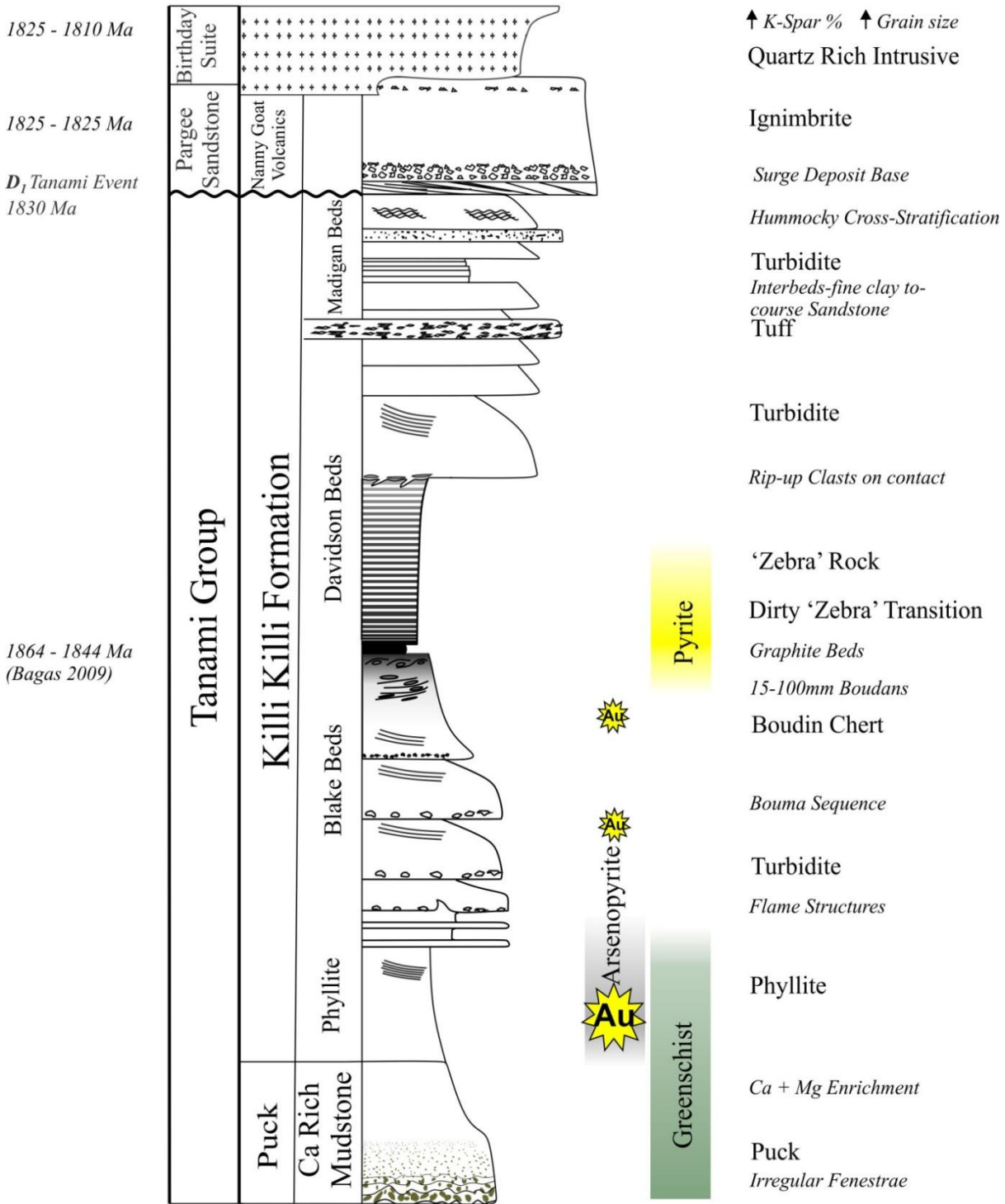


Figure 29: Interpreted stratigraphy of Oberon, a basal unit of Dolomitic mudstone grades up into the overlying fine grained meta-siltstone phyllite. Overlying this is the turbidite sequence which grades into graphitic siltstone with distinctive chert Boudins. The Boudin Chert then increases its feldspathic and quartz content in beds, defining the Zebra unit. The zebra unit is then conformably overlying by another turbiditic sequence, which grades up into a interlayer mudstone, siltstone and sandstone unit. This is in turn overlain by an ignimbrite.



Figure 30 a) and b): Rock chip samples collected from approx 1km from the discovery hole demonstrate that regional the amphibolite facies. Visible mineral assemblage is garnet (Figure 21) – sillimanite - tourmaline (Figure 22)



Figure 31 a) and b): The brittle fracturing of the 'zebra' rock that has been re-cemented with a late stage calcite. Bedding has been faulted and then re-cemented by late stage calcite alteration, demonstrating that the carbonate alteration post-dates mineralisation. Thin section image 24 shows micro scale relationship of the broken beds, calcite groundmass is one crystal.



Figure 32: Ductile deformation of a quartz vein (811m) that has undergone multiple stages of deformation. Shearing can also be seen in the cross cutting vein shown by the arrows.

Figure 33

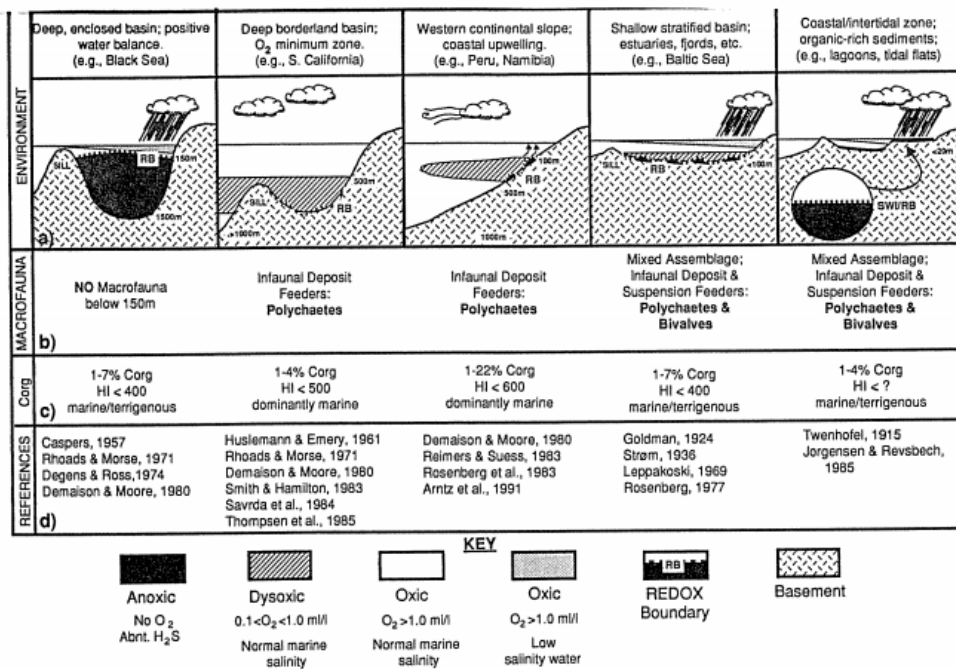


Figure 33: Marine environment organic matter accumulation demonstrating the Anoxic environment represented by figure a) and c) (Arthur & Sageman 1994).

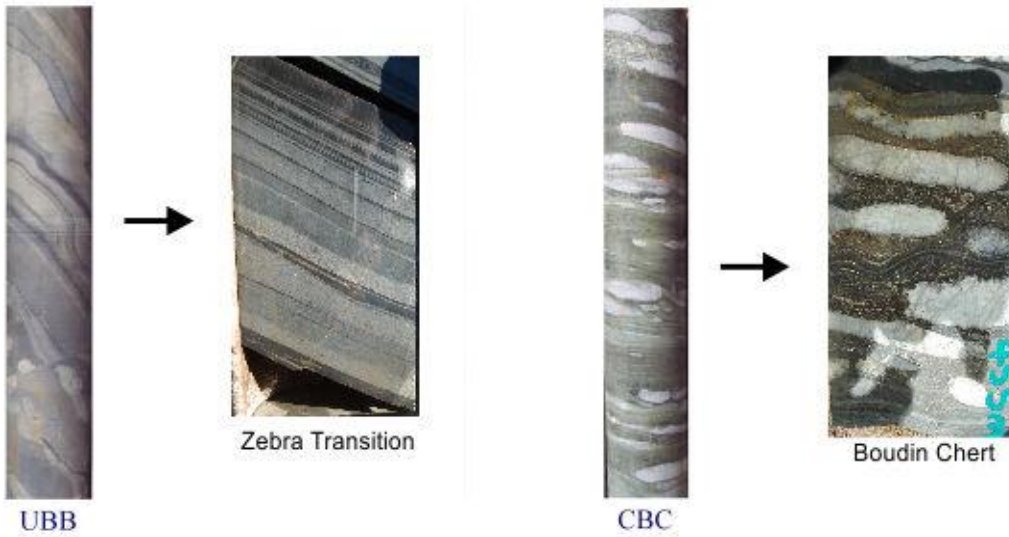


Figure 34: Comparison between the Callie mine stratigraphy and the Oberon stratigraphy.

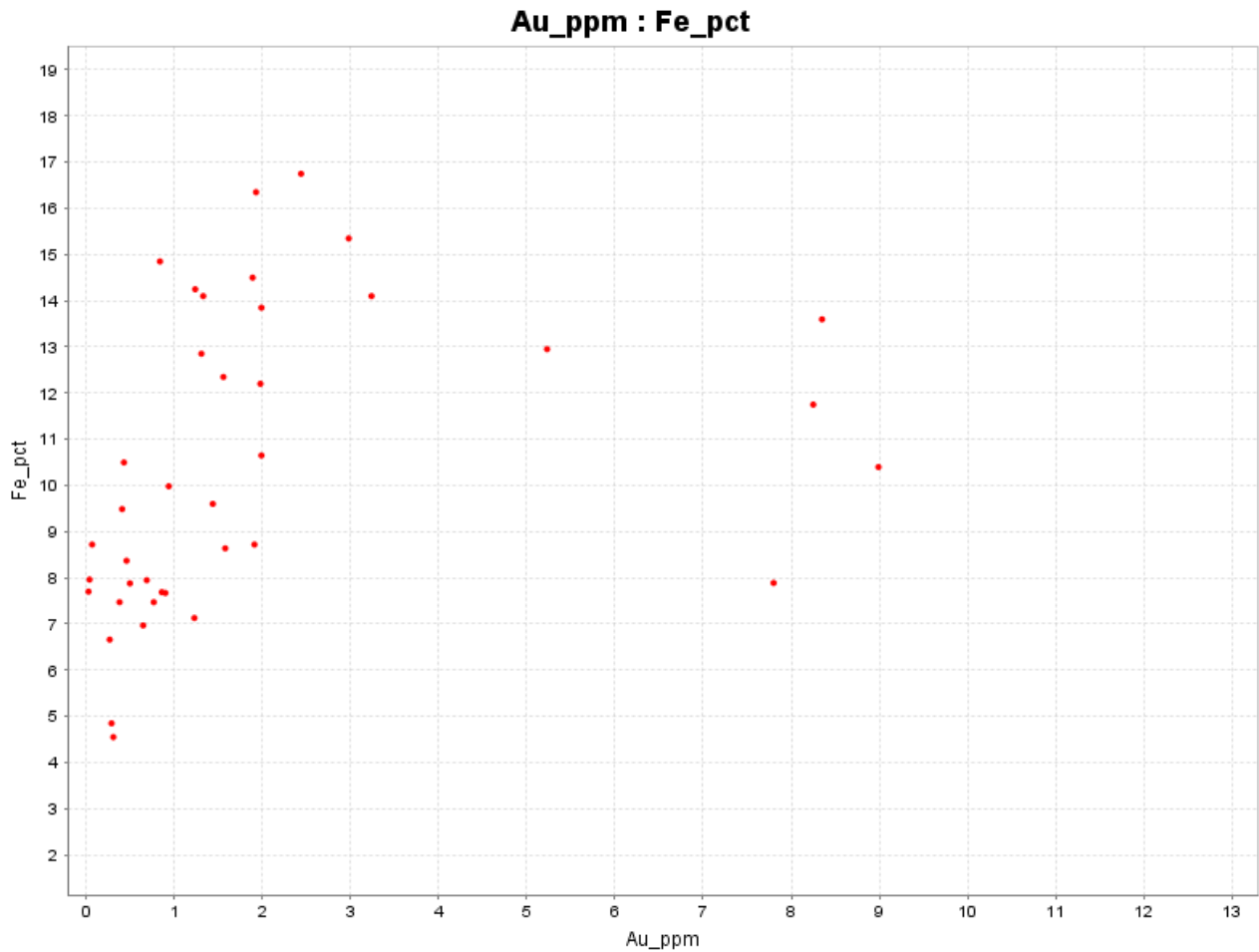


Figure 35: Positive correlation between the Fe and Au grades in the Boudan Chert unit. This is the only unit that demonstrates this correlation and may be an indicator that gold precipitation is associated with higher Fe grades in the host unit.

- ARNOLD G. L., ANBAR A. D., BARLING J. & LYONS T. W. 2004. Molybdenum isotope evidence for widespread anoxia in mid-proterozoic oceans. *Science* **304**, 87-90.
- ARTHUR M. A. & SAGEMAN B. B. 1994. MARINE BLACK SHALES - DEPOSITIONAL MECHANISMS AND ENVIRONMENTS OF ANCIENT-DEPOSITS. *Annual Review of Earth and Planetary Sciences* **22**, 499-551.
- BAGAS L., ANDERSON J. A. C. & BIERLEIN F. P. 2009. Palaeoproterozoic evolution of the Killi Killi Formation and orogenic gold mineralization in the Granites-Tanami Orogen, Western Australia. *Ore Geology Reviews* **35**, 47-67.
- BLAKE D. H. 1979. *Geology of the Granites-Tanami Region, Northern Territory and Western Australia*. Australian Govt. Pub. Service (Canberra).
- COOPER J. A. & DING P. Q. 1997. Zircon ages constrain the timing of deformation events in the the Granites-Tanami region, northwest Australia. *Australian Journal of Earth Sciences* **44**, 777-787.
- CRISPE A., VANDENBERG L. & SCRIMGEOUR I. 2007. Geological framework of the Archean and Paleoproterozoic Tanami Region, Northern Territory. *Mineralium Deposita* **42**, 3-26.
- CRISPE A. J. C. A. J. 2006. SHRIMP U–Pb analyses of detrital zircon: a window to understanding the Paleoproterozoic development of the Tanami Region, northern Australia. *Miner Deposita* **42:27–50**.
- DOTT R. H. & BOURGEOIS J. 1982. HUMMOCKY STRATIFICATION - SIGNIFICANCE OF ITS VARIABLE BEDDING SEQUENCES. *Geological Society of America Bulletin* **93**, 663-680.
- GOLDFARB R. J., GROVES D. I. & GARDOLL S. 2001. Orogenic gold and geologic time: a global synthesis. *Ore Geology Reviews* **18**, 1-75.
- GROVES D. I., GOLDFARB R. J., GEBRE-MARIAM M., HAGEMANN S. G. & ROBERT F. 1998. Orogenic gold deposits: A proposed classification in the context of their crustal distribution and relationship to other gold deposit types. *Ore Geology Reviews* **13**, 7-27.
- HENDRICKX M. 2000. Palaeoproterozoic stratigraphy of the Tanami Region. *Northern Territory Geological Survey* **GS 2000-13**.
- HUSTON D., VANDENBERG L., WYGRALAK A., MERNAGH T., BAGAS L., CRISPE A., LAMBECK A., CROSS A., FRASER G., WILLIAMS N., WORDEN K., MEIXNER T., GOLEBY B., JONES L., LYONS P. & MAIDMENT D. 2007. Lode-gold mineralization in the Tanami region, northern Australia. *Mineralium Deposita* **42**, 175-204.
- LAMBECK A., HUSTON D. & BAROVICH K. 2010. Typecasting prospective Au-bearing sedimentary lithologies using sedimentary geochemistry and Nd isotopes in poorly exposed Proterozoic basins of the Tanami region, Northern Australia. *Mineralium Deposita* **45**, 497-515.
- LAMBECK A., MERNAGH T. P. & WYBORN L. 2011. ARE IRON-RICH SEDIMENTARY ROCKS THE KEY TO THE SPIKE IN OROGENIC GOLD MINERALIZATION IN THE PALEOPROTEROZOIC? *Economic Geology* **106**, 321-330.
- MERNAGH T. & WYGRALAK A. 2007. Gold ore-forming fluids of the Tanami region, Northern Australia. *Mineralium Deposita* **42**, 145-173.
- MORITZ R. 2002. *What have we learnt about orogenic lode gold deposits over the past 20 years? Section des Sciences de la Terre, University of Geneva, Switzerland*.
- PHILLIPS G. N. 1986. Geology and alteration in the Golden Mile, Kalgoorlie. *Economic Geology* **Vol. 81**, pp. 779-808.
- QUEROL X., MORENO N., UMANA J. C., ALASTUEY A., HERNANDEZ E., LOPEZ-SOLER A. & PLANA F. 2002. Synthesis of zeolites from coal fly ash: an overview. *International Journal of Coal Geology* **50**, 413-423.
- READING H. G. & RICHARDS M. 1994. TURBIDITE SYSTEMS IN DEEP-WATER BASIN MARGINS CLASSIFIED BY GRAIN-SIZE AND FEEDER SYSTEM. *Aapg Bulletin-American Association of Petroleum Geologists* **78**, 792-822.
- SMITH L. D., PRING PI, SANDO BG 1998. Dead bullock soak gold deposits. *Aust IMM Monogr* **22**, 449–460.
- TUCKER M. E. 2001. *Sedimentary petrology : an introduction to the origin of sedimentary rocks*. Wiley-Blackwell.
- TUNKS A. & COOKE D. 2007. Geological and structural controls on gold mineralization in the Tanami District, Northern Territory. *Mineralium Deposita* **42**, 107-126.
- WILLIAMS N. 2007. The role of decarbonization and structure in the Callie gold deposit, Tanami Region of northern Australia. *Mineralium Deposita* **42**, 65-87.

Label	mineral	O% total	Depth (m)	Lithology	W%(F)	W%(Cl)	Ox%(F)	Ox%(Na)
05DS01	Chlorite	85.1684	230.1	Turbidite	0.0003	0.0001	0.0003	0.047
05DS03	Chlorite	86.8589	230.1	Turbidite	0.0004	0.0001	0.0004	0.0256
05DS04	Chlorite	82.9933	230.1	Turbidite	0.0003	0.0001	0.0003	0.0323
05DS06	Chlorite	84.0296	230.1	Turbidite	0.0003	0.0001	0.0003	0.0368
05DS08	Chlorite	86.2861	230.1	Turbidite	0.0003	0.0001	0.0003	0.0059
05DS09	Chlorite	83.5754	230.1	Turbidite	0.0003	0.0001	0.0003	0.1681
05DS10	Chlorite	82.491	230.1	Turbidite	0.0003	0.0001	0.0003	0.0348
05DS11	Chlorite	84.4825	230.1	Turbidite	0.0003	0.0001	0.0003	0.2098
05DS15	Chlorite	85.9066	230.1	Turbidite	0.0004	0.0001	0.0004	0.0454
10DS02	Chlorite	84.9056	345.9	Sandstone	0.0294	0.0249	0.0418	0.0303
10DS05	Chlorite	85.0974	345.9	Sandstone	0.0739	0.0001	0.1051	0.0197
10DS07	Chlorite	82.7385	345.9	Sandstone	0.2204	0.0031	0.3133	0.0402
10DS08	Chlorite	84.1375	345.9	Sandstone	0.0003	0.0109	0.0004	0.0025
10DS09	Chlorite	84.8872	345.9	Sandstone	0.0003	0.0001	0.0004	0.0238
10DS15	Chlorite	84.2111	345.9	Sandstone	0.0003	0.0001	0.0004	0.0322
18DS04	Chlorite	82.5083	462.5	Boudan Ch	0.0927	0.0143	0.1318	0.0063
18DS05	Chlorite	85.7716	462.5	Boudan Ch	0.1061	0.0098	0.1508	0.0209
18DS06	Chlorite	88.8917	462.5	Boudan Ch	0.1408	0.0461	0.2001	0.132
18DS07	Chlorite	84.9983	462.5	Boudan Ch	0.0934	0.0381	0.1327	0.03
18DS08	Chlorite	86.9962	462.5	Boudan Ch	0.2206	0.0271	0.3134	0.0543
18DS09	Chlorite	86.908	462.5	Boudan Ch	0.2438	0.0332	0.3465	0.0143
18DS10	Chlorite	85.982	462.5	Boudan Ch	0.1566	0.0239	0.2226	0.0112
18DS12	Chlorite	85.3987	462.5	Boudan Ch	0.0309	0.0143	0.0439	0.0643
18DS13	Chlorite	86.0551	462.5	Boudan Ch	0.1544	0.0301	0.2194	0.0307
18DS19	Chlorite	85.5935	462.5	Boudan Ch	0.2318	0.0301	0.3294	0.0221
18DS20	chlorite	89.3673	462.5	Boudan Ch	0.3132	0.0064	0.4451	0.1606
18DS21	Chlorite	89.5389	462.5	Boudan Ch	0.141	0.008	0.2004	0.2684
19DS01	Chlorite	84.3411	467	Boudan Ch	0.1237	0.0001	0.1758	0.0496
19DS02	Chlorite	91.2422	467	Boudan Ch	0.0172	0.0001	0.0244	0.0514
19DS04	Chlorite	86.9371	467	Boudan Ch	0.0003	0.0079	0.0005	0.0003
19DS05	Chlorite	85.8471	467	Boudan Ch	0.2011	0.0001	0.2858	0.0823
19DS07	Chlorite	85.5907	467	Boudan Ch	0.0312	0.0111	0.0444	0.0157
19DS08	Chlorite	88.7647	467	Boudan Ch	0.017	0.0403	0.0241	0.1478
19DS09	Chlorite	89.6732	467	Boudan Ch	0.0345	0.0081	0.049	0.3433
19DS10	Chlorite	90.7991	467	Boudan Ch	0.2427	0.0065	0.3448	0.4194
19DS11	Chlorite	82.8927	467	Boudan Ch	0.1233	0.026	0.1752	0.1348
19DS12	Chlorite	84.0939	467	Boudan Ch	0.1216	0.0178	0.1728	0.1813
20DS01C	Chlorite	86.3137	475.8	Boudan Ch	0.385	0.0001	0.5471	0.0205
20DS03F	Chlorite	86.3968	475.8	Boudan Ch	0.2693	0.0001	0.3827	0.0721
20DS07A	Chlorite	86.0865	475.8	Boudan Ch	0.7602	0.0001	1.0802	0.0118
20DS08C	Chlorite	85.2704	475.8	Boudan Ch	0.482	0.0147	0.685	0.0329
20DS09C	Chlorite	86.6335	475.8	Boudan Ch	0.414	0.0169	0.5883	0.0813
20DS10C	Chlorite	85.9405	475.8	Boudan Ch	0.5128	0.0121	0.7288	0.0267
20DS10F	Chlorite	85.9517	475.8	Boudan Ch	0.357	0.0124	0.5074	0.0356
20DS11C	Chlorite	85.2268	475.8	Boudan Ch	0.2687	0.0074	0.3818	0.0583
20DS12C	Chlorite	86.5103	475.8	Boudan Ch	0.2163	0.0222	0.3074	0.0513
20DS13C	Chlorite	86.5734	475.8	Boudan Ch	0.2834	0.0001	0.4028	0.005
20DS15C	Chlorite	85.9875	475.8	Boudan Ch	0.3594	0.0001	0.5107	0.0429
20DS16F	Chlorite	85.0285	475.8	Boudan Ch	0.3251	0.0169	0.462	0.0072

20DS17C	chlorite	85.3793	475.8 Boudan Ch	0.0754	0.0458	0.1071	0.0442
20DS18F	Chlorite	87.9247	475.8 Boudan Ch	0.0969	0.0001	0.1377	0.126
20DS19F	Chlorite	87.3978	475.8 Boudan Ch	0.3447	0.0272	0.4899	0.1285
20DS20F	Chlorite	89.3407	475.8 Boudan Ch	0.3422	0.0637	0.4864	0.1307
20DS21F	Chlorite	88.3195	475.8 Boudan Ch	0.4838	0.0548	0.6875	0.1038
20DS22C	Chlorite	84.3898	475.8 Boudan Ch	0.3265	0.0316	0.464	0.0755
20DS23C	Chlorite	83.0561	475.8 Boudan Ch	0.315	0.0394	0.4476	0.0149
20DS24C	Chlorite	87.2031	475.8 Boudan Ch	0.3439	0.0001	0.4887	0.0711
25DS01C	Chlorite	86.3237	530.2 Sandstone	0.3034	0.0188	0.4312	0.0003
25DS02C	Chlorite	84.8599	530.2 Sandstone	0.3315	0.0257	0.4711	0.0201
25DS04C	Chlorite	81.7948	530.2 Sandstone	0.3119	0.0306	0.4433	0.0698
25DS05	Chlorite	87.0707	530.2 Sandstone	0.3309	0.0001	0.4702	0.0003
25DS08C	Chlorite	86.5058	530.2 Sandstone	0.165	0.0001	0.2344	0.0349
25DS16C	Chlorite	86.4226	530.2 Sandstone	0.3686	0.0001	0.5239	0.1058
25DS17C	Chlorite	86.6007	530.2 Sandstone	0.3996	0.0023	0.5679	0.0782
25DS18C	Chlorite	86.1161	530.2 Sandstone	0.3183	0.0165	0.4524	0.115
25DS24C	Chlorite	87.4698	530.2 Sandstone	0.2783	0.0094	0.3955	0.0143
25DS25D	Chlorite	86.6543	530.2 Sandstone	0.3625	0.0071	0.5151	0.0224
27.2ch1	Chlorite	85.9404	562 Turbidite	0.3448	0.0782	0.49	0.0032
27.2ch2	Chlorite	86.9049	562 Turbidite	0.2954	0.0049	0.4198	0.0057
27DS06	Chlorite	83.9278	562 Turbidite	0.2544	0.0404	0.3615	0.1641
27DS07	Chlorite	89.9023	562 Turbidite	0.2465	0.0001	0.3503	0.0467
27DS08	Chlorite	85.4379	562 Turbidite	0.2939	0.0048	0.4176	0.7648
27DS09	Chlorite	85.3079	562 Turbidite	0.3172	0.0145	0.4508	0.0663
27DS10	Chlorite	82.4416	562 Turbidite	0.3023	0.0886	0.4296	0.2367
27DS15	Chlorite	86.9158	562 Turbidite	0.2247	0.0371	0.3193	0.1263
27DS16	Chlorite	83.1143	562 Turbidite	0.1943	0.0579	0.2762	0.1855
27DS18	Chlorite	86.6792	562 Turbidite	0.2541	0.0162	0.361	0.1178
30DS06C	Chlorite	84.1473	682.2 Sed Puck	0.3111	0.0016	0.4421	0.1576
30DS07C	Chlorite	85.4304	682.2 Sed Puck	0.3161	0.0582	0.4493	0.0748
30DS09c	Chlorite	85.6587	682.2 Sed Puck	0.3601	0.0047	0.5117	0.042
30DS11C	Chlorite	84.354	682.2 Sed Puck	0.2422	0.0047	0.3441	0.0974
30DS15C	Chlorite	84.0092	682.2 Sed Puck	0.4011	0.0564	0.57	0.1295
30DS16C	Chlorite	85.6721	682.2 Sed Puck	0.4041	0.0207	0.5743	0.0824
30DS17C	Chlorite	85.8668	682.2 Sed Puck	0.2756	0.0319	0.3917	0.1368
30DS18C	Chlorite	86.3212	682.2 Sed Puck	0.3662	0.0173	0.5204	0.1485
30DS19C	Chlorite	85.9998	682.2 Sed Puck	0.2371	0.0659	0.337	0.1461
31DS03?	Chlorite	86.5663	707.6 Sed Puck	0.3588	0.0032	0.5099	0.0363
31DS10c	Chlorite	82.3578	707.6 Sed Puck	0.3608	0.021	0.5127	0.0576
31DS11c	Chlorite	80.3063	707.6 Sed Puck	0.4458	0.0001	0.6335	0.0671
31DS12c	Chlorite	84.9451	707.6 Sed Puck	0.2733	0.0275	0.3884	0.0176
31DS20c	Chlorite	84.8724	707.6 Sed Puck	0.3175	0.0001	0.4511	0.1226
31DS25c	Chlorite	86.3761	707.6 Sed Puck	0.3616	0.013	0.5138	0.0265
33DS09	Chlorite	84.7958	750.1 Puck (Biotit	0.1584	0.0064	0.2252	0.0274
33DS11	Chlorite	84.5466	750.1 Puck (Biotit	0.2217	0.0001	0.315	0.0222
33DS15	Chlorite	84.9532	750.1 Puck (Biotit	0.1578	0.0254	0.2242	0.0205
33DS17	Chlorite	84.3579	750.1 Puck (Biotit	0.238	0.0001	0.3382	0.0003
33DS19	Chlorite	84.3995	750.1 Puck (Biotit	0.2053	0.0207	0.2917	0.002
35DS01	Chlorite	86.7163	761.9 Sed Puck (C	0.3759	0.0096	0.5342	0.08
35DS02	Chlorite	86.4217	761.9 Sed Puck (C	0.3345	0.008	0.4753	0.0752

35DS05	Chlorite	86.6799	761.9 Sed Puck (C	0.3064	0.0144	0.4354	0.055
35DS06	Chlorite	84.6651	761.9 Sed Puck (C	0.3924	0.008	0.5577	0.0302
35DS07	Chlorite	86.1536	761.9 Sed Puck (C	0.3653	0.0144	0.5192	0.1179
35DS09	Chlorite	85.205	761.9 Sed Puck (C	0.3562	0.008	0.5062	0.0717
35ds10c	Chlorite	86.1037	761.9 Sed Puck (C	0.3044	0.0001	0.4326	0.0331
35ds12c	Chlorite	87.799	761.9 Sed Puck (C	0.2657	0.021	0.3775	0.0586
35ds13c	Chlorite	83.6424	761.9 Sed Puck (C	0.3474	0.0001	0.4937	0.0479
35ds14c	Chlorite	84.8157	761.9 Sed Puck (C	0.3704	0.0128	0.5263	0.0526
35ds15c	Chlorite	85.4573	761.9 Sed Puck (C	0.2984	0.0304	0.424	0.2352
35ds18c	Chlorite	83.6561	761.9 Sed Puck (C	0.2906	0.0001	0.413	0.1037
35ds21c	Chlorite	87.0462	761.9 Sed Puck (C	0.3605	0.0128	0.5123	0.0003
35ds23c	Chlorite	88.648	761.9 Sed Puck (C	0.3522	0.008	0.5005	0.0516
38ds01	Chlorite	85.8144	794.7 Sed Puck	0.3146	0.0973	0.4471	0.2789
38ds02	Chlorite	85.2329	794.7 Sed Puck	0.3654	0.0848	0.5192	0.248
38ds08	Chlorite	86.707	794.7 Sed Puck	0.2205	0.0144	0.3134	0.1365
38ds16	Chlorite	86.7052	794.7 Sed Puck	0.2792	0.0144	0.3968	0.0548
38ds17	Chlorite	85.7033	794.7 Sed Puck	0.2495	0.0032	0.3546	0.0901
38ds18	Chlorite	85.7331	794.7 Sed Puck	0.2618	0.0272	0.3721	0.0769
38ds19	Chlorite	85.0694	794.7 Sed Puck	0.3278	0.0112	0.4659	0.0419
40DS03	Chlorite	86.275	833.1 Puck (Biotii	0.1818	0.0032	0.2583	0.2053
40DS04	Chlorite	86.3665	833.1 Puck (Biotii	0.0003	0.0001	0.0005	0.0551
40DS08	Chlorite	84.3482	833.1 Puck (Biotii	0.0661	0.0321	0.0939	0.0003
40DS10	Chlorite	86.4226	833.1 Puck (Biotii	0.0003	0.0081	0.0005	0.4335
40DS11	Chlorite	83.8718	833.1 Puck (Biotii	0.0824	0.0161	0.1171	0.0251
40DS19	Chlorite	83.7967	833.1 Puck (Biotii	0.0164	0.0161	0.0234	0.0215
40DS21	Chlorite	85.4467	833.1 Puck (Biotii	0.0816	0.0001	0.116	0.0479
40DS22	Chlorite	84.8991	833.1 Puck (Biotii	0.281	0.0289	0.3994	0.0439
40DS29	Chlorite	84.618	833.1 Puck (Biotii	0.2636	0.0129	0.3747	0.0496
40DS31	Chlorite	87.8456	833.1 Puck (Biotii	0.6976	0.0434	0.9913	0.0568
40DS32	Chlorite	89.3171	833.1 Puck (Biotii	1.0658	0.0063	1.5145	0.0326
43DS01	Chlorite	85.8766	858.7 Puck	0.0003	0.0001	0.0003	0.0252
43DS02	Chlorite	85.5841	858.7 Puck	0.0003	0.0001	0.0003	0.0098
43DS03	Chlorite	86.6854	858.7 Puck	0.0003	0.0001	0.0003	0.0354
43DS04	Chlorite	85.3913	858.7 Puck	0.0003	0.0001	0.0003	0.0541
43DS06	Chlorite	87.2616	858.7 Puck	0.0003	0.0001	0.0003	0.1166
43DS07	Chlorite	85.6101	858.7 Puck	0.0003	0.0001	0.0003	0.0731
43DS08	Chlorite	86.7473	858.7 Puck	0.0003	0.0001	0.0003	0.0478
45DS04C	Chlorite	81.292	881.6 Puck	0.2737	0.0239	0.3889	0.103
45DS10C	Chlorite	85.8904	881.6 Puck	0.348	0.0452	0.4945	0.0994
45DS11C	chlorite	86.0169	881.6 Puck	0.3082	0.0001	0.438	0.0822
45DS12C	Chlorite	86.4817	881.6 Puck	0.3289	0.0119	0.4674	0.0858
45DS15C	Chlorite	85.803	881.6 Puck	0.2909	0.0167	0.4134	0.0912
45DS18C	Chlorite	81.8424	881.6 Puck	0.2227	0.0094	0.3165	0.0701
45DS22C	Chlorite	86.7304	881.6 Puck	0.2198	0.0001	0.3124	0.0334
45DS23C	Chlorite	86.8722	881.6 Puck	0.3557	0.019	0.5055	0.0788
45DS24C	Chlorite	86.3843	881.6 Puck	0.311	0.0118	0.442	0.0376
45DS27M	Chlorite	86.7569	881.6 Puck	0.294	0.0048	0.4177	0.039
45DS28A	Chlorite	83.5422	881.6 Puck	0.2277	0.0131	0.3236	0.0319
46DS03	Chlorite	84.8998	893.8 Puck	0.0003	0.0182	0.0005	0.0564
46DS07	Chlorite	85.6005	893.8 Puck	0.2023	0.0001	0.2874	0.0071

46DS08	Chlorite	84.7154	893.8 Puck	0.223	0.002	0.3169	0.0914
46DS11	Chlorite	82.0688	893.8 Puck	0.1208	0.0001	0.1717	0.0402
46DS12	Chlorite	82.1259	893.8 Puck	0.1424	0.0001	0.2024	0.0342
46DS14	Chlorite	86.7396	893.8 Puck	0.0403	0.0284	0.0573	0.0372
46DS20	Chlorite	82.5681	893.8 Puck	0.0806	0.0001	0.1145	0.0003

Ox%(Mg)	Ox%(Al)	Ox%(Si)	Ox%(P)	Ox%(Cl)	Ox%(K)	Ox%(Ca)	Ox%(Ti)	Ox%(Cr)
18.032	20.7011	26.7018	0.0001	0.0001	0.0445	0.0964	0.0309	0.0002
19.6248	20.6247	28.5307	0.0001	0.0001	0.0328	0.0205	0.0568	0.0051
16.9757	19.8779	25.6381	0.0001	0.0001	0.0001	0.0002	0.0121	0.0118
18.1459	19.4135	26.2334	0.0001	0.0001	0.0089	0.0064	0.0002	0.0002
17.5589	21.8597	25.9724	0.0001	0.0001	0.0217	0.0171	0.0002	0.0185
16.9327	20.8888	25.3699	0.0001	0.0001	0.0188	0.0792	0.0403	0.0002
17.4476	19.5549	25.5605	0.0001	0.0001	0.0524	0.0139	0.0002	0.0002
18.0552	20.0221	26.0584	0.0001	0.0001	0.0445	0.0236	0.0175	0.0304
19.6684	19.8614	27.9078	0.0001	0.0001	0.0318	0.014	0.0662	0.0205
6.253	20.3844	22.4376	0.0003	0.0306	0.013	0.0122	0.1076	0.0002
6.8044	19.7343	23.3467	0.0183	0.0002	0.0158	0.0061	0.0494	0.0002
6.3382	19.5843	22.1369	0.0037	0.0038	0.0001	0.0193	0.0633	0.0002
6.4101	20.4127	23.1844	0.0003	0.0134	0.139	0.0173	0.0673	0.0049
6.3934	20.4357	23.0669	0.0037	0.0002	0.0317	0.0244	0.0799	0.0002
6.2067	19.4381	22.6071	0.0003	0.0001	0.0139	0.0425	0.0139	0.0096
10.9684	19.5573	24.0176	0.0003	0.0175	0.0208	0.0021	0.0155	0.0002
7.2538	11.6498	48.164	0.0003	0.012	0.0253	0.0785	0.0295	0.0035
13.4386	18.8403	27.6926	0.0411	0.0565	0.0228	0.0808	0.0156	0.0185
12.5384	19.3068	24.9676	0.0224	0.0467	0.0085	0.1303	0.048	0.0002
13.6884	18.6598	27.477	0.015	0.0332	0.019	0.0031	0.0143	0.0168
10.8088	19.3442	25.2708	0.0297	0.0407	0.0001	0.0165	0.0348	0.0002
12.4322	20.5235	25.561	0.0598	0.0292	0.0076	0.0197	0.0002	0.0002
11.7734	19.093	25.2728	0.0003	0.0175	0.0275	0.0712	0.0427	0.0002
11.6998	19.2464	25.5178	0.0149	0.0369	0.0379	0.0681	0.0002	0.0067
11.9519	18.393	26.0215	0.0003	0.0369	0.0104	0.0072	0.0285	0.0002
13.7115	20.5471	26.7522	0.0003	0.0078	0.0095	0.0259	0.0273	0.0002
13.7129	20.571	26.8946	0.0149	0.0097	0.0019	0.0052	0.0247	0.0002
12.6355	19.7562	24.1719	0.0003	0.0002	0.0103	0.0297	0.1107	0.0002
10.3651	14.9656	44.8508	0.0003	0.0002	0.0144	0.023	0.0608	0.0121
13.5506	19.3149	25.4937	0.0296	0.0096	0.032	0.0021	0.0528	0.0017
13.0439	20.0437	24.9228	0.0148	0.0002	0.0001	0.0092	0.0567	0.015
14.3537	19.3499	25.429	0.0037	0.0135	0.0387	0.0288	0.0246	0.0002
24.5868	20.1086	28.9576	0.0003	0.0494	0.0164	0.0348	0.0776	0.0002
25.9006	20.6107	30.0746	0.0003	0.0099	0.0077	0.0254	0.0002	0.0089
26.7348	20.7463	30.8096	0.0382	0.0079	0.0213	0.0127	0.0002	0.0002
24.5394	19.8924	28.6064	0.0003	0.0319	0.0701	0.0075	0.0339	0.009
24.8025	19.7915	28.0562	0.0153	0.0219	0.0223	0.1082	0.0243	0.0179
18.3467	17.8251	34.3025	0.0003	0.0002	0.3236	0.0683	0.0639	0.0002
25.8914	19.5301	32.1204	0.0003	0.0002	1.0728	0.0627	0.141	0.0002
20.5785	17.0466	24.9636	5.3655	0.0002	0.1673	6.2876	0.0002	0.0316
19.2471	17.9496	32.3085	0.0003	0.018	0.04	0.0472	0.0247	0.027
16.5153	18.2364	30.9147	0.0726	0.0208	0.044	0.0306	0.0122	0.0002
20.8845	20.5387	27.4267	0.0112	0.0149	0.0309	0.0002	0.0594	0.0574
29.5582	18.859	30.9388	0.0003	0.0152	0.0105	0.0002	0.0002	0.0002
17.4642	14.9806	40.5832	0.0003	0.0091	0.1059	0.1017	0.0229	0.0002
25.2519	19.4496	32.0221	0.0398	0.0272	0.7594	0.0346	0.021	0.0002
17.1423	20.1173	26.8	0.0003	0.0002	0.0044	0.032	0.0303	0.0224
17.8859	20.1886	26.6702	0.0003	0.0002	0.0088	0.0192	0.0061	0.0002
17.5609	19.8587	26.9653	0.0222	0.0207	0.0001	0.0433	0.0122	0.0263

17.2713	20.2836	27.1302	0.0003	0.0561	0.6018	0.0289	0.0203	0.1169
18.4613	15.7626	43.8472	0.0003	0.0002	0.087	0.0775	0.0002	0.0119
20.7304	18.3428	39.9322	0.0003	0.0333	1.5032	0.0596	0.0929	0.0002
18.9203	21.3898	37.3502	0.0003	0.0781	3.0247	0.0265	0.1599	0.052
18.8291	18.5114	25.9302	0.0601	0.0672	0.0521	0.073	8.255	0.0116
19.3675	19.9001	28.8914	0.0003	0.0387	0.7955	0.0276	0.0308	0.0193
25.1322	17.3018	31.3042	0.0003	0.0483	0.0597	0.0723	0.0021	0.0002
16.6297	20.3602	26.9325	0.0166	0.0002	0.0262	0.0002	0.0504	0.0746
8.7988	20.7298	24.4806	0.0108	0.0231	0.268	0.0704	0.1235	0.0071
5.6035	18.7308	24.0441	0.0323	0.0315	0.1499	0.107	0.0542	0.021
8.0768	20.0306	22.7392	0.0487	0.0375	0.4218	0.1048	0.0686	0.1285
9.3121	21.402	25.3039	0.0109	0.0002	0.4187	0.0314	0.122	0.0216
9.4788	20.9331	24.279	0.0108	0.0002	0.2109	0.0016	0.0823	0.0002
6.7947	22.2319	26.0377	0.0003	0.0002	1.4208	0.1796	0.0988	0.0217
8.2095	20.7955	24.0262	0.0054	0.0029	0.1963	0.245	0.0606	0.0142
7.3284	21.4656	25.4097	0.0003	0.0202	0.9315	0.2039	0.0787	0.0251
9.7205	20.7981	24.0662	0.0003	0.0115	0.0085	0.2385	0.0547	0.0002
9.5568	20.5676	24.6739	0.0108	0.0087	0.3606	0.1033	0.0098	0.0036
9.1025	20.6723	24.0607	0.0113	0.0959	0.2291	0.0076	0.0706	0.1631
9.6895	21.4335	23.9316	0.0338	0.006	0.0276	0.1289	0.0394	0.0371
8.3368	21.1883	26.2771	0.1226	0.0495	1.7057	0.1113	0.125	0.0275
5.5182	10.212	55.6868	0.0039	0.0002	0.0201	0.021	0.0685	0.0444
9.1314	19.7795	26.7108	0.0149	0.0059	0.0372	0.0547	0.0404	0.0468
10.5884	20.0826	23.8442	0.037	0.0178	0.0799	0.0513	0.13	0.0002
9.9957	19.8388	23.0806	0.1038	0.1086	0.04	0.3008	0.0497	0.0049
8.8443	22.3129	26.2117	0.0705	0.0455	1.5104	0.069	0.1247	0.01
9.517	20.1037	22.9646	0.0555	0.071	0.1052	0.1037	0.0563	0.0464
8.8729	19.4712	28.3151	0.1079	0.0198	0.3681	0.0871	0.0931	0.0049
7.0135	19.6985	23.9443	0.1587	0.0019	0.0598	0.1508	0.0547	0.0002
6.3513	18.212	28.1635	0.0543	0.0713	0.0228	0.0782	0.0002	0.0237
6.4384	18.6114	27.7308	0.0434	0.0058	0.0475	0.0824	0.0431	0.0119
6.4817	19.2103	24.4723	0.0072	0.0058	0.0767	0.0986	0.0376	0.0002
6.8847	18.8514	24.9392	0.1009	0.0691	0.0664	0.1144	0.0703	0.0165
6.4195	15.2732	37.2702	0.0003	0.0254	0.0463	0.0518	0.0399	0.0073
6.2719	14.9882	38.0777	0.0003	0.0391	0.0531	0.0614	0.0266	0.0073
8.2507	20.2664	25.6115	0.1121	0.0212	0.0295	0.145	0.1321	0.0024
6.8975	18.7587	26.9699	0.2095	0.0808	0.1026	0.1991	0.0509	0.0095
7.5638	20.6778	23.2035	0.0558	0.004	0.0303	0.0525	0.0335	0.0898
7.0084	18.7155	22.2471	0.0408	0.0257	0.0469	0.0386	0.0963	0.0411
6.5851	17.9333	21.0398	0.0703	0.0001	0.0146	0.0448	0.0773	0.0529
7.351	19.9933	22.6967	0.0186	0.0337	0.0001	0.0343	0.087	0.0363
7.212	20.0345	22.6587	0.0074	0.0001	0.0088	0.0086	0.0991	0.0945
7.96	20.6287	23.5679	0.0559	0.0159	0.0265	0.0473	0.0915	0.0439
14.8621	20.1315	24.7438	0.0224	0.0078	0.0371	0.0218	0.1436	0.0002
15.1212	19.7727	24.8186	0.0003	0.0002	0.0105	0.0415	0.0653	0.0118
14.8049	19.401	25.1184	0.0149	0.0312	0.0931	0.0145	0.133	0.0034
15.1619	18.1718	25.8432	0.0075	0.0002	0.1036	0.0353	0.0666	0.2217
14.3797	19.8609	24.6048	0.1083	0.0253	0.0209	0.113	0.0587	0.076
7.0062	19.6232	23.8155	0.0003	0.0117	0.0396	0.0328	0.078	0.0215
6.8878	20.0264	24.0349	0.0184	0.0098	0.2806	0.0021	0.0862	0.0048

7.8264	19.102	24.3403	0.0441	0.0176	0.1142	0.018	0.2056	0.1803
7.8786	17.7783	23.4377	0.0003	0.0098	0.0319	0.0085	1.2945	0.0193
7.4056	19.6781	23.9297	0.0883	0.0176	0.1724	0.0149	0.0372	0.0048
6.437	19.7826	23.6286	0.1212	0.0098	0.1712	0.0265	0.106	0.0983
7.2813	19.6951	24.4709	0.0037	0.0001	0.4273	0.0064	0.5376	0.0508
5.7042	19.31	31.0987	0.0297	0.0257	1.3395	0.0054	0.1147	0.0518
6.8748	19.7149	22.6087	0.0074	0.0001	0.1113	0.0191	0.11	0.0672
6.8102	19.5091	23.1506	0.0514	0.0157	0.1005	0.2437	0.2027	0.0672
6.8293	20.1316	23.2539	0.1471	0.0372	0.2004	0.0722	0.1009	0.0288
6.7637	19.0147	23.588	0.0994	0.0001	0.0707	0.1539	0.0504	0.0601
6.2284	20.4538	25.5788	0.0184	0.0157	0.9977	0.0384	0.1348	0.0024
6.7965	21.7052	26.8685	0.0517	0.0098	1.1923	0.0075	0.239	0.0662
7.9854	18.6519	26.1381	0.0771	0.1193	0.1991	0.036	0.1062	0.1304
7.1916	17.2976	21.1777	0.1184	0.1039	0.2858	0.0449	8.8578	0.1088
7.7784	20.7839	24.1516	0.0515	0.0176	0.0406	0.0001	0.0756	0.13
7.8965	19.8129	24.4103	0.0221	0.0176	0.091	0.1815	0.089	0.0698
7.7985	19.7309	23.6878	0.0368	0.0039	0.0822	0.0498	0.0849	0.048
7.741	19.7874	24.3684	0.0294	0.0333	0.2953	0.0276	0.0744	0.07
7.4715	19.7737	24.0233	0.0221	0.0137	0.4028	0.034	0.0492	0.0506
18.0369	20.5235	27.4133	0.053	0.0039	0.0337	0.0515	0.0531	0.0764
18.1737	20.3037	27.4319	0.0719	0.0002	0.0356	0.0357	0.0331	0.0659
17.9894	19.3677	26.3704	0.0718	0.0394	0.0836	0.0598	0.1166	0.3364
17.9431	19.2947	28.7302	0.0682	0.0099	0.3082	0.0568	0.0199	0.0157
18.4177	18.8884	26.6491	0.0003	0.0197	0.0308	0.0535	0.0398	0.0676
18.6859	18.4414	26.53	0.0492	0.0197	0.0606	0.0189	0.0756	0.0919
18.1586	19.9245	25.9265	0.0377	0.0002	0.1996	0.0388	0.0688	0.038
18.5439	19.4201	26.7752	0.0003	0.0355	0.2316	0.084	0.0796	0.1025
18.635	19.1052	26.3728	0.0264	0.0157	0.3306	0.0242	0.1857	0.0295
15.4386	15.8132	36.0455	0.0151	0.0532	2.4483	0.0255	0.5866	0.0088
14.8166	15.1479	34.3062	0.0408	0.0078	7.4495	0.031	1.6399	0.0733
10.4837	20.2342	24.5335	0.0001	0.0001	0.1501	0.2506	0.0326	0.0306
9.6904	20.4181	25.4299	0.0001	0.0001	0.3754	0.0137	0.0745	0.0242
10.5354	18.4839	27.7661	0.0001	0.0001	0.0398	0.0473	0.0419	0.0002
9.8994	19.9149	25.8099	0.0001	0.0001	0.1514	0.0357	0.0379	0.0226
10.2979	21.2648	25.3291	0.0001	0.0001	0.1709	0.0736	0.0366	0.0129
10.4758	20.6394	24.1065	0.0001	0.0001	0.0902	0.0094	0.1279	0.0193
10.7476	20.394	24.4864	0.0001	0.0001	0.0242	0.3724	0.0953	0.0002
12.603	19.5424	26.648	0.1655	0.0294	0.9196	0.1823	0.0222	0.0747
13.9535	20.7973	25.2121	0.0439	0.0555	0.049	0.1758	0.0538	0.0002
13.8892	20.5005	24.8974	0.0003	0.0002	0.0072	0.0522	0.0894	0.0002
13.1736	20.9839	26.7748	0.055	0.0146	0.5586	0.0827	0.0681	0.0002
13.7081	20.4602	25.2275	0.0989	0.0205	0.0535	0.1189	0.0299	0.022
13.2853	18.2675	20.9817	0.0003	0.0115	0.0513	4.5247	0.0301	0.0074
14.0024	20.6555	24.8631	0.0328	0.0002	0.0316	0.2779	0.0002	0.0002
13.0536	19.9724	26.2138	0.0764	0.0233	0.0345	0.0773	1.9299	0.0002
13.5876	19.2046	23.9972	0.1733	0.0145	0.2089	0.0471	4.3116	0.0296
13.9337	20.7726	25.4366	0.0329	0.0058	0.0317	0.0601	0.0437	0.0002
1.3694	18.0207	0.0818	0.0003	0.0161	0.0664	0.0001	3.1719	17.7912
14.6005	19.5867	24.9689	0.0095	0.0223	0.0533	0.0568	0.8527	0.3575
15.1594	20.2891	25.3146	0.0191	0.0002	0.0001	0.0106	0.0849	0.0002

15.3803	19.8828	25.1755	0.0003	0.0025	0.0001	0.0331	0.0002	0.0002
14.8684	19.9747	23.2246	0.0333	0.0002	0.0001	0.0502	0.0698	0.0002
15.9681	18.5135	24.5228	0.1335	0.0002	0.0001	0.0635	0.1634	0.0002
15.8047	19.2874	25.9335	0.0286	0.0348	0.0036	0.004	0.0914	0.028
14.2875	19.7505	24.2164	0.0143	0.0002	0.0133	0.0594	0.0665	0.0002

Ox%(Mn)	Ox%(Fe)	NbCat(Al)	NbCat(Si)	MgO/FeO	Fe+Mg	B.Current
0.2908	19.2235	37.5463	37.4128	0.003236	0.031	19.82
0.0309	17.9068	37.5625	37.4641	0.001761	0.0569	19.81
0.2594	20.1855	37.4206	37.4203	0.008264	0.0122	19.8
0.2393	19.9448	38.33	38.3033	0.5	0.0003	19.8
0.2153	20.6162	38.3904	38.3253	0.5	0.0003	19.79
0.2496	19.8276	37.0099	36.9535	0.002481	0.0404	19.79
0.212	19.6143	37.2739	37.1167	0.5	0.0003	19.79
0.1915	19.8293	38.076	37.9425	0.005714	0.0176	19.8
0.1617	18.1292	37.9593	37.8639	0.001511	0.0663	19.78
0.2205	35.4159	41.8894	41.8504	0.231413	0.1325	19.97
0.276	34.8263	41.9067	41.8593	0.002024	0.0495	19.98
0.1849	34.3636	40.8867	40.8864	0.048973	0.0664	19.98
0.1431	33.7425	40.2957	39.8787	0.161961	0.0782	19.98
0.1948	34.6325	41.2207	41.1256	0.001252	0.08	19.98
0.2362	35.6105	42.0534	42.0117	0.007194	0.014	19.99
0.0002	27.9021	38.8707	38.8083	0.922581	0.0298	19.9
0.0002	18.5338	25.7878	25.7119	0.332203	0.0393	19.9
0.0002	28.5527	41.9915	41.9231	2.955128	0.0617	19.9
0.0629	27.8365	40.4378	40.4123	0.79375	0.0861	19.91
0.0366	26.9787	40.7037	40.6467	1.895105	0.0414	19.91
0.0296	31.3183	42.1567	42.1564	0.954023	0.068	19.9
0.0002	27.3372	39.7696	39.7468	119.5	0.0241	19.9
0.0298	29.006	40.8092	40.7267	0.334895	0.057	19.9
0.0463	29.3494	41.0955	40.9818	150.5	0.0303	19.9
0.0562	29.0653	41.0734	41.0422	1.05614	0.0586	19.91
0.0531	28.0718	41.8364	41.8079	0.234432	0.0337	19.92
0.0066	28.0288	41.7483	41.7426	0.323887	0.0327	19.92
0.2398	27.3367	40.212	40.1811	0.000903	0.1108	20.08
0.1476	20.7509	31.2636	31.2204	0.001645	0.0609	20.09
0.1445	28.3053	42.0004	41.9044	0.149621	0.0607	20.08
0.1314	27.527	40.7023	40.702	0.001764	0.0568	20.09
0.122	26.2109	40.6866	40.5705	0.45122	0.0357	20.08
0.0068	14.7784	39.372	39.3228	0.51933	0.1179	20.08
0.0002	12.6914	38.5922	38.5691	40.5	0.0083	20.09
0.0136	11.9949	38.7433	38.6794	32.5	0.0067	20.09
0.0171	9.5499	34.1064	33.8961	0.766962	0.0599	20.07
0.0068	11.0457	35.855	35.7881	0.73251	0.0421	20.09
0.0426	15.3198	33.7091	32.7383	0.001565	0.064	13.44
0.1192	7.3864	33.397	30.1786	0.000709	0.1411	13.44
0.0377	11.5959	32.2121	31.7102	0.5	0.0003	13.41
0.0747	15.5004	34.8222	34.7022	0.595142	0.0394	13.41
0.0739	20.6315	37.2207	37.0887	1.385246	0.0291	13.41
0.0743	16.8156	37.7744	37.6817	0.203704	0.0715	13.43
0.0002	6.5333	36.0917	36.0602	62	0.0126	13.43
0.0161	11.8843	29.3646	29.0469	0.323144	0.0303	13.43
0.0487	8.8045	34.1051	31.8269	1.057143	0.0432	13.43
0.0367	22.3825	39.5615	39.5483	0.0033	0.0304	13.44
0.0683	21.0968	39.051	39.0246	0.016393	0.0062	13.45
0.0002	20.5114	38.0725	38.0722	1.385246	0.0291	13.44

0.0842	19.7415	37.097	35.2916	2.256158	0.0661	13.45
0.0325	9.518	28.0118	27.7508	0.5	0.0003	13.43
0.0869	6.4875	27.3048	22.7952	0.292788	0.1201	13.45
0.0812	8.127	27.1285	18.0544	0.398374	0.2236	13.44
0.0477	16.3783	35.2551	35.0988	0.006638	8.3098	13.46
0.133	15.1101	34.6106	32.2241	1.025974	0.0624	13.45
0.0002	9.1199	34.2523	34.0732	18.7619	0.0415	13.44
0.1311	22.9103	39.6711	39.5925	0.001984	0.0505	13.42
0.1125	31.6988	40.6101	39.8061	0.152227	0.1423	13.48
0.0506	36.0149	41.669	41.2193	0.47417	0.0799	13.47
0.0307	30.0378	38.1453	36.8799	0.446064	0.0992	13.48
0.1436	30.304	39.7597	38.5036	0.00082	0.1221	13.49
0.0511	31.4229	40.9528	40.3201	0.001215	0.0824	13.5
0.0772	29.4539	36.3258	32.0634	0.001012	0.0989	13.47
0.0002	32.9667	41.1764	40.5875	0.037954	0.0629	13.48
0.0002	30.5375	37.8661	35.0716	0.209657	0.0952	13.49
0.1581	32.3989	42.2775	42.252	0.171846	0.0641	13.51
0.1023	31.2345	40.8936	39.8118	0.72449	0.0169	13.5
0.085	31.4391	40.6266	39.9393	1.107649	0.1488	19.47
0.1205	31.4513	41.2613	41.1785	0.124365	0.0443	19.48
0.0953	25.7246	34.1567	29.0396	0.3232	0.1654	19.76
0.0002	18.2803	23.7987	23.7384	0.00146	0.0686	19.76
0.0527	28.7988	37.9829	37.8713	0.118812	0.0452	19.76
0.0002	30.41	40.9986	40.7589	0.111538	0.1445	19.76
0.035	28.647	38.6777	38.5577	1.782696	0.1383	19.76
0.0247	27.5658	36.4348	31.9036	0.297514	0.1618	19.76
0.042	29.8634	39.4224	39.1068	1.028419	0.1142	19.75
0.0703	29.151	38.0942	36.9899	0.174006	0.1093	19.75
0.0544	32.8529	39.9208	39.7414	0.02925	0.0563	20.19
0.0648	32.3135	38.7296	38.6612	291	0.0584	20.2
0.0341	32.5679	39.0404	38.8979	0.109049	0.0478	20.2
0.0814	33.7848	40.3479	40.1178	0.125	0.0423	20.21
0.0238	32.743	39.6515	39.4523	0.802276	0.1267	20.21
0.0553	26.4005	32.8753	32.7364	0.518797	0.0606	20.21
0.045	26.1594	32.4763	32.317	1.199248	0.0585	20.2
0.0136	31.5882	39.8525	39.764	0.130961	0.1494	20.22
0.0341	32.5411	39.4727	39.1649	1.294695	0.1168	20.21
0.0666	34.7524	42.3828	42.2919	0.095522	0.0367	19.54
0.0735	33.9663	41.0482	40.9075	0.218069	0.1173	19.53
0.0209	34.4001	41.0061	40.9623	0.001294	0.0774	19.54
0.056	34.6205	42.0275	42.0272	0.316092	0.1145	19.53
0.1227	34.5034	41.8381	41.8117	0.001009	0.0992	19.52
0.0562	33.8558	41.872	41.7925	0.142077	0.1045	19.52
0.0765	24.7216	39.6602	39.5489	0.044568	0.15	19.96
0.1031	24.5792	39.8035	39.772	0.001531	0.0654	19.97
0.0166	25.3017	40.1232	39.8439	0.190977	0.1584	19.96
0.0002	24.7456	39.9077	39.5969	0.001502	0.0667	19.96
0.0233	25.1266	39.5296	39.4669	0.352641	0.0794	19.96
0.09	35.9175	43.0137	42.8949	0.123077	0.0876	19.75
0.0659	34.9296	41.8833	41.0415	0.092807	0.0942	19.75

0.0659	34.7105	42.6028	42.2602	0.070039	0.22	19.75
0.0521	34.1239	42.0546	41.9589	0.00618	1.3025	19.74
0.0902	34.5969	42.0927	41.5755	0.387097	0.0516	19.74
0.0002	34.7519	41.1891	40.6755	0.075472	0.114	19.75
0.0626	33.5348	40.8787	39.5968	0.000186	0.5377	19.75
0.0632	29.9975	35.7649	31.7464	0.183086	0.1357	19.75
0.0416	34.0394	40.9558	40.6219	0.000909	0.1101	19.74
0.0277	34.5843	41.4222	41.1207	0.063148	0.2155	19.75
0.0347	34.386	41.25	40.6488	0.301288	0.1313	19.74
0.0555	33.6959	40.5151	40.303	0.001984	0.0505	19.74
0.1045	33.473	39.8059	36.8128	0.094955	0.1476	19.74
0.077	31.5827	38.4562	34.8793	0.033473	0.247	19.75
0.0208	32.0712	40.0774	39.4801	0.916196	0.2035	19.88
0.0696	29.7288	36.99	36.1326	0.009573	8.9426	19.86
0.0416	33.4996	41.3196	41.1978	0.190476	0.09	19.81
0.052	34.0077	41.9562	41.6832	0.161798	0.1034	19.78
0.0002	34.0902	41.8889	41.6423	0.037691	0.0881	19.78
0.0486	33.1808	40.9704	40.0845	0.365591	0.1016	19.79
0.0798	33.1068	40.6581	39.4497	0.227642	0.0604	19.78
0.0002	19.8242	37.8613	37.7602	0.060264	0.0563	19.93
0.0606	20.0991	38.3334	38.2266	0.003021	0.0332	19.94
0.0168	19.896	37.9022	37.6514	0.2753	0.1487	19.92
0.0002	19.5422	37.4855	36.5609	0.407035	0.028	19.93
0.1111	19.5687	38.0975	38.0051	0.404523	0.0559	19.94
0.0002	19.8018	38.4879	38.3061	0.212963	0.0917	19.92
0.0336	20.9725	39.1647	38.5659	0.001453	0.0689	19.93
0.091	19.4915	38.1264	37.4316	0.363065	0.1085	19.94
0.064	19.7793	38.4783	37.4865	0.069467	0.1986	19.93
0.0645	17.2895	32.7926	25.4477	0.073986	0.63	19.93
0.034	15.7375	30.5881	8.2396	0.003842	1.6462	19.93
0.0734	30.0625	40.6196	40.1693	0.003067	0.0327	19.8
0.0802	29.4677	39.2383	38.1121	0.001342	0.0746	19.8
0.0368	29.6984	40.2706	40.1512	0.002387	0.042	19.8
0.0535	29.4117	39.3646	38.9104	0.002639	0.038	19.8
0.0335	29.9255	40.2569	39.7442	0.002732	0.0367	19.78
0.0067	30.0616	40.5441	40.2735	0.000782	0.128	19.79
0.1236	30.4556	41.3268	41.2542	0.001049	0.0954	19.78
0.0002	21.0017	33.6049	30.8461	1.076577	0.0461	13.46
0.0002	25.4497	39.4034	39.2564	0.840149	0.099	13.48
0.0155	26.4826	40.3873	40.3657	0.001119	0.0895	13.48
0.0052	24.6792	37.858	36.1822	0.174743	0.08	13.46
0.0002	25.9721	39.6804	39.5199	0.558528	0.0466	13.45
0.0831	24.5294	37.8978	37.7439	0.312292	0.0395	13.47
0.0465	26.7866					
0.0622	25.3498	40.8355	40.7407	0.009845	1.9489	13.49
0.0467	24.7256	38.4656	38.3621	0.002737	4.3234	13.49
0.0259	26.3747	38.3599	37.7332	0.10984	0.0485	13.49
0.0582	42.9342	40.3343	40.2392	0.00413	3.185	13.49
0.1062	24.229	44.3618	44.1626	0.021344	0.8709	13.49
0.0763	24.6389	38.9357	38.7758	0.001178	0.085	15.67

0.1189	24.0301	39.8746	39.8743	10	0.0022	15.67
0.0593	23.7478	39.5293	39.529	0.001433	0.0699	15.66
0.0679	22.6585	38.6755	38.6752	0.000612	0.1635	15.68
0.1143	25.3721	38.6945	38.6942	0.310722	0.1198	15.69
0.0763	24.0832	41.2911	41.2803	0.001504	0.0666	15.68
		38.447	38.4071	#DIV/0!	0	15.7